



Declaration

UNIVERSITEIT • STELLENBOSCH • UNIVERSITY  
jou kennisvenoot • your knowledge partner

Meganiese Ingenieurswese – Mechanical Engineering

**Design, building and testing of a fibre optic force sensor and  
its application in an *in vitro* and *in vivo* study investigating  
the biomechanical properties of the patella tendon**

by

**Jacobus Hendrik Müller**

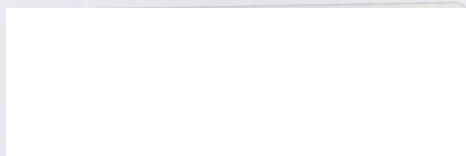
Thesis presented at the University of Stellenbosch  
in partial fulfilment of the requirements for the  
degree of

**Masters of Science in Mechanical Engineering**

Department of Mechanical and Mechatronic Engineering  
University of Stellenbosch  
Private Bag X1, 7602, Matieland, South Africa

**Promoter: Prof. Cornie Scheffer**

April 2007



## Declaration

I, the undersigned, hereby declare that the work contained in this thesis is my own original work and that I have not previously in its entirety or in part submitted it at any university for a degree.

Signature:

Date: 14/02/2007

## Abstract

*Background:* A fibre optic force sensor (two transmitters and receivers, a driver circuit and the load sensing optic fibre) was designed, built and tested to be used in *in vitro* and *in vivo* patella tendon experiments.

*Methods:* Hysteresis in the sensor output, the sensor's frequency response and its measurement repeatability were quantified through two loading tests in a hydraulic press and a cadaveric patella tendon. The sensor and loadcell measurements of the cadaveric patella tendon loading test were also used to derive five constants of a mathematical expression that models soft tissue stress relaxation. The results obtained from the sensor measurements (local stress relaxation) were compared to the results obtained from the loadcell (overall stress relaxation). The loads in the anterior third and posterior third of the right patella tendon were measured when volunteers performed a one leg squat and a leg extension as well as a step and jump exercise.

*Results:* The sensor has an average hysteresis error of 20% full scale output (FSO), its measurement repeatability is 93% FSO and its measurement sensitivity decreases when the loading frequency increases. The stress relaxation measured by the loadcell differed from the relaxation measured by the sensor (loadcell: 70%, sensor: 57%). The *in vivo* study results were submitted for statistical analysis and showed that posterior loads were significantly higher than anterior loads as the ratio of the peak anterior load over the peak posterior load indicates (squat: concentric = 0.56 [SD = 0.4] and eccentric 0.54 [SD = 0.41], leg extension: 0.33 [SD = 0.17], step: up = 0.28 [SD = 0.094] and down = 0.29 [SD = 0.066], jump: 0.34 [SD = 0.14]).

*Discussion:* The hysteresis was within acceptable limits for the study. The measurement repeatability and frequency response results suggest that it will be best to make use of subject and rate specific calibrations for the sensor. The sensor gives the possibility of measuring local stress relaxation, something that is not possible with the loadcell. The *in vivo* results provide insight into the loading patterns within the patella tendon.

## Uittreksel

*Agtergrond:* 'n Veseloptiese krag sensor (twee senders en ontvangers, 'n drywerbaan en krag sensitiewe optiese vesel) is ontwerp, vervaardig en getoets wat gebruik kan word tydens *in vitro* en *in vivo* patellapees eksperimente.

*Metodes:* Histerese in die omsetter uitreesein, die omsetter se frekwensierespons en metingherhaalbaarheid was gekwantifiseer m.b.v. twee belastingstoetses in 'n hidrouliese pers en 'n kadawer patellapees toetsopstelling in 'n trektoetsraam. Die omsetter en lassel metings van die *in vitro* belastingstoets is gebruik om vyf konstantes van 'n wiskundige model waarmee die ontspanningsgedrag van sagte weefsel gesimuleer word, te bepaal. Die resultate verkry deur die lassel data (totale ontspanning) en die omsetter data (lokale ontspanning) is met mekaar vergelyk. Die kragte in die voorste en agterste derde van vrywilligers se regter patellapees is gemeet tydens 'n stel oefeninge: hurk, een-been-ekstensie, trap en spring.

*Resultate:* Die gemiddelde histerese fout is bereken op 8.9%-vol-skaal-uitset (VSO) en metingherhaalbaarheid was 93% VSO. Die omsetter se sensitiwiteit het afgeneem vir toenemende frekwensie. Die ontspanning gemeet deur die lassel verskil van die ontspanning gemeet deur die omsetter (lassel: 70%, omsetter: 57%). Die *in vivo* studie resultate is ingehandig vir statistiese analise en die bevinding was dat agterste maksimum kragte in die patellapees aansienlik groter was as die voorste maksimum kragte. Die verhouding van die voorste maksimum krag oor die agterste maksimum krag vir die oefeninge was: hurk - konsentries = 0.56 [SD = 0.4] en eksentries 0.54 [SD = 0.41]; been-ekstensie - 0.33 [SD = 0.17]; trap - op = 0.28 [SD = 0.094] en af = 0.29 [SD = 0.066]; spring = 0.34 [SD = 0.14].

*Bespreking:* Die histerese fout was binne aanvaarbare limiete vir die studie. Die metingherhaalbaarheid en frekwensierespons resultate dui daarop dat die omsetter se kalibrasies afhanklik is van die tempo van belasting en varieer tussen optiese vesels. Die omsetter kan gebruik word om lokale ontspanning te meet, iets wat nie moontlik is met 'n lassel nie. Die *in vivo* resultate ondersteun die hipotese dat agterste patellapees vesels meer belas is as die voorste patellapees vesels.

## Acknowledgements

The following persons should be thanked for their assistance during the project. Special thanks are given to:

Prof. Cornie Scheffer  
Dr. Edwin Dillon  
Dr. Spike Erasmus  
Dr. Richard de Villiers  
Dr. Alex Alvin

The following persons also made worth mentioning contributions. They are thanked in no specific order:

Mr Jonathan Gunton  
Mr. Sean Moffet  
Mr. Lukusa Kabula  
Mrs. Lee Smith  
Mr. Ockert Strydom  
Mr. Cobus Zietsman  
Mr. Ferdi Zietsman  
Dr. Martin Kidd

Thank you to all the people who volunteered for the *in vivo* study. It would not have been possible to complete the project without them.

## Dedications

To my family and all who supported me throughout my undergraduate and post-graduate studies.

## Table of contents

Abstract .....	ii
Uittreksel .....	iii
Acknowledgements .....	iv
Dedications .....	v
List of figures .....	ix
List of tables .....	xii
Nomenclature .....	xiv
List of abbreviations .....	xiv
List of symbols .....	xiv
Chapter 1: Introduction .....	1
1.1 Scope of work .....	2
Chapter 2: Literature survey .....	4
2.1 Knee anatomy .....	4
2.2 Connective tissue .....	6
2.2.1 Anatomy .....	6
2.2.2 Biomechanics .....	7
2.3 Solution techniques for mathematical models .....	10
2.4 Force and strain transducers used in biomechanical studies .....	11
2.5 Fibre optic technology .....	14
Chapter 3: Hardware and software .....	16
3.1 Fibre optic force sensor .....	16
3.1.1 Working principle .....	16
3.1.2 Composing elements .....	18
3.2 Data acquisition .....	20

Chapter 4: Characterisation of the sensor output.....	21
4.1 Introduction .....	21
4.2 Hydraulic press loading test.....	22
4.2.1 Introduction.....	22
4.2.2 Hardware setup .....	22
4.2.3 Test procedure.....	24
4.2.4 Data processing.....	25
4.2.5 Results.....	29
4.3 In vitro patella tendon loading test .....	32
4.3.1 Introduction.....	32
4.3.2 Hardware setup .....	32
4.3.3 Test procedure.....	34
4.3.4 Data processing procedure.....	35
4.3.5 Results.....	36
4.4 In vivo sensor calibration .....	38
4.4.1 Introduction.....	38
4.4.2 Hardware setup .....	39
4.4.3 Test procedure.....	40
4.4.4 Data processing.....	40
4.4.4 Results.....	41
4.5 Conclusion .....	42
Chapter 5: Stress relaxation measured by a loadcell and the sensor.....	47
5.1 Introduction .....	47
5.2 QLV theory.....	48
5.3 Elastic response.....	50
5.4 Reduced relaxation function .....	50



5.5	Test setup .....	54
5.6	Test procedure.....	55
5.7	Matlab programming .....	56
5.8	Data processing procedure.....	58
5.9	Results.....	60
5.10	Conclusion.....	64
Chapter 6: <i>In vivo</i> investigation into the loading patterns of the patella tendon.....		68
6.1	Introduction .....	68
6.2	Hardware setup and test procedure.....	69
6.3	Data processing procedure.....	70
6.4	Results.....	72
6.5	Conclusion.....	73
Chapter 7: Conclusions .....		75
Chapter 8: Recommendations.....		77
References.....		78
Appendix A: Results from the sensor output tests.....		I
A-1	Hydraulic press loading test.....	I
A-2	In vitro patella tendon loading test .....	V
Appendix B: QLV model of patella tendon stress relaxation.....		VI
B-1	Linear solid model.....	VI
B-2	Reformulation of QLV theory for programming .....	VII
B-3	Patternsearch-algorithm.....	IX
B-4	Stress relaxation graphs .....	XI
B-5	Cyclic loading graphs.....	XII
Appendix C: <i>In vivo</i> investigation into the loading patterns of the patella tendon ..		XIV
C-1	Results.....	XIV

## List of figures

Figure 1: Knee anatomy, adopted from <a href="http://lipscombcclinic.com">http://lipscombcclinic.com</a> (23/06/06) .....	4
Figure 2: Schematic diagram illustrating the six degrees of freedom of the human knee joint. Edited version from <a href="http://www.aclsolutions.com">www.aclsolutions.com</a> (23/06/06) .....	5
Figure 3: Hierarchical structure of a tendon, adopted from <a href="http://www.engin.umich.edu/class/bme456/ligten/ligten.htm">http://www.engin.umich.edu/class/bme456/ligten/ligten.htm</a> (23/06/06).....	6
Figure 4: Idealised stress vs. strain curve from a load to failure test.....	7
Figure 5: Illustration of stress relaxation, creep and hysteresis. The top graphs signify the input and the bottom graphs show the connective tissue's response.....	8
Figure 6: 1. Buckle transducers and the insertion of a buckle transducer into a ligament or tendon. 2. Implantable force transducers and insertion of an Implantable force transducer into a ligament or tendon. Adopted from Ravary <i>et al.</i> (2004). .....	13
Figure 7: Illustration of the possibilities when a light ray strikes the core/cladding interface. ....	15
Figure 8: Illustration of a macro bend .....	16
Figure 9: 1. Illustration of a micro bend. 2. Illustration of a micro bend induced by an external load.....	16
Figure 10: Elongations that result from tensile loading.....	17
Figure 11: Schematic of the driving circuit for the sensor.....	19
Figure 12: Schematic of the hydraulic press test hardware setup. ....	23
Figure 13: Suspension of the optical fibre in the hydraulic assembly .....	23
Figure 14: Hydraulic press loading test: data processing of sequential test recordings	25
Figure 15: Subdivision of cycle into sub-cycles .....	26
Figure 16: Hydraulic press loading test: data processing of random test recordings....	27
Figure 17: Posterior channel (20 mm plate) - 0.1 Hz cyclic load @ maximum 250 N....	31
Figure 18: Posterior channel (20 mm plate) – 1 Hz cyclic load @ maximum 250 N.....	31
Figure 19: Schematic of the <i>in vitro</i> patella tendon study hardware setup .....	33

Figure 20: Steel cylinders fixed in MTS hydraulic press .....	33
Figure 21: Optic fibres inserted through the patella tendon.....	34
Figure 22: <i>In vitro</i> patella tendon loading test: data processing of sequential test recordings .....	35
Figure 23: FFT for optic fibres far apart.....	36
Figure 24: FFT for optic fibres in close proximity.....	36
Figure 25: Insertion of optic fibre into the patella tendon.....	39
Figure 26: <i>In vivo</i> patella tendon loading test: data processing of cyclic recordings.....	40
Figure 27: Maxwell model (Fung, 1965).....	47
Figure 28: Kelvin/Voight model (Fung, 1965).....	47
Figure 29: Linear solid model (Fung, 1965).....	51
Figure 30: Modulus and internal damping plotted against frequency $\omega$ .....	53
Figure 31: Harvesting of patella tendon complex .....	54
Figure 32: Patella tendon complex potted into steel cylinders.....	55
Figure 33: Optimisation strategy.....	59
Figure 34: Raw strain measured by displacement sensor.....	60
Figure 35: 3 <sup>rd</sup> order polynomial fit to loadcell measurements .....	60
Figure 36: 3 <sup>rd</sup> order polynomial fit to sensor measurements.....	60
Figure 37: Loadcell stress relaxation prediction: squared error objective function .....	62
Figure 38: Sensor stress relaxation prediction: squared error objective function .....	62
Figure 39: Loadcell output: squared error objective function.....	63
Figure 40: Sensor output: squared error objective function.....	63
Figure 41: Indication of Patellar Tendinopathy on a MRI photograph.....	69
Figure 42: Steps followed during processing of the <i>in vivo</i> data.....	71
Figure 43: Linear solid model .....	VI
Figure 44: Dashpot and elastic spring in series free body diagram.....	VI

Figure 45: Poll method .....	X
Figure 46: Loadcell stress relaxation prediction: chi squared objective function .....	XI
Figure 47: Loadcell stress relaxation prediction: least squares curve fit.....	XI
Figure 48: Sensor stress relaxation prediction: chi squared objective function .....	XI
Figure 49: Sensor stress relaxation prediction: least squares curve fit.....	XI
Figure 50: Loadcell cyclic stress relaxation prediction: chi squared objective function	XII
Figure 51: Loadcell cyclic stress relaxation prediction: least squares curve fit.....	XII
Figure 52: Sensor cyclic stress relaxation prediction: chi squared objective function..	XII
Figure 53: Sensor cyclic stress relaxation prediction: least squares curve fit.....	XII
Figure 54: Squat exercise: volunteer #4.....	XVII
Figure 55: Leg extension: volunteer #4 .....	XVII
Figure 56: Step up: volunteer #4 .....	XVIII
Figure 57: Step down: volunteer #4.....	XVIII
Figure 58: Step down: volunteer #4.....	XVIII
Figure 59: Jump exercise: volunteer #4 .....	XVIII
Figure 60: Squat exercise: Concentric contraction [ $p = 0.132$ ].....	XIX
Figure 61: Squat exercise: Eccentric contraction [ $p = 0.115$ ] .....	XIX
Figure 62: Leg extension exercise: Concentric contraction [ $p = 0.0213$ ].....	XIX
Figure 63: Leg extension exercise: Eccentric contraction [ $p = 0.0211$ ] .....	XIX
Figure 64: Step up exercise [ $p = 0.0194$ ].....	XIX
Figure 65: Step down exercise [ $p = 0.0188$ ].....	XIX
Figure 66: Jump exercise [ $p = 0.00193$ ] .....	XX

## List of tables

Table 1: Hysteresis error and RMS error for the sensor.....	30
Table 2: Hysteresis of the force input from the hydraulic press.....	30
Table 3: Signal-to-noise ratio for each channel .....	30
Table 4: $A_{\text{output}}/A_{\text{input}}$ for the static calibration, 0.1 Hz cycle and 1 Hz cycle .....	31
Table 5: Calibration results for anterior channel.....	32
Table 6: FFT results on sensor output for different optic fibre configurations.....	36
Table 7: Hysteresis in the recordings of the sequential test .....	37
Table 8: Signal to noise ratio and FSO of the loadcell and sensor.....	37
Table 9: Best calibration and average static sensitivity .....	37
Table 10: Average sensor recordings for the three isokinetic tests .....	41
Table 11: Maximum exerted torque as reported by the Biodex test system .....	41
Table 12: Sensor calibration results of <i>in viitro</i> and <i>in vivo</i> patella tendon loading test	42
Table 13: Static sensitivity of posterior channel .....	42
Table 14: Overall hysteresis contribution from the sensor.....	43
Table 15: QLV-constants for the loadcell output.....	61
Table 16: QLV-constants for the sensor output.....	61
Table 17: Stress relaxation measured by loadcell for relaxation test.....	62
Table 18: Stress relaxation measured by sensor for relaxation test.....	62
Table 19: Stress relaxation measured by loadcell for cyclic loading.....	63
Table 20: Stress relaxation measured by sensor for cyclic loading .....	63
Table 21: Estimation error for the QLV-constants .....	64
Table 22: <i>In vivo</i> test results for the different exercises.....	72
Table 23: Probabilities as determined by the repeated measures analysis for the condition that the anterior loads are smaller than the posterior loads for the different exercises .....	73

Table 24: Anterior channel calibration: 250 N, 20 mm plate.....	I
Table 25: Anterior channel calibration: 500 N, 20 mm plate.....	I
Table 26: Anterior channel calibration: 500 N, 15 mm plate.....	I
Table 27: Posterior channel calibration: 250 N, 20 mm plate .....	II
Table 28: Posterior channel calibration: 500 N, 20 mm plate .....	II
Table 29: Results from the calibrations for anterior channel .....	III
Table 30: Results from the calibrations for posterior channel.....	III
Table 31: Static sensitivity for each test – anterior channel.....	IV
Table 32: Static sensitivity for each test – posterior channel.....	IV
Table 33: Calibration constants for anterior channel .....	V
Table 34: Calibration constants for posterior channel .....	V
Table 35: Stress relaxation prediction for cyclic loading: loadcell predictions .....	XIII
Table 36: Stress relaxation prediction for cyclic loading: sensor predictions.....	XIII
Table 37: Squat: Concentric contraction .....	XIV
Table 38: Squat: Eccentric contraction.....	XV
Table 39: Leg extension .....	XV
Table 40: Step up.....	XVI
Table 41: Step down .....	XVI
Table 42: Jump.....	XVII

## Nomenclature

### List of abbreviations

	<b>A</b>		
ACL	anterior cruciate ligament	MTS	materials testing system
A/D	analogue to digital		<b>P</b>
	<b>C</b>	PC	personal computer
CPU	central processing unit	PCL	posterior cruciate ligament
	<b>D</b>	PID	proportional, integral and differential
DC	direct current	PT	Patellar Tendinopathy
	<b>E</b>		<b>Q</b>
EMG	electromyogram	QLV	Quasi-linear viscoelastic theory
	<b>F</b>		<b>R</b>
FFT	Fast Fourier Transform	RAM	random access memory
FSO	full scale output	RMS	root mean square
	<b>I</b>		<b>S</b>
IA	instrumentation amplifier	SD	standard deviation
I/O	input-output	S/N	signal-to-noise
	<b>L</b>		<b>U</b>
LCL	lateral collateral ligament	USB	universal serial bus
LED	light emitting diode		<b>V</b>
LMSG	liquid metal strain gauge	V/I	voltage-current
	<b>M</b>	VR	voltage regulator
MB	megabyte		
MCL	medial collateral ligament		

### List of symbols

<i>A</i>	QLV-function constant	<i>S</i>	function of QLV time constants
<i>B</i>	QLV-function constant	<i>T</i>	tensile load
<i>C</i>	QLV-function constant	<i>U</i>	displacement
<i>F</i>	force	<i>V</i>	speed of light in a material
<i>G</i>	reduced relaxation function	<i>a</i>	lower integration limit for Simpson's rule
<i>J</i>	reduced creep function	<i>b</i>	upper integration limit for Simpson's rule
<i>K</i>	stress response	<i>c</i>	speed of light in a vacuum
<i>M</i>	complex modulus	<i>f</i>	function
<i>N</i>	refractive index	<i>g</i>	function
<i>P</i>	confidence interval		

$i$	index of a vector	$A_{output}$	maximum FFT value for the output
$\ell$	length	$A_0$	reference area
$m$	polynomial order	$C_{\#}$	capacitor, $\# = 1..n, n \in Z$
$n$	number of samples	$E_R$	ratio of linear solid model time constants
$p$	probability constant	$E_x$	longitudinal elastic modulus
<b>r</b>	stress response to ramp increase in strain, vector	$E_y$	transverse elastic modulus
<b>s</b>	stress response to stress relaxation, vector	$E_{\dagger}$	exponential integral
$s$	Laplace parameter	$OBJ_{\#}$	objective function, $\# = 1..n, n \in Z$
$t$	time	$R_{\#}$	resistor, $\# = 1..n, n \in Z$
$u$	displacement	$S_{a0}$	zero error
$x$	longitudinal distance, measurement, independent variable	$S_{a1}$	sensitivity error
$y$	transverse distance, measurement, dependent variable	$S_x$	standard deviation of independent variable measurements
$\alpha$	constant	$S_{yx}$	standard error of polynomial fit
$\delta$	phase shift between strain and stress	$V_N$	voltage noise level
$\delta x$	perturbation in longitudinal direction	$V_S$	voltage signal level
$\delta y$	perturbation in transverse direction	$e_{h,max}$	maximum hysteresis error
$\delta \varepsilon$	infinitesimal change in strain	$e_{L,max}$	linearity error
$\varepsilon$	strain	$e_{R,max}$	measurement repeatability
$\gamma$	strain rate, $\frac{\partial \varepsilon}{\partial t}$	$k_{\#}$	Spring constant, $\# = 1..n, n \in Z$
$\mu$	dashpot damping constant	$\ell_0$	reference length
$\nu$	degrees of freedom	$r_0$	full scale output
$\theta$	substitute for QLV-constants	$t_0$	time at the end of the ramp phase
$\sigma$	tensile stress	$x_i$	independent variable
$\tau$	time, integration parameter	$x_0$	longitudinal reference length
$\omega$	angular frequency	$y_{c,i}$	polynomial prediction
$\xi$	time difference	$y_i$	actual measurement
$\psi$	edited reduced creep function	$y_{i,downscale}$	dependent variable entries when de-scaling
$f^{-1}$	derivative of function, $f$		
$\chi^2$	chi squared error		
$\sigma^{(e)}$	elastic response		
$A_{input}$	maximum FFT value for the input		



$y_{i,upscale}$	dependent variable entries when ascending		ramp phase
$y_0$	transverse reference length	$\tau_\epsilon$	stress relaxation time constant
$\epsilon_x$	longitudinal strain	$\tau_\sigma$	creep time constant
$\epsilon_y$	transverse strain	$\tau_1$	lower boundary value of relaxation spectrum
$\nu_{long}$	Poisson ratio in longitudinal direction	$\tau_2$	upper boundary value of relaxation spectrum
$\nu_{Poisson}$	Poisson ratio	$\dot{F}$	first time derivative for force
$\nu_{trans}$	Poisson ratio in transverse direction	$\bar{G}$	Laplace transform of reduced stress relaxation function
$\theta_A$	angle of acceptance	$\bar{J}$	Laplace transform of reduced creep function
$\theta_C$	critical angle	$\dot{u}$	first time derivative of displacement
$\theta_\#$	angle, incidence angle, refraction angle, $\# = 1..n, n \in \mathbb{Z}$	$\bar{\sigma}$	Laplace transform of tensile stress
$\sigma_f$	stress left in specimen at the end of the relaxation period	$\bar{\sigma}^{(e)}$	Laplace transform of elastic response
$\sigma_{relax}$	stress relaxation ratio	$1(t)$	step input
$\sigma_0$	stress in sample at the end of the		

## Chapter 1: Introduction

The mechanical properties of the patella tendon have been derived from various *in vitro* studies (Almekinders, Vellema & Weinhold, 2002; Basso, Amis, Race & Johnson, 2002; Hashemi, Chandrashekar & Slauterbeck, 2005; Haut & Powlison, 1990; Johnson, Tramaglini, Levine, Ohno, Choi & Woo, 1994) but it is results from *in vivo* studies (Finni, Komi & Lepola, 2000; Komi, Belli, Huttunen, Bonnefoy, Geysantt and Lacour 1996; Hansen, Bojsen-Moller, Aagaard, Kjaer & Magnusson, 2006) that are of greater value to researchers and clinicians (Komistek, Kane, Mahfouz, Ochoa & Dennis, 2005). This has led to the development of various techniques and methods (mathematical modelling and experimental techniques) with which soft tissue and joint loads can be approximated in the biomechanics field (Meyer, 2003). One cannot, however, apply the two techniques separately, since experimental results serve as validation for mathematical model results and mathematical models use experimental results to simulate situations that are not easy to monitor experimentally.

The need for experimental procedures has seen the development of advanced transducers with which the necessary measurements can be taken, as described by Ravary, Pourcelot, Bortolussi, Konieczka and Crevier-Denoix (2004). Since introduced by Komi *et al.* (1996), the fibre optic force sensor (sensor) has been used in biomechanical studies (Arndt, Komi, Brüggemann & Lukkariniemi, 1998; Finni *et al.*, 2000; Finni, Komi & Lukkariniemi, 1998) and its properties have been investigated (Erdemir, Hamel, Piazza & Sharkney, 2003; Erdemir, Piazza & Sharkney, 2002). The technique provides a minimally invasive and inexpensive method of taking *in vitro* and *in vivo* force measurements in ligaments and tendons for biomechanical studies.

The viscoelastic behaviour of soft tissue have mainly been investigated through *in vitro* test set-ups (Abramowitch & Woo, 2004; Hashemi *et al.*, 2005; Johnson *et al.*, 1994; Moon, Woo, Takakura, Gabriel & Abramowitch, 2006; Nigul & Nigul, 1987; Toms, Dakin, Lemons & Eberhardt, 2002; Wu, Levenston & Chaikof, 2006) although one *in vivo* study have been found that looks at the viscoelastic creep behaviour of the patella tendon (Hansen *et al.*, 2006). The sensor provides an attractive method with which investigations into the viscoelastic nature of soft tissue - both *in vitro* and *in vivo* - can be conducted due to its minimally invasive character. The measurement capabilities of the sensor were compared to those of a loadcell during a stress relaxation test on a patella

tendon complex in a hydraulic press. Experimental data have been combined with a mathematical model (Fung, 1972) that simulates the stress relaxation behaviour of soft tissues.

Two *in vitro* investigations have been conducted on the differential loading patterns of the anterior and posterior patella tendon fibres (Almekinders *et al.*, 2002; Basso *et al.*, 2002). The results on whether the anterior or posterior side of the patella tendon endures greater loads are conflicting for these two studies and more research into the *in vivo* loading patterns of the anterior and posterior patella tendon fibres are needed (Almekinders *et al.*, 2002; Basso *et al.*, 2002; Hamilton & Purdam, 1973).

Tasks for this study can be summarised as:

- The development and testing of a sensor that is suitable for the *in vitro* and *in vivo* measurement of connective tissue loads;
- An *in vitro* investigation into the stress relaxation behaviour of the patella tendon with a loadcell, the sensor and a mathematical model.
- An *in vivo* investigation into the differential loading patterns of the patella tendon with the sensor.

## **1.1 Scope of work**

The literature survey focuses on four distinct areas. The anatomy and biomechanics of the knee joint is investigated with the centre of attention directed to the connective tissues that act as supporting structures for the knee joint. The study is largely based on the patella tendon, and therefore the properties and characteristics of connective tissue are needed for the successful completion of the study. A mathematical model has to be solved which approximates the stress relaxation nature of the patella tendon. This model is indeterminate, and methods that have been employed in the past to solve indeterminate systems need to be investigated. Drawbacks of these methods also need to be considered, since the mathematical model is based on a biologic system, and a mathematically correct answer might not correspond to a physiologically correct answer. Transducers that have been employed in biomechanical studies are investigated. A transducer needs to be found with which the required measurements for the study can be taken. A fibre optic force sensor was decided upon and therefore the mechanics of light propagation through an optic fibre are considered next. The investigation is di-

rected towards the principles that influence the effective propagation of light through an optic fibre.

In Chapter 3 a discussion on the hardware that was developed for the project is provided. The working principle of the sensor is explained after which the components making up the sensor are discussed in more detail. Thereafter the data acquisition system that was developed is discussed. Since the sensor was custom designed and developed, it was necessary to characterise its properties and measurement capabilities. The methods that were used are described in Chapter 4.

Chapter 4 is comprised of three major sections that describe the three test set-ups that were used to characterise the sensor's properties. A hydraulic press loading test, an *in vitro* patella tendon loading test and an *in vivo* patella tendon loading test are described. During the discussion on the characterisation tests, the focus rests on the hysteresis effect in force recordings, the signal-to-noise ratio of the measurements as well as the frequency response of the sensor. Applicable calibrations and measurement repeatability for the two channels of the sensor are also considered. The difference in sensitivity between the two channels is considered as well as the influence that two optic fibres in close proximity have on the force measurements.

In Chapter 5 the viscoelastic behaviour of the patella tendon was investigated with the main focus on a phenomenon known as stress relaxation. Two transducers were used to measure the stress relaxation that results when the tendon undergoes a constant increase in strain that is maintained afterwards. A loadcell inside the MTS hydraulic press was used as well as the sensor. The purpose of the study was to compare the local stress relaxation measured by the sensor to the stress relaxation measured by the loadcell. A mathematical tool, known as Quasi-linear Viscoelastic (QLV) theory (Fung, 1972) was used as a method to compare the local and overall measured stress relaxation.

The sensor was used in an investigation of the differential forces that occur in the anterior and posterior fibres of the patella tendon. In Chapter 6 the test method and results of this *in vivo* study is described. The results of this study provide insight into the question of whether anterior or posterior loads in the patella tendon are greater, since results in the literature are conflicting.

## Chapter 2: Literature survey

The purpose of this chapter is to provide the necessary background on the work that is presented in this report. The topics that are discussed include the following:

- the basic anatomy of the knee joint;
- the basic anatomy and biomechanics of connective tissue;
- mathematical model solution techniques;
- the transducers that have been used in previous biomechanical studies to measure connective tissue loads and strains ; and
- the basic science of fibre optic systems, with the focus on light propagation through an optic fibre.

### 2.1 Knee anatomy

The knee joint, shown in Figure 1, consists of skeletal elements (two femoral condyles, a tibial plateau and the patella) that are connected to one another through ligaments. Knee joint articulation is established through the excitation of the quadriceps muscles and the hamstring muscles that is connected to the skeletal elements through tendons. During articulation, the femoral condyles roll across the medial and lateral meniscus while the patella, shown in Figure 2, slides inside the femoral groove. The menisci, situated between the femoral condyles and the tibial plateau, are fibro-cartilage pads that conform to the articulating surfaces.

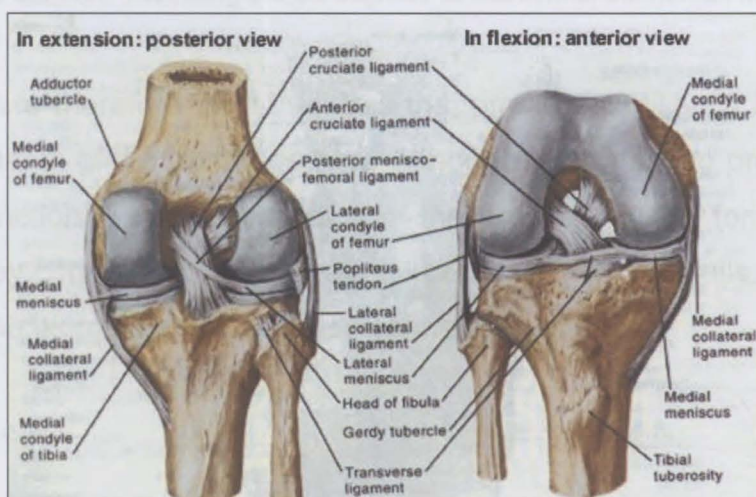


Figure 1: Knee anatomy, adopted from <http://lipscomclinic.com> (23/06/06)

Knee joint articulation can be described by means of three translations and three rotations that act along three principle axes. These axes are the tibial shaft axis, the epicondylar axis and the anterior/posterior axis. The orientation of the axes and the kinematics along each axis are illustrated in Figure 2.

Ligaments inside the knee joint together with the quadriceps muscles and the hamstring muscles are responsible for knee joint stability. The medial collateral ligament (MCL) and the lateral collateral ligament (LCL) support the medial and lateral surfaces respectively when the knee joint is in full extension. Anterior and posterior movement of the tibia relative to the femur is limited by the anterior cruciate ligament (ACL) and the posterior cruciate ligament (PCL). Support at the front of the knee joint is provided by the patella tendon-patella-quadriceps tendon complex.

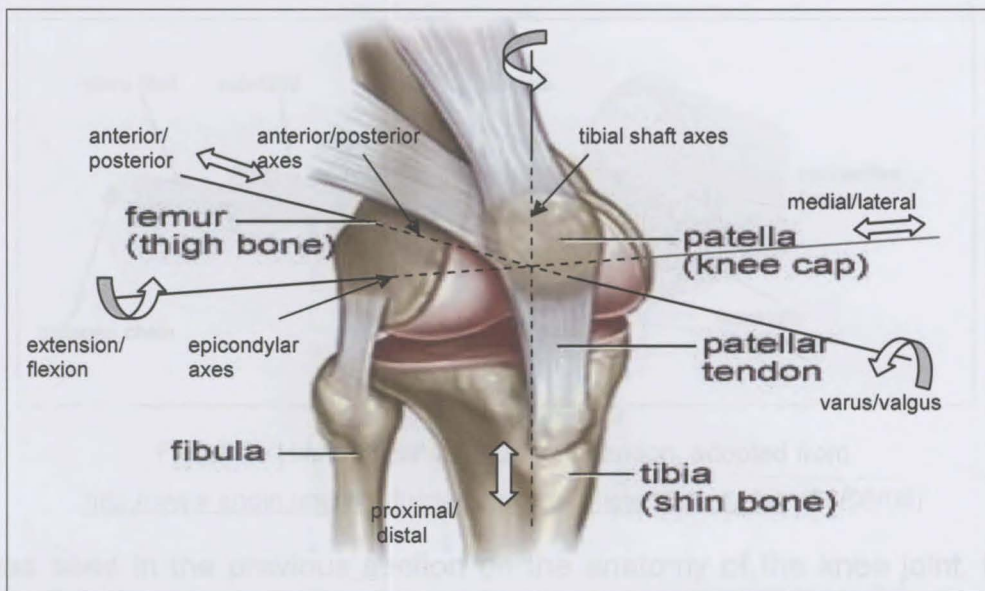


Figure 2: Schematic diagram illustrating the six degrees of freedom of the human knee joint. Edited version from [www.aclsolutions.com](http://www.aclsolutions.com) (23/06/06)

Ligaments are therefore the structures that provide stability by keeping the different skeletal elements of the joint together. Although tendons also provide some stability, their main function is the transmission of the skeletal muscle forces to the skeletal elements that they connect to. In the next section the emphasis falls on the basic anatomy as well as the biomechanics<sup>i</sup> of these connective tissues.

<sup>i</sup> Biomechanics is the research and analysis of the mechanics of living tissue. (Fung YC, 1993)

## 2.2 Connective tissue

### 2.2.1 Anatomy

Tendons and ligaments are composed of water and densely packed elements that have a hierarchical structure (Woo, Debski, Withrow & Janashek, 1999). The different organisational levels in this hierarchical structure are illustrated in Figure 3. Connective tissue is a composition of fascicles that are subdivided into smaller units known as fibrils. The fibrils have a zigzag crimp configuration when the connective tissue is unloaded. Each fibril contains sub-fibrils that in turn contain micro-fibrils. Type1 Collagen, the major load bearing structure, is located inside the micro-fibrils (Woo *et al.*, 1999).

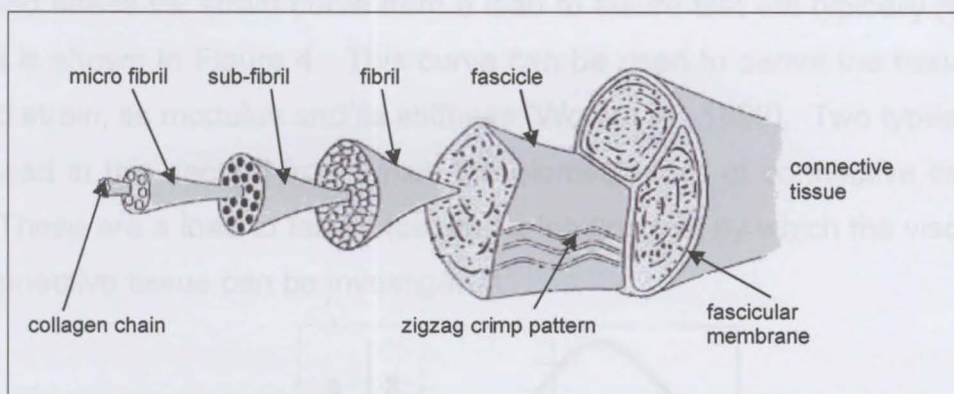


Figure 3: Hierarchical structure of a tendon, adopted from

<http://www.engin.umich.edu/class/bme456/ligten/ligten.htm> (23/06/06)

It was seen in the previous section on the anatomy of the knee joint, that a tendon's major function is the transmission of skeletal muscle forces. In order to accommodate these tensile forces, the tendon's fibrils are arranged parallel to the direction of loading. A ligament is responsible for knee joint stability and therefore it should be able to accommodate loads that are exerted from different directions. A ligament's fibrils are therefore arranged longitudinally as well as oblique or spirally.

Connective tissue will only function properly if the transition from the soft tissue into the harder bone material is of good quality. There are two insertion types (Thomopoulos, Williams, Gimbel, Favata & Soslowsky, 2003). A direct insertion consists of four morphological zones that include the connective tissue, fibro-cartilage, mineralised fibro-cartilage and the bone material. An indirect insertion refers to the direct transition

from the soft connective tissue to a superficial layer that connects directly to the periosteum<sup>ii</sup>, with deeper layers that anchor to the bone material via Sharpey's fibres<sup>iii</sup>.

When the strength of connective tissue is considered, both the material properties and the quality of the insertion of the soft tissue into the skeletal element must be kept in mind. This project focuses exclusively on the biomechanics of the soft tissue of the patella tendon. It is therefore not necessary to consider the biomechanics surrounding the insertion site, as was done by Thomopoulos *et al.* (2003).

### 2.2.2 Biomechanics

The biomechanics of connective tissue are based on empirical results, for example the derivations from the characteristics on a stress vs. strain curve (Woo *et al.*, 1999). An idealised stress vs. strain curve from a load to failure test will typically resemble the curve that is shown in Figure 4. This curve can be used to derive the tissue's ultimate stress and strain, its modulus and its stiffness (Woo *et al.*, 1999). Two types of tests will be discussed in this section from which the biomechanics of connective tissue can be derived. These are a load to failure test and a loading test by which the viscoelastic nature of connective tissue can be investigated.

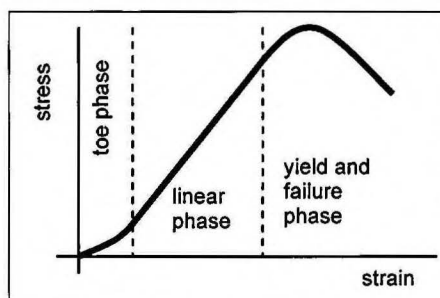


Figure 4: Idealised stress vs. strain curve from a load to failure test

The load to failure test has three distinct phases: the toe phase, the linear phase and a yield and failure phase (Woo *et al.*, 1999). During the toe phase, the fibrils of the connective tissue extend from its crimp pattern as the applied load increases. It is evident from the slope that the stiffness of the connective tissue increases gradually with the load during this phase.

---

<sup>ii</sup> Periosteum is a layer of fibrous connective tissue that surrounds a skeletal element. Definition supplied by: <http://www.medterms.com/script/main/art.asp?articlekey=7907>, (26/10/2006).

<sup>iii</sup> Sharpey's fibres are strong collagenous fibres that extend from the periosteum to the outer circumferential and interstitial lamellae of the skeletal element. Definition supplied by: <http://www.amershamhealth.com/medcyclopaedia/medical/Volume%20III%201/SARPEYS%20FIBRES.asp>; (19/07/2005).



As the fibrils become fully stretched, they align in the loading direction and the collagen chains become the major load bearing units. This signifies the beginning of the linear phase, which is the general operating range of the connective tissue. The modulus (the slope of the curve) and the stiffness (product of the slope and the ratio of the reference area and length) of the connective tissue are based on this part of the curve.

If the applied load is further increased, some of the collagen chains start to fail. This point indicates the transition from the linear phase to the yield phase. The load capacity and the stiffness of the connective tissue decrease as more of the collagen chains fail. The connective tissue will ultimately rupture upon further loading. There are two rupture modes, namely intra-substance failure, i.e. the connective tissue ruptures, or insertion site failure, i.e. the connective tissue tears from the skeletal element. The ultimate stress and ultimate strain of the connective tissue are derived from this part of the curve if the failure mode was intra-substance.

Although the properties derived from a load to failure test are valuable, it only gives estimates of the derived properties and it does not account for all the properties of the connective tissue. Connective tissue is a viscoelastic material and its response to induced loads or elongations is therefore time and history dependent (Woo *et al.*, 1999). A viscoelastic material's behaviour is described according to three quantities known as stress relaxation, creep and hysteresis. Figure 5 illustrates each of these properties schematically.

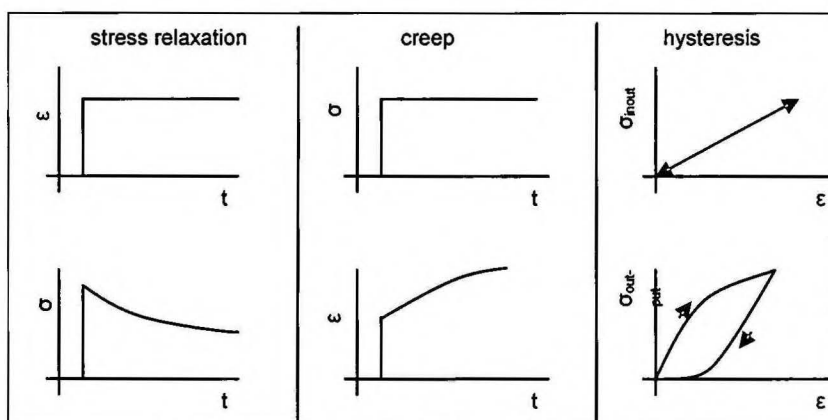


Figure 5: Illustration of stress relaxation, creep and hysteresis. The top graphs signify the input and the bottom graphs show the connective tissue's response.

Stress relaxation is a term that describes the decrease in stress over time that occurs when a body is suddenly strained and the strain is maintained at a constant magni-

tude afterwards (Fung, 1993). Creep on the other hand describes the increase in deformation over time that occurs when a body is suddenly loaded and the load is maintained at a constant magnitude afterwards. Hysteresis refers to the difference between the energy needed when a material is loaded and the usable energy available when the material unloads, i.e. the loading and unloading paths are different.

The viscoelastic properties can be derived from specific characteristics on a stress vs. time curve or a strain vs. time curve as will be discussed hereafter. When the connective tissue is strained to a level and that level is maintained over a period of time, the resulting stress vs. time curve together with a mathematical model can be used to characterise the stress relaxation behaviour of the tissue. The same applies to the creep behaviour. Instead of a constant strain level being held, a constant stress level is maintained for a period of time. Hysteresis can be characterised by applying a cyclic load over the connective tissue and using the resulting stress vs. time curve with a mathematical model.

Fung (1972) derived mathematical models that can be employed together with data from the stress vs. time curve and the strain vs. time curve to derive the parameters that describe the stress relaxation and creep respectively. Different expressions exist for the hysteresis, e.g. based on energy (Erdemir *et al.*, 2002) or actual force values (Figliola & Beasley, 2006). When the expression that is based on the energy principle is employed, the hysteresis is defined as the ratio of the areas under the loading and the unloading curve. The expression based on the actual stress or force values, is defined as the ratio of the maximum difference between the corresponding loading and unloading value and the difference between the maximum and minimum load or stress.

The viscoelastic properties of connective tissue play an important role in everyday joint function (Woo *et al.*, 1999). The laxity of a person's joints increases with time during physical exercise. This serves as a protective measure during sports since the person's joints are able to endure greater degrees of motion without rupturing the connective tissue. After a period of rest however, the joints regain their original laxity.

Stress relaxation together with hysteresis serve as a protective mechanism against fatigue failure in connective tissue. During cyclic loading the connective tissue experiences a continuous decrease in stress and the peak loads thus decrease. After a number of cycles, typically ten (Fung, 1972), the loading and unloading curves become

repeatable. This phenomenon is important to keep in mind when experimental testing is performed on connective tissue, since repeatable results will only be achieved after the tissue has been preconditioned.

When the results of different studies are compared, it is important to keep the following in mind: Reported values of a property from different studies might display variability. This variability can be ascribed to biologic factors, i.e. effects of maturation and age, effects of exercise and effects of immobilisation and remobilisation, and experimental testing factors, i.e. specimen orientation, effects of testing temperature, testing strain rate and specimen storage and freezing (Woo *et al.*, 1999). It is therefore important to pay attention to the test samples that was used, the test procedure that was applied and the assumptions that were made for a study when its results are compared to the results of another.

The biomechanics can therefore be based on *in vitro* or *in vivo* measurements. Parameters can be directly derived from the experimental data but some parameters are derived from empirical models. The results are then verified with additional experimental data.

### **2.3 Solution techniques for mathematical models**

In the biomedical field, mathematical models are used to describe the behaviour and function of a system inside the human body (Komistek *et al.*, 2005). The utilised mathematical model will normally have limitations in its application since it will only approximate a response to a defined condition, i.e. stress response of a tendon to a step increase in strain (Meyer, 2003). These models are normally indeterminate and numerical solution techniques should be applied to solve the model unknowns.

Optimisation techniques are used when the governing equation(s) of the mathematical model can be rewritten as an objective function,  $f(x)$ , where  $x$  represents the model unknowns. After the objective function has been derived and equality constraints and inequality constraints as well as bounds for the model unknowns have been derived, the objective function is optimised by means of a suitable optimisation algorithm, e.g. Newton's method. The choice of a proper cost function is critical since it will determine the kind of optimisation algorithm that will work best. Optimisation techniques have been applied by Abramowitch *et al.* (2004), Anderson & Pandy (2001), Crowin-

shield (1978), Johnson *et al.* (1994), Piazza & Delp (2001), Seireg & Arvikar (1973a), Seireg & Arvikar (1973b), Toms *et al.* (2002).

Another method that has been utilised is reduction methods (Komistek, Stiel & Dennis, 1998; Lu, O'Connor, Taylor & Walker, 1998; Lu, Taylor, O'Connor & Walker, 1997; Mikosz, Andriacchi & Anderson, 1988; Schipplein & Andriacchi, 1991). The logic of this technique is based on the fact that some muscles do not influence the system significantly when a specific motion path of a joint is modelled (Komistek *et al.*, 2005). When reduction methods are applied, elements that play an insignificant role are ignored or grouped together. The model is then reduced to a determinate set of equations.

There is need for caution when one of the abovementioned techniques is used. Although the results obtained with an optimisation technique or a reduction method may be mathematically correct, it will not necessarily be physiologically correct. The mathematical results therefore need to be verified against experimental results.

## **2.4 Force and strain transducers used in biomechanical studies**

The need for the measurement of muscle, ligament and tendon loads or elongations in biomechanical studies has led to the development of application specific transducers. Muscle loads are recorded via electromyography (EMG) whereas many types of transducers exist that can be used in the recording of ligament or tendon loads. The latter can be divided into three groups namely transducers that work on the principle of variation of electrical resistance, variation of magnetic fields or light intensity modulation (Ravary *et al.*, 2004).

There are also more advanced transducers that have been used before which fall in different categories. Examples of these are the application of photoelasticity (Yamamoto, Hirokawa & Kawada, 1998) and ultrasound (Hansen *et al.*, 2006) in the measurement of connective tissue loads or strains. For the purposes of this study, only the conventional transducers were considered, the reason being that these have been most widely applied. In the remainder of this section the working principle and examples as well as the main advantages and disadvantages for each category will be presented. For more information on these transducers, the reader is referred to the review of Ravary *et al.* (2004).

The Hall-effect transducer is an example of a transducer that is based on the variation of a magnetic field. This transducer consists of a magnetic core that slides inside a steel tube connected to a Hall generator. The opposing ends of the core and tube are fixed to the connective tissue in a proximal/distal direction. When the connective tissue elongates, the magnetic core translates relative to the steel tube. The voltage output from the Hall generator changes and the change is proportional to the magnitude of the connective tissue's elongation. The transducer is effective and accurate over short distances. The installation cost for the transducer is expensive and the transducer is maximally invasive, which will lead to prolonged recovery periods.

Liquid metal strain gauge (LMSG's), a transducer that is based on the variation of electrical resistance, consists of soft polymer capillaries that are filled with a liquid metal at room temperature. The capillary ends are closed with platinum wire onto which lead wires are soldered. The liquid metal resistance is proportional to the liquid metal temperature and capillary length and indirect proportional to the capillary cross-section. When the LMSG is inserted into the connective tissue, it is fixed to the connective tissue's fibres in a proximal/distal direction. As the connective tissue's fibres are strained, the LMSG's length and cross section change, which lead to a change in resistance. The LMSG has a constant current supply and therefore the change in resistance will lead to a change in the voltage output that represents the magnitude of the connective tissue's strain.

LMSG's are small in size and will have a small influence on the orientation of the connective tissue fibres. The transducers are hazardous due to the toxic liquid metal and care should be taken when inserting it into the ligament or tendon. The service life of the transducer is limited and the transducer's output is temperature dependent.

Buckle transducers, implantable force transducers and pressure transducers are also examples of transducers that work on the principle of varying electrical resistance. These transducers are inserted into the tendon or ligament in such a way that the normal orientation of the tendon or ligament fibres is disturbed. When the ligament or tendon is then loaded, the disturbed fibres tend to return to their original orientation, causing a transverse force to the loading direction being exerted onto the transducer. A strain gauge is fitted to the transducer in such a way that it measures the strain resulting from the transverse force. The transverse force is proportional to the tensile load in the connective tissue according to Poisson's ratio. A buckle transducer and an implantable

force transducer are shown in Figure 6. Pressure transducers are modified commercial pressure transducers with a Teflon button fitted onto the diaphragm.

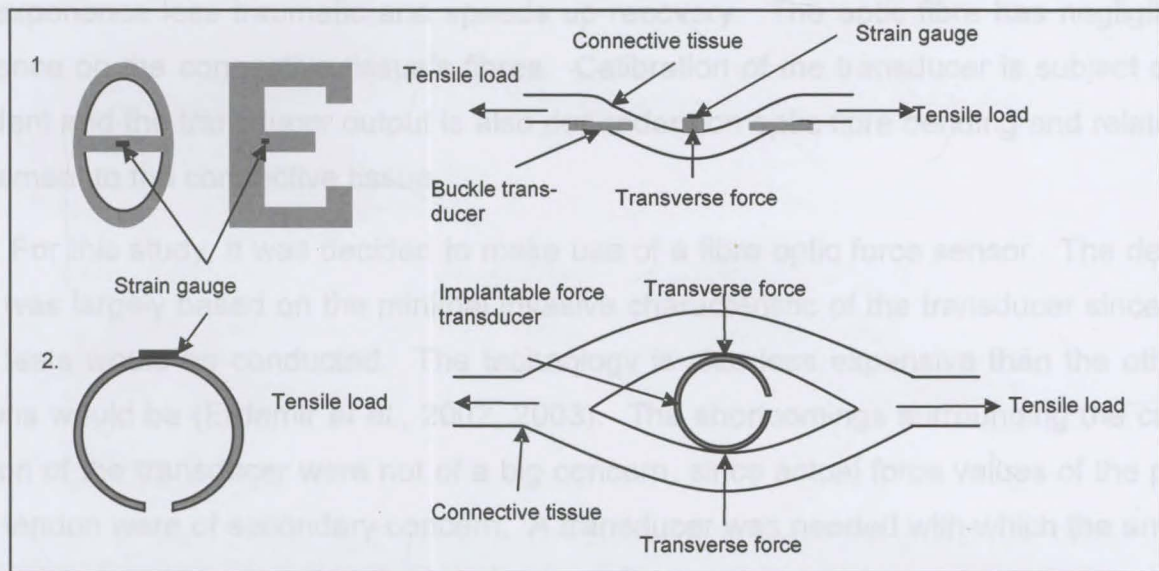


Figure 6: 1. Buckle transducers and the insertion of a buckle transducer into a ligament or tendon. 2. Implantable force transducers and insertion of an Implantable force transducer into a ligament or tendon.

Adopted from Ravary *et al.* (2004).

Buckle transducers, implantable force transducers and pressure transducers are rigid and small in size, but still have a noticeable effect on the normal orientation of the connective tissue's fibres. The transducers are easy to manufacture and are also commercially available. There is a risk of possible impingement onto the bone when these transducers are used, and this together with the maximal invasive nature of these transducers, will lead to prolonged recovery periods. Calibration of the buckle transducer can be standardised, but the calibrations of the implantable force transducer and pressure transducer are subject dependent.

Optic fibres consist of a core through which a light signal propagates and a cladding material, which induces internal reflection of the light signal into the core and covers and protects the core. Light propagation through the optic fibre is dependent on the geometry as well as the properties of the optic fibre, as will be discussed in the next section. Therefore, it is possible to manipulate the output from the fibre optic system, by means of modifying the geometry of the optic fibre. If the optic fibre is inserted through the cross section of the ligament or tendon, the transverse force will cause the geometry to deform, which will induce a change in the output signal that represents the tensile load.

These types of transducers are easy to implant since they are minimally invasive and only the optic fibre need to be inserted through the ligament or tendon. This makes the experience less traumatic and speeds up recovery. The optic fibre has negligible influence on the connective tissue's fibres. Calibration of the transducer is subject dependent and the transducer output is also dependent on optic fibre bending and relative movement to the connective tissue.

For this study, it was decided to make use of a fibre optic force sensor. The decision was largely based on the minimal invasive characteristic of the transducer since *in vivo* tests would be conducted. The technology is also less expensive than the other options would be (Erdemir *et al.*, 2002, 2003). The shortcomings surrounding the calibration of the transducer were not of a big concern, since actual force values of the patella tendon were of secondary concern. A transducer was needed with which the anterior and the posterior loads in the proximal patella tendon could be compared. In order to be able to do this, the raw transducer output would be sufficient.

## **2.5 Fibre optic technology**

A fibre optic system consists of a transmitter unit, a receiver unit, the two unit's driver circuit and a communication channel (optic fibre) that connects the two units to one another. It is normally used for the quick transfer of information over relatively short distances. Information enters the fibre optic system as a voltage signal and is converted into an electromagnetic wave in the near visible light region (transmitter unit) for transmission through an optic fibre. On the other end of the optic fibre the receiver unit senses the transmitted light and converts it back to a voltage signal. This information is then ready for output from the fibre optic system. In this section the fundamental principles of the physics surrounding the transmission of a light signal through the optic fibre is explained.

When a light signal propagates through the core, it will strike the core/cladding interface sooner or later. The light ray will then either undergo total internal reflection (Figure 7.1) or it will disperse into the cladding material leading to communication losses (Figure 7.2). A combination of reflection and dispersion is also possible (Figure 7.3). The former is desirable for successful transmission and it is dependent on two factors: the angle of incidence on the core/cladding interface, and the refractive indexes of the core and the cladding material.

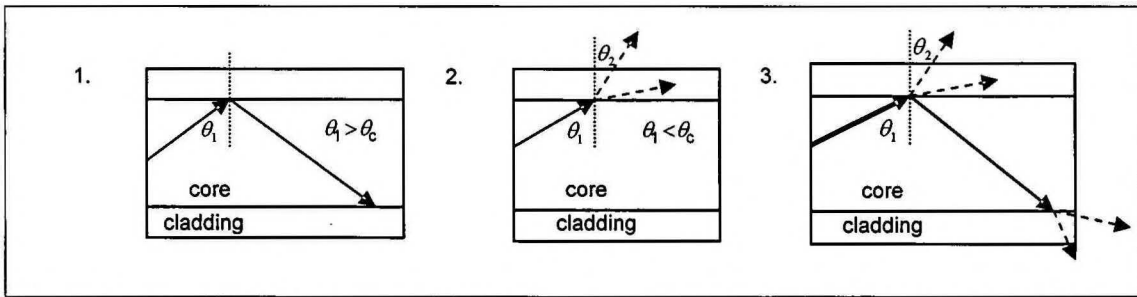


Figure 7: Illustration of the possibilities when a light ray strikes the core/cladding interface.

A materials refractive index,  $N$ , is defined as the ratio of the speed of light in a vacuum,  $c$ , to the speed of light in the material,  $V$ , as (Bailey, 2003)

$$N = \frac{c}{V} \quad \text{Equation 1}$$

A core with a higher refractive index than that of the cladding, will lead to a greater percentage of the incident light being internally reflected. As the angle of incidence is increased, the angle of refraction grows until it is equal to  $90^\circ$ . The critical angle refers to the angle of incidence at which the angle of refraction is equal to  $90^\circ$  as is depicted in Figure 7. An angle of incidence greater than the critical angle will result in total internal reflection of the incident light signal.

The main purpose of fibre optic systems is the sufficient transfer of information between two distant points. Losses due to diffraction are therefore undesirable. Successful operation of the sensor on the other hand is dependent on induced losses in the fibre optic system as will be discussed in the next chapter. Chapter 3 will introduce the hardware that was used.



## Chapter 3: Hardware and software

### 3.1 Fibre optic force sensor

#### 3.1.1 Working principle

In the previous chapter the principles of refraction and internal reflection was discussed on the basis of the incidence angle and the core and cladding material's refractive indexes. During the operation of the sensor, of these two, only the angle of incidence can be modified and this is achieved through the mechanical modification of the optic fibre's geometry. The light intensity that is sensed by the receiver unit is indirect proportional to the amount of light rays that refract into the cladding material of the optic fibre. The sensor's output can therefore be modified by changing the angle of incidence of the incident light (deformation of the optic fibre geometry) to induce incidence angles smaller than the critical angle.

The deformations that alter the angle of incidence can be subdivided into macro-bends and micro-bends (Bailey, 2003). Figure 8 and Figure 9.1 illustrates how a macro and a micro-bend will alter the incidence angle. Macro-bends are associated with bends having radii typically ten times that of the optic fibre's diameter while micro-bends result from imperfections in the cladding material or ripples in the core/cladding interface or tiny cracks in the optic fibre (Bailey, 2003). An external applied load on the optic fibre surface will also induce a micro bend, as is shown in Figure 9.2.

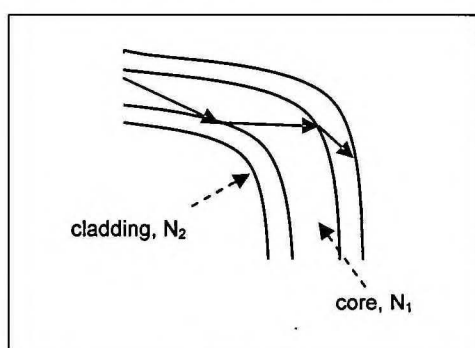


Figure 8: Illustration of a macro bend

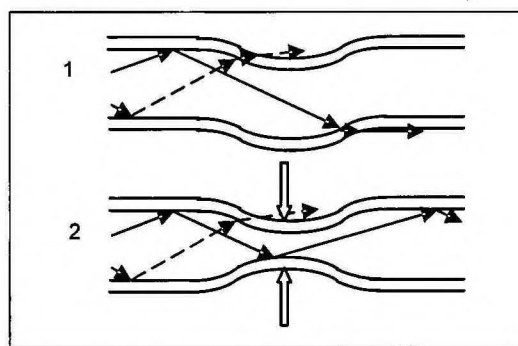


Figure 9: 1. Illustration of a micro bend. 2. Illustration of a micro bend induced by an external load.

The sensor's working principle is therefore based on light intensity modulation through the mechanical deformation of the optic fibre's geometry. The mechanical deformation is caused by an external force that is exerted onto the optic fibre. If the exter-

nal force is increased, the effect of the micro bend on the sensor output becomes more prominent. In other words, a larger external force will result in a lower sensor output since more light rays will refract into the cladding material. The aim therefore is to insert the optic fibre into the connective tissue in such a way that the induced loads inside the connective tissue will induce a micro-bend. In order to achieve this, the mechanics of connective tissue need to be considered more closely.

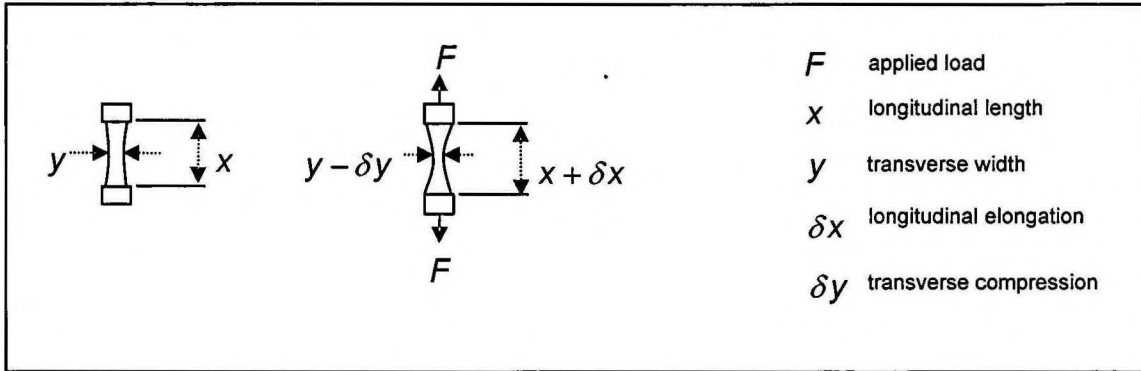


Figure 10: Elongations that result from tensile loading

When the connective tissue is loaded, its fibres are strained along the loading direction and along the transverse direction as is illustrated in Figure 10. Poisson's ratio,  $\nu_{Poisson}$ , relates this longitudinal strain,  $\epsilon_x$ , and the transverse strain,  $\epsilon_y$ , through (Shigley & Mischke, 2001)

$$\nu_{Poisson} = -\frac{\epsilon_y}{\epsilon_x}$$

where Equation 2

$$\epsilon_x = \frac{\delta X}{X_0} \text{ and } \epsilon_y = \frac{\delta y}{y_0}$$

Since connective tissue are viscoelastic, the strain is both a function of the induced stress,  $\sigma$ , and time,  $t$ . The stress,  $\sigma_x$  and  $\sigma_y$ , inside the connective tissue can be related to the strain,  $\epsilon_x$  and  $\epsilon_y$ , through the connective tissue's modulus,  $E_x$  and  $E_y$ , as

$$\sigma_x = E_x \epsilon_x \text{ or } \sigma_y = E_y \epsilon_y \quad \text{Equation 3}$$

By substituting Equation 3 into Equation 2, the compressive stress  $\sigma_y$  can be mathematically related to the tensile stress,  $\sigma_x$ , as

$$\sigma_y = \frac{E_y}{E_x} \nu_{Poisson} \sigma_x \quad \text{Equation 4}$$

If the optic fibre is passed through the connective tissue in a direction normal to the loading direction, the compressive stress will induce a micro bend in the optic fibre. Since the compressive stress is proportional to the tensile stress as is shown through

Equation 4, the sensor output will be indirect proportional to the tensile stress. An increase in the tensile stress will result in an increase in the compressive stress that will lead to a decrease in the sensor's output.

Erdemir *et al.* (2002, 2003) reported a non-linear relationship between the sensor output and the applied compressive load. These findings contradict the results of Finni *et al.* (1998) who reported a linear relationship. Hysteresis effects as well as the difference in loading rate during calibration and measurement have however not been investigated thoroughly by Finni *et al.* (1998).

### 3.1.2 Composing elements

The sensor comprise of a pair of transmitter units, a pair of receiver units, two pieces of optic fibre that connect the transmitter and receiver units through ST-connectors and a driver circuit. A schematic presentation of the sensor's driver circuit is shown in Figure 11. The voltage input to the transmitter unit and the receiver unit was supplied by 9 V batteries that drove voltage regulators (LP2951, National Semiconductor). The voltage regulator output was governed by capacitor, C1, to give a 5 V output signal.

The transmitter driving circuit consisted of the transmitter unit (HFBR 1414T, Agilent Technologies Inc.), the voltage supply circuit and resistors R1 and R2. Resistor R1 governed the maximum current in the transmitter circuit while variable resistor R2 gave the possibility of varying the transmitted light intensity. The receiver driving circuit consisted of the receiver unit (HFBR 2416T, Agilent Technologies Inc.), the voltage supply circuit, an instrumentation amplifier (AD620, Analog Devices Inc.) and a passive low pass filter. The variable resistor, R3, varied the DC offset of the output signal (pin 2) to ensure that it fell within the range of the A/D converter. Amplification of the output signal was not necessary. The low pass filter was designed to have a cut-off frequency of 16 Hz, since testing frequencies would initially not go beyond 10 Hz.

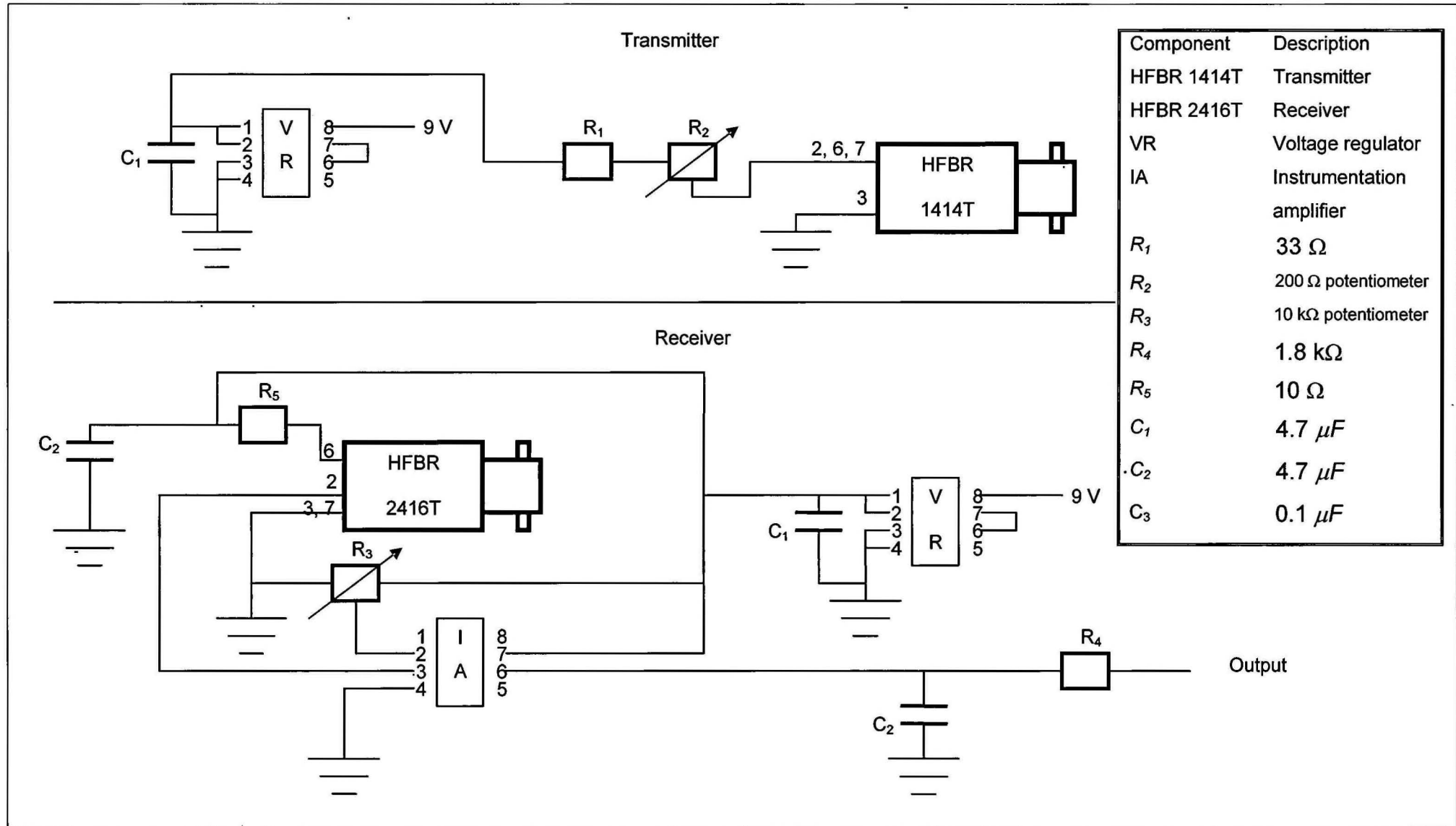


Figure 11: Schematic of the driving circuit for the sensor.

### **3.2 Data acquisition**

The data acquisition strategy entailed the following: Sensors that were used during the project were connected to a PC through an USB based I/O module (PMD-1608FS, Measurement Computing). This device has eight 16-bit single-ended analogue channels. Each channel has its own A/D converter and all channels could be scanned simultaneously during data sampling. The sensors connected to this device through BNC cables.

Data acquisition was performed with a customised LabVIEW application (LabVIEW 7.1) that consisted of universal libraries that was supplied with the USB based I/O module. The amount of channels that need to be scanned on the module, the amount of required data points, the sampling frequency and the voltage range in which the sampled data fell were specified by the user. After data collection of each trial, all the sampled data was exported to a \*.txt file from where it could be loaded into a post-processing application.

## Chapter 4: Characterisation of the sensor output

### 4.1 Introduction

Although fibre optic force sensors have been used before (Arndt *et al.*, 1998; Finni *et al.*, 2000, 1998) it is subjected to significant error. Erdemir *et al.* (2002, 2003) examined different phenomena that lead to erroneous force recordings with a sensor similar to the one that was used during this project. Hysteresis error, varying loading rates between calibration and experiments as well as loading at different locations along the optic fibre were investigated.

These parameters were based on the force recordings with the optic fibre inserted through an Achilles tendon complex inside a materials testing machine. The Achilles tendon was loaded at different loading rates, i.e. 20 N/s, 200 N/s and 1000 N/s, from 0 N to a maximum load of 1000 N. The discussion in Chapter 3 showed that the sensor's output is influenced by a compressive transverse load that can be related to the tensile load through Poisson's ratio and the modulus of the connective tissue.

Values of the Poisson ratio for connective tissue are not widely published though. Hewitt, Guilak, Glisson & Vail (2001) conducted a study on the hip joint ligaments and determined a Poisson value of  $\nu_{Poisson} = 1.4$  ( $SD = 0.8$ ,  $n = 10$ ). It was also stated in Chapter 2 that there exists significant variability in the published results on biomechanical parameters. The lack and uncertainty of biomechanical properties of connective tissue (Woo *et al.*, 1999) therefore render it an unsuitable testing medium when the sensor's behaviour needs to be considered. It is unfortunately difficult to simulate the loading mode of connective tissue with another test medium.

In this chapter the behaviour of the sensor was investigated by means of three test set-ups:

- A hydraulic press loading test
- An *in vitro* patella tendon loading test
- An *in vivo* patella tendon loading test

## 4.2 Hydraulic press loading test

### 4.2.1 Introduction

A hydraulic press was used to apply pressure on a segment of the optic fibre that was connected to the sensor. This setup had the following advantages above the *in vitro* and *in vivo* setup. The applied load on the optic fibre was measurable and its magnitude was controllable, which led to repeatable loading conditions. This was not achievable with the *in vitro* or *in vivo* setup because of the uncertainty and unavailability of the biomechanical properties of connective tissue. It is for instance difficult to quantify the hysteresis effect in the sensor recordings since connective tissue is viscoelastic.

The hydraulic press loading test was based on two tests. The optic fibre's hysteresis effect, signal-to-noise ratio and frequency response were typified from the force measurements taken during a sequential test. The static sensitivity and measurement repeatability of the two channels were derived from force measurements taken during a random test.

### 4.2.2 Hardware setup

A schematic of the hardware setup for the hydraulic press loading test is shown in Figure 12. The transverse compressive force that results when connective tissue is tensioned was simulated by the piston of the hydraulic cylinder (1) that pressed onto the optic fibre inside the hydraulic press. A servo valve (Moog Inc. Jamison Rd. East Aurora, NY 14052, 02-307a; 2) regulated the fluid pressure to the cylinder and governed the magnitude of the applied force on the optic fibre. The servo valve's solenoid received a control signal from a V/I driver that was connected to a PID controller (3).

The PID controller had two reference inputs and one feedback input. A variable resistor (single turn 10 k $\Omega$  potentiometer; 4) regulated a voltage signal from a DC power supply (Dual tracking DC power supply, 6306D, Topward Electric Instruments CO., LTD.; 5) that was used as the reference signal for DC load control. A signal generator (723963, Topward Electric Instruments CO., LTD.; 6) generated a sinusoidal signal which was used as a reference signal for AC load control. The feedback signal was supplied by a loadcell (506335-04, Revere Transducers Inc.; 7) in the hydraulic press whose output was amplified by a full bridge amplifier (KWS 0373, HBM; 8).

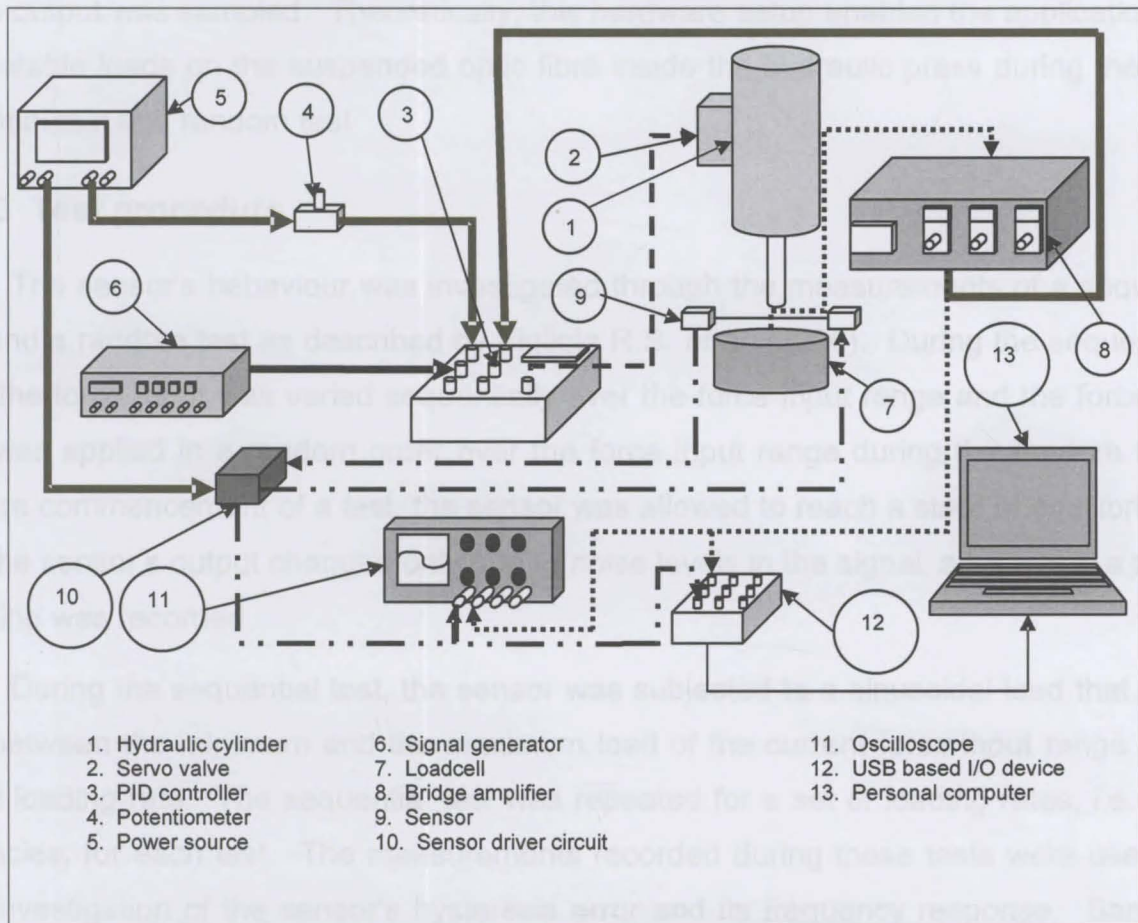


Figure 12: Schematic of the hydraulic press test hardware setup.

Figure 13 illustrates how the sensor (9) was mounted inside the hydraulic press. The optic fibre was compressed between two polished metal plates. The first plate rested on top of the suspended optic fibre and the second plate rested on top of the loadcell. The hydraulic cylinder pressed down onto the first polished plate.

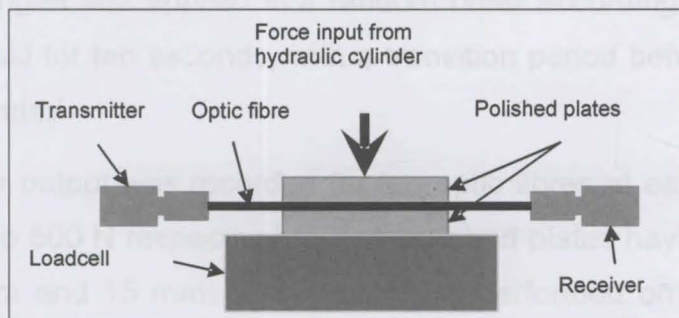


Figure 13: Suspension of the optical fibre in the hydraulic assembly

An oscilloscope (TDS 2014, Tektronix Inc.; 11) was used to show the control signals and the sensor output during the experiment. Data acquisition was done with the system described in Chapter 3 (12: USB based I/O module, 13: Personal computer (Intel(R) Pentium 4, CPU 2.8 GHz, 496 MB RAM)). Only the loadcell's output and the sen-



sensor's output was sampled. Theoretically, this hardware setup enabled the application of repeatable loads on the suspended optic fibre inside the hydraulic press during the sequential test and random test.

### 4.2.3 Test procedure

The sensor's behaviour was investigated through the measurements of a sequential and a random test as described by Figliola R.S. *et al.* (2006). During the sequential test the force input was varied sequentially over the force input range and the force input was applied in a random order over the force input range during the random test. Before commencement of a test, the sensor was allowed to reach a state of equilibrium, i.e. the sensor's output changed only due to noise levels in the signal, after which a zero reading was recorded.

During the sequential test, the sensor was subjected to a sinusoidal load that varied between the minimum and the maximum load of the current force input range at a fixed loading rate. The sequential test was repeated for a set of loading rates, i.e. frequencies, for each test. The measurements recorded during these tests were used in the investigation of the sensor's hysteresis error and its frequency response. Sample times were chosen for each trial to contain at least ten cycles when the sampling rate was 100 Hz.

After completion of the sequential test trials, the random test followed. The current force input range was divided into ten equal intervals to form ten sub loads. These sub-loads were arranged and applied in a random order according to the hat method<sup>iv</sup>. A sub-load was held for ten seconds, with a transition period between the sub-loads lasting twenty seconds.

The sensor output was recorded for ten optic fibres at each input range of 0 N to 250 N and 0 N to 500 N respectively. Two polished plates having different widths were used, i.e. 20 mm and 15 mm. Ten trials were performed on the one channel with a force input range of 0 N to 500 N and a polished plate with a width of 15 mm. All other tests were conducted with the 20 mm polished plate.

---

<sup>iv</sup> Each state is assigned a number. The numbers are thrown into a hat and then taken out one by one to form a random sequence of numbers.

## 4.2.4 Data processing

The aim of the sequential tests was to obtain a value of the maximum hysteresis error for the sensor in the applied loading ranges as well as a signal-to-noise ratio and the frequency response of the sensor. Measurements from the sequential test were also used in the calculation of the force prediction error in terms of a RMS error when a straight line was fitted through the cyclic measurements. The processing procedure can be divided into a pre-processing stage and a processing stage, as shown in Figure 14.

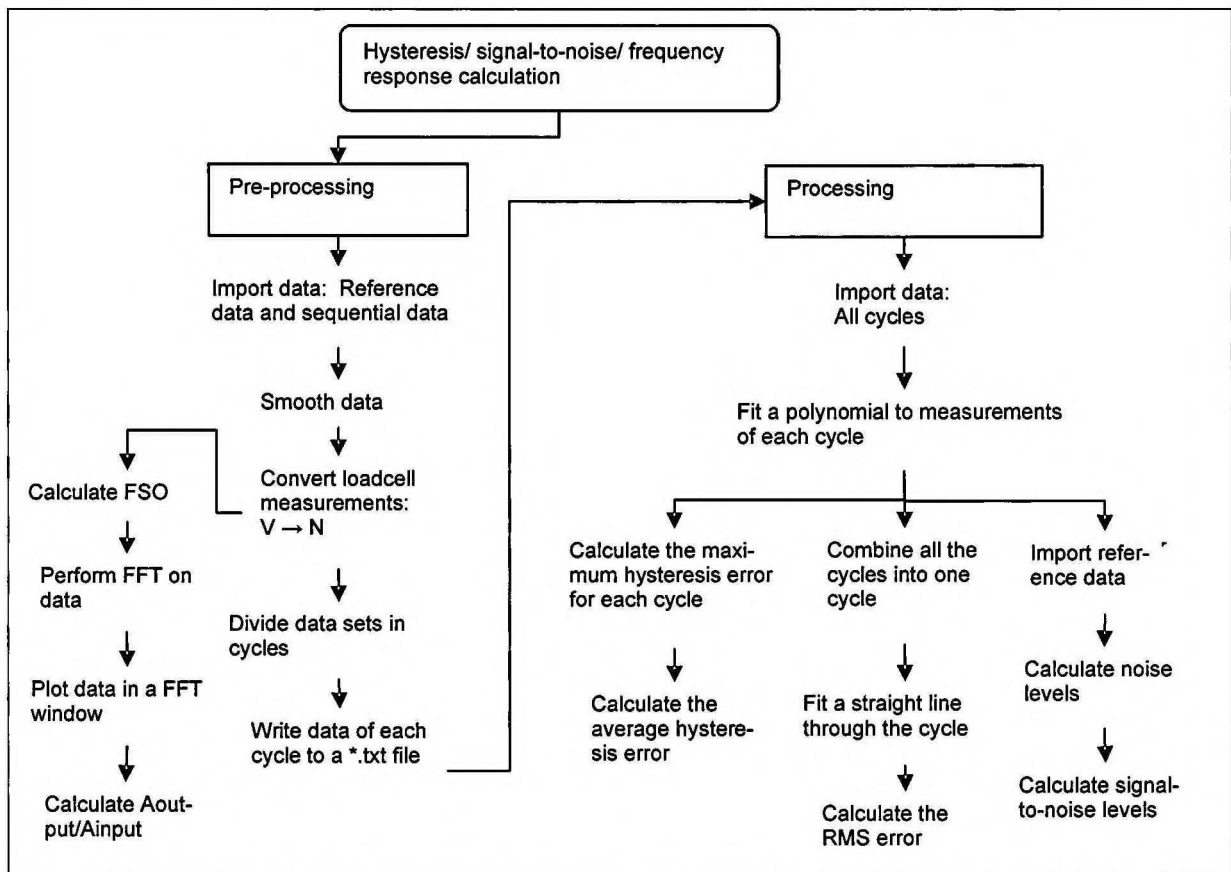


Figure 14: Hydraulic press loading test: data processing of sequential test recordings

During the pre-processing stage, each trial's measurements were imported into Matlab (Version 7.0.1.24704 (R14)) and smoothed to minimise the effect of noise by applying a moving average (10 points). The loadcell's voltage output was converted to its corresponding force output, i.e. voltage values to Newton values.

Before the sensor's frequency response could be calculated, the sensor's full scale output (FSO) was calculated by subtracting the force output from the reference measurements, i.e. the zero load recordings. After the FSO was calculated, the N-point one-sided absolute value FFT of the sensor signal and loadcell signal were calculated. A preliminary investigation showed that 10 cycles per sample gave good results. The

peak output in the FFT that contained the output from the loadcell, was inspected to see whether it corresponded with the peak output in the FFT that contained the sensor output. The peak sensor output,  $A_{output}$ , was divided by the corresponding loadcell value,  $A_{input}$ , to give the ratio  $A_{output}/A_{input}$ . This ratio was calculated for both the 0.1 Hz and the 1 Hz test. The calculated ratios were combined with the predictions of the static calibrations as will be shown in the results.

After the calculation of the frequency response, each trial's sensor recordings and loadcell recordings were subdivided into sub-cycles with a sub-cycle containing a loading and an unloading phase as is illustrated in Figure 15.

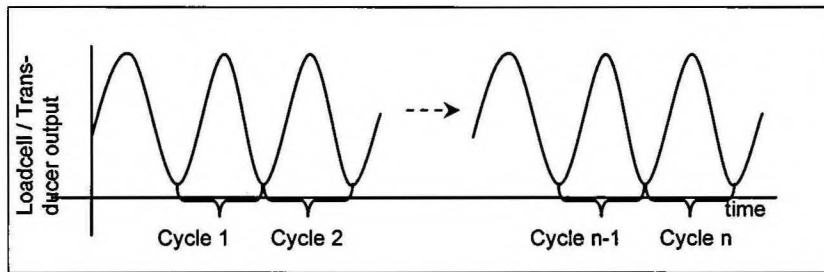


Figure 15: Subdivision of cycle into sub-cycles

The sub-cycles were separated into its loading phase and unloading phase and polynomials were fitted to the two phases with Matlab's *polyfit*-function. The *polyfit*-function, based on a least squares method, provided the means of determining the quality of the polynomial fit to the recorded data in terms of the error made in subsequent predictions. The best polynomial fit was chosen by comparing the maximum errors made by polynomials of different degrees fitted to the data.

After the data was processed into the sub-cycles, the hysteresis error,  $e_{h_{max}}$ , could be calculated in terms of the FSO,  $r_0$ , according to (Figliola *et al.*, 2006)

$$\%e_{h_{max}} = \frac{|y_{i, \text{up scale}} - y_{i, \text{down scale}}|_{\max}}{r_0} \times 100 \quad \text{Equation 5}$$

The sensor recordings for the unloading phase,  $y_{i, \text{down scale}}$ , were subtracted from the corresponding sensor recordings for the loading phase,  $y_{i, \text{up scale}}$ . Equation 5 was applied on every cycle of every trial. The average values of the trials were then calculated and taken as the average hysteresis error for that input range and sensor channel, i.e. the anterior channel or posterior channel.

The RMS error was calculated by fitting a straight line through the combination of the loading and unloading measurements for each cycle. The root mean square on the

difference of the prediction of the straight line,  $y_{c,i}$  and the actual measurement,  $y_i$ , was then computed as (Erdemir *et al.*, 2002)

$$\text{RMS} = \sqrt{\sum_{i=1}^n (y_{c,i} - y_i)^2} \quad (n = \text{amount of samples}) \quad \text{Equation 6}$$

The reference measurements of each test were used in the calculation of the signal-to-noise ratio, S/N. The reference measurements were scanned for the maximum deflection. Because the sensor was unloaded when the reference measurements were taken, the maximum deflection would correspond to noise in the signal and drift in the output signal. In order to avoid a situation where the drift was mistaken for noise, only local deflections were calculated. This was done by searching for a maximum deflection in small blocks having user defined sizes in the output signal. The signal-to-noise ratio was based on the maximum noise level,  $V_s$ , and the FSO,  $V_n$

$$\text{S/N} = 20 \log_{10}(V_s / V_n) \quad \text{Equation 7}$$

Sources of noise could primarily be attributed to electrical noise from the electric motor in the power pack of the hydraulic cylinder.

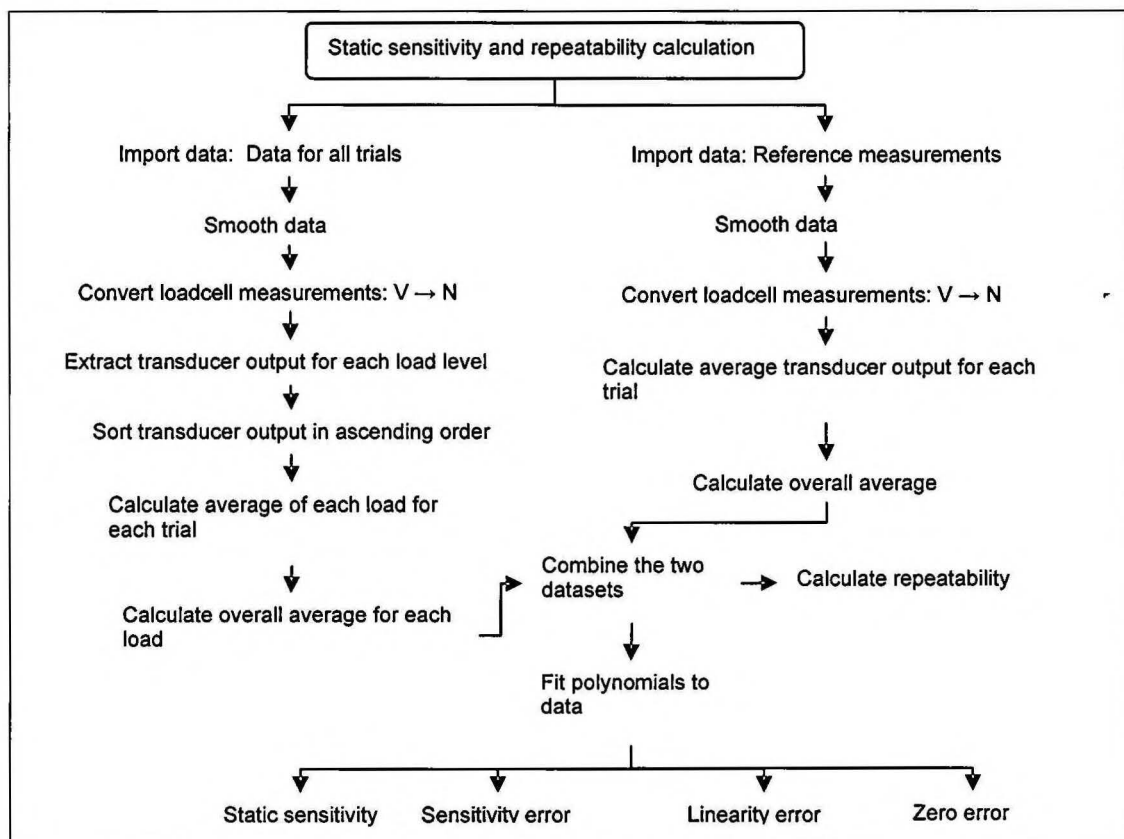


Figure 16: Hydraulic press loading test: data processing of random test recordings

The recordings from the random tests were used to obtain calibrations from which the sensor's static sensitivity and the repeatability of force measurements were calcu-

lated. The data processing procedure on the random test recordings are shown in Figure 16.

Each random trial's recordings as well as the corresponding reference measurements were imported into Matlab. The signals were smoothed and the loadcell's voltage output was converted to force output using the same methods that were described earlier. Since the sub-loads were applied in a random order, it needed to be extracted and organised sequentially. The force measurements for each sub-load were averaged. Each trial's sub-loads were combined with the reference measurements to form one vector and polynomials were fitted to the data with Matlab's *polyfit*-function. Based on these polynomial fits, the static sensitivity of the two channels and the repeatability of the sensor could be calculated.

The average static sensitivity of the sensor was calculated from the average value of the first derivative of each polynomial fit. The sensor's repeatability,  $\%e_{R_{\max}}$ , which is based on the standard deviation of the sensor output,  $S_x$ , and the FSO  $r_0$ , was calculated with (Figliola *et al.*, 2006)

$$\%e_{R_{\max}} = \frac{2S_x}{r_0} \times 100 \quad \text{Equation 8}$$

The linearity error, static sensitivity, sensitivity error and zero error were calculated for the calibrations. The linearity error,  $e_{L_{\max}}$ , was calculated in terms of the FSO of the loadcell,  $r_0$ , by subtracting the measured loadcell output,  $y_i$ , from the corresponding value predicted by the polynomial fit,  $y_{c,i}$  (Figliola *et al.*, 2006)

$$\%e_{L_{\max}} = \frac{|y_i - y_{c,i}|_{\max}}{r_0} \times 100 \quad \text{Equation 9}$$

The linearity error,  $e_{L_{\max}}$ , provided a measure that described the maximum error that occurred for the current polynomial fit. The standard error of the polynomial fit,  $S_{yx}$ , was calculated with (Figliola *et al.*, 2006)

$$S_{yx} = \sqrt{\frac{\sum_{i=1}^n (y_i - y_{c,i})^2}{\nu}} \quad \text{Equation 10}$$

and was based on the summation of the squared error,  $\sum_{i=1}^n (y_i - y_{c,i})^2$ , between the actual measurements,  $y_i$ , and the predictions of the polynomial,  $y_{c,i}$ , divided by the degrees of freedom,  $\nu$ . The degrees of freedom,  $\nu$ , depends on the amount of measurements,  $n$ , and the order of the polynomial,  $m$ , as defined by (Figliola *et al.*, 2006)

$$v = n - (m + 1) \quad \text{Equation 11}$$

The sensitivity error,  $S_{a1}$ , a statistical measure of the random error in the estimate of the slope of the calibration, can be calculated from the standard error of the polynomial fit,  $S_{yx}$ , and the independent variable,  $x_i$ , on which the calibration is based as (Figliola *et al.*, 2006)

$$S_{a1} = S_{yx} \sqrt{\frac{n}{n \sum_{i=1}^n x_i^2 - (\sum_{i=1}^n x_i)^2}} \quad \text{Equation 12}$$

If the sensitivity is constant, but the zero intercept of the calibration drifts, the zero error,  $S_{a0}$ , can be used to quantify the resulting error as (Figliola *et al.*, 2006)

$$S_{a0} = S_{yx} \sqrt{\frac{n \sum_{i=1}^n x_i^2}{n \left[ n \sum_{i=1}^n x_i^2 - (\sum_{i=1}^n x_i)^2 \right]}} \quad \text{Equation 13}$$

#### 4.2.5 Results

The hysteresis error and the RMS error calculated from the sensor output taken during the sequential tests are shown in Table 1. In Table 2 the hysteresis of the force input from the hydraulic press is shown. The average hysteresis in the loadcell recordings was 9.83%FSO [SD = 2.69] while the average hysteresis in the anterior and posterior channel recordings was 16.7%FSO [SD = 9.10] and 11.2%FSO [SD = 5.05] respectively. If the hysteresis in the anterior channel recordings for the 500 N and 15 mm plate is ignored, the average hysteresis for the anterior channel measurements would be 11.5%FSO [SD = 1.22].

The average RMS error calculated when the straight line was fitted through the anterior channel measurements and the posterior channel measurements were 7.80%FSO [SD = 3.14] and 5.96%FSO [SD = 0.801] respectively. Erdemir *et al.* (2002) obtained an average RMS value of 5%FSO from their *in vitro* Achilles tendon study.

Table 1: Hysteresis error and RMS error for the sensor

Channel	Load, N (plate, mm)	Hysteresis, %FSO	RMS error, %FSO
Anterior (n = 10)	250 (20)	10.6	7.61
	500 (20)	12.4	4.76
	500 (15)	27.2	11.0
Average [SD]		16.7 [9.10]	7.80 [3.14]
Posterior (n = 10)	250 (20)	7.61	5.39
	500 (20)	14.8	6.52
Average [SD]		11.2 [5.05]	5.96 [0.801]

Table 2: Hysteresis of the force input from the hydraulic press

Channel	Load, N (plate, mm)	Hysteresis, %FSO
Anterior (n = 10)	250 (20)	12.1
	500 (20)	7.39
	500 (15)	9.10
Posterior (n = 10)	250 (20)	13.2
	500 (20)	7.37
Average [SD]		9.83 [2.69]

The signal-to-noise ratio obtained for the anterior and the posterior channel for the five different tests are given in Table 3.

Table 3: Signal-to-noise ratio for each channel

Channel	Load, N (plate, mm)	Signal to noise ratio, dB
Anterior (n = 10)	250N (20)	41.23
	500N (20)	51.51
	500N (15)	46.04
Posterior (n = 10)	250N (20)	47.97
	500N (20)	60.45

The frequency response of the sensor was quantified by calculating the ratio of the maximum loadcell output and maximum sensor output as calculated by the FFT of the signals. Samples of the FFT signals are shown in Figure 17 and Figure 18 for the posterior channel when the input was 250 N at 0.1 Hz cycle and 250 N at 1 Hz cycle respectively. Table 4 shows the ratio  $A_{output}/A_{input}$  of the anterior and posterior channel's output and the corresponding loadcell's output in terms of the FSO. The ratios in the static calibration and static sensitivity columns were derived from the static calibrations that were obtained from the random tests recordings.

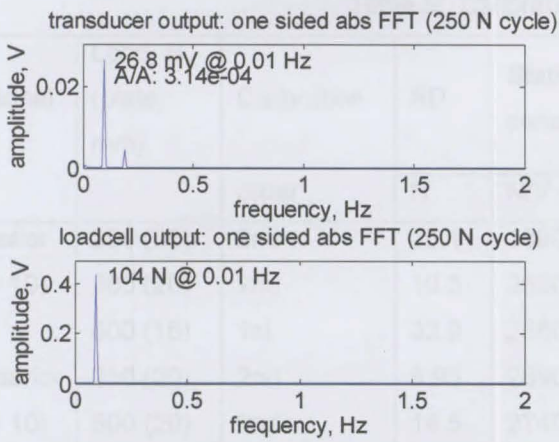


Figure 17: Posterior channel (20 mm plate) - 0.1 Hz cyclic load @ maximum 250 N

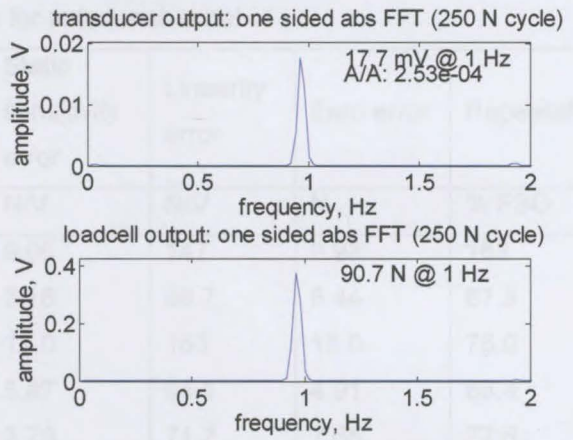


Figure 18: Posterior channel (20 mm plate) - 1 Hz cyclic load @ maximum 250 N

Table 4:  $A_{output}/A_{input}$  for the static calibration, 0.1 Hz cycle and 1 Hz cycle

Channel	Load, N (plate, mm)	Frequency, Hz	Static, V/N	Dynamic, V/N
Anterior (n = 10)	250 (20)	0.1	7.50e-04	1.95e-04
		1	7.64e-04	1.95e-04
	500 (20)	0.1	2.60e-04	1.84e-04
		1	2.60e-04	1.64e-04
Posterior (n = 10)	250 (20)	0.1	3.69e-04	3.22e-04
		1	3.78e-04	2.43e-04
	500 (20)	0.1	3.94e-04	2.79e-04
		1	3.95e-04	2.46e-04
500 (15)	0.1	3.54e-04	3.56e-04	
	1	2.28e-04	1.94e-04	

Table 5 contains the results from the random test for the anterior and the posterior channel and contain only the parameters that are based on the chosen calibrations. In Appendix A the results of all the calibrations for the two channels are shown. The average static sensitivity for the anterior and the posterior channel were 2720 N/V [SD = 213] and 2710 N/V [SD = 149] respectively. The repeatability of force measurements were poor with average values of 102%FSO [SD = 53.2] and 83.1%FSO [SD = 7.50] for the anterior channel and posterior channel respectively.



Table 5: Calibration results for anterior channel

Channel	Load, N (plate, mm)	Calibration order	SD	Static sensitivity	Static sensitivity error	Linearity error	Zero error	Repeatability
			N	N/V [SD]	N/V	N/V	N	% FSO
Anterior (n = 10)	250 (20)	2nd	16.1	1890 [612]	9.06	147	9.93	163
	500 (20)	2nd	10.3	3690 [361]	3.16	69.7	5.44	67.3
	500 (15)	1st	32.9	2580 [206]	13.0	163	18.0	75.0
Posterior (n = 10)	250 (20)	2nd	8.93	2690 [331]	5.87	94.1	4.91	88.4
	500 (20)	2nd	14.5	2740 [154]	3.79	71.7	7.65	77.8

### 4.3 In vitro patella tendon loading test

#### 4.3.1 Introduction

The behaviour of the sensor was examined for the case where the optic fibre was inserted through a patella tendon that was loaded inside a hydraulic press. During the test the effect that two optic fibres in close proximity inside the patella tendon had on the sensor output was investigated. The hysteresis in the sensor recordings was compared to the hysteresis in the recordings of the MTS hydraulic press loadcell and displacement transducer. The signal-to-noise ratio was calculated as well as the static sensitivity of the two channels of the sensor.

#### 4.3.2 Hardware setup

The hardware setup is shown in Figure 19. The test sample consisted of a patella-patella tendon-tibial tubercle complex<sup>v</sup> that was harvested from a amputated human leg (Female, ±80 years old). The bony ends were potted into the cylinders with an epoxy (Epidermix 372, ABE Construction Chemicals (Pty)Ltd.) and the connective tissue exposed to the atmosphere. While the sensor was tested, the connective tissue was constantly hydrated with 0.9% saline as is described by Johnson *et al.* (1994) to prevent the sample from drying out.

<sup>v</sup> The preparation of the patella-patella tendon-tibial tubercle complex is described in Chapter 6.

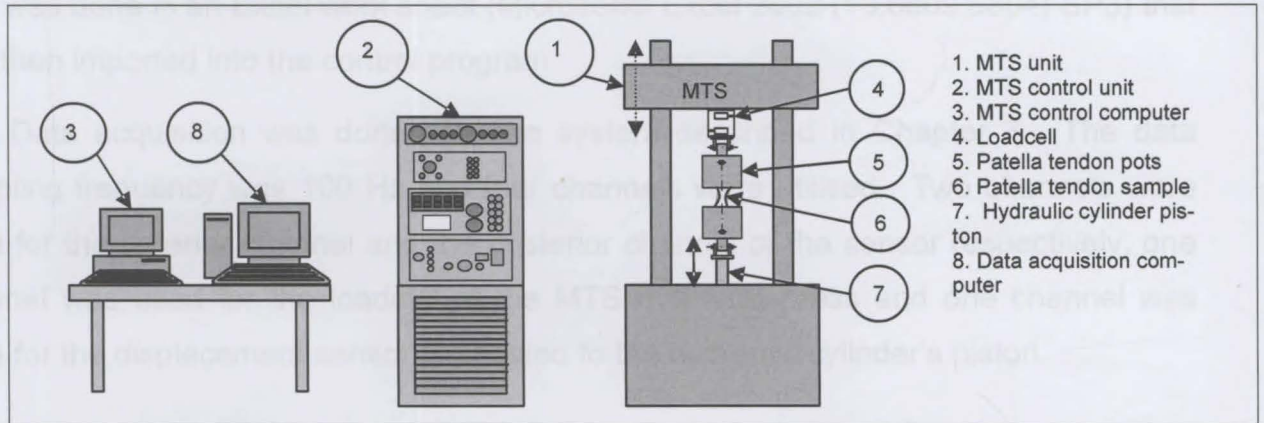


Figure 19: Schematic of the *in vitro* patella tendon study hardware setup

The steel cylinders were attached to clevis clamps and fixed inside the MTS hydraulic press, Figure 20. One clevis clamp was fixed to the piston of the hydraulic cylinder and the other clevis was fastened to the loadcell. The loadcell was fixed to a stationary sleeve, which was adjustable along the guide rods of the MTS hydraulic press. The hydraulic cylinder piston's motion was controlled by a servo valve, whose solenoid was controlled by the MTS control unit that consisted of an MTS 442 Controller, an MTS 425 transducer conditioner and an MTS 413 master control panel.

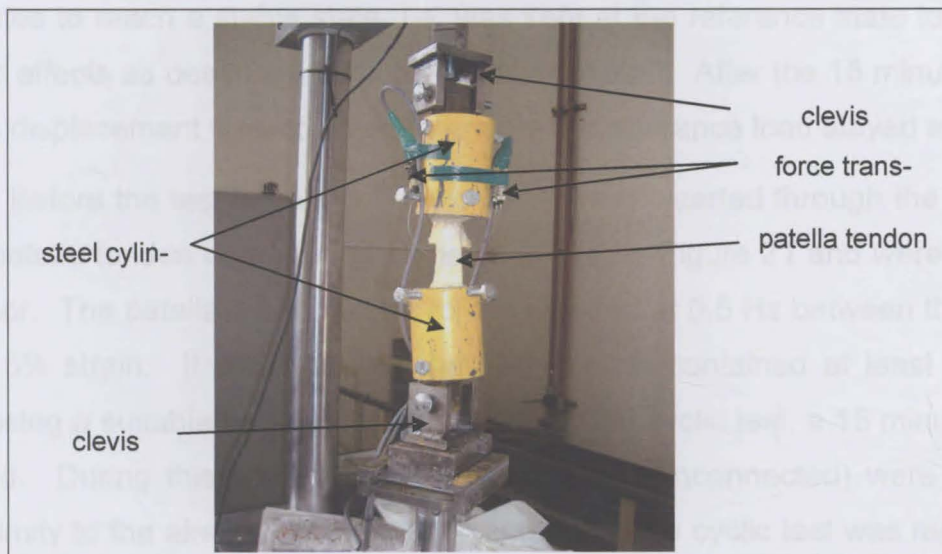


Figure 20: Steel cylinders fixed in MTS hydraulic press

The control strategy was based on displacement feedback control. Input into the control system was supplied by a PC that ran the MTS hydraulic press control program. Four ranges of motion could be chosen on the MTS 442 controller. The sensitivity in terms of V/mm was known for each range of motion and the input and feedback voltage range was 0 V to 10 V. With the sensitivity and the maximum allowed voltage known, the desired motion of the cylinder's piston could be programmed as voltage values.

This was done in an Excel work sheet (Microsoft® Excel 2002 (10.6809.6804) SP3) that was then imported into the control program.

Data acquisition was done with the system described in Chapter 3. The data sampling frequency was 100 Hz and four channels were utilised. Two channels were used for the anterior channel and the posterior channel of the sensor respectively, one channel was used for the loadcell of the MTS hydraulic press and one channel was used for the displacement sensor connected to the hydraulic cylinder's piston.

### 4.3.3 Test procedure

After the patella tendon complex was inserted into the MTS hydraulic press, the patella tendon was manually tensioned to a load level of 12 N by changing the position of the hydraulic cylinder's piston via an offset knob on the MTS 442 controller. The patella tendon's length, depth and width were measured afterwards with a vernier calliper. The patella tendon's cross section was assumed to be rectangular as described by Hashemi *et al.* (2005). To precondition the patella tendon, it was cyclically loaded between the reference state and 2% strain after which the patella tendon was left for 15 minutes to reach a stable state, i.e. was kept at the reference state to minimise viscoelastic effects as described by Johnson *et al.* (1994). After the 15 minute period, the piston's displacement was adjusted to ensure the reference load stayed at 12 N.

Before the test began, two optic fibres were inserted through the mid-substance of the patella tendon in the frontal plane as shown in Figure 21 and were connected to the sensor. The patella tendon was cyclically loaded at 0.5 Hz between the reference state and 5% strain. It was ensured that the sample contained at least twenty cycles by choosing a suitable sampling time. After the first cyclic test, a 15 minute rest period followed. During this time, two extra optic fibres (unconnected) were inserted in close proximity to the already inserted optic fibres and the cyclic test was repeated. The data processing procedure is described in the next section.



Figure 21: Optic fibres inserted through the patella tendon

### 3.3.4 Data processing procedure

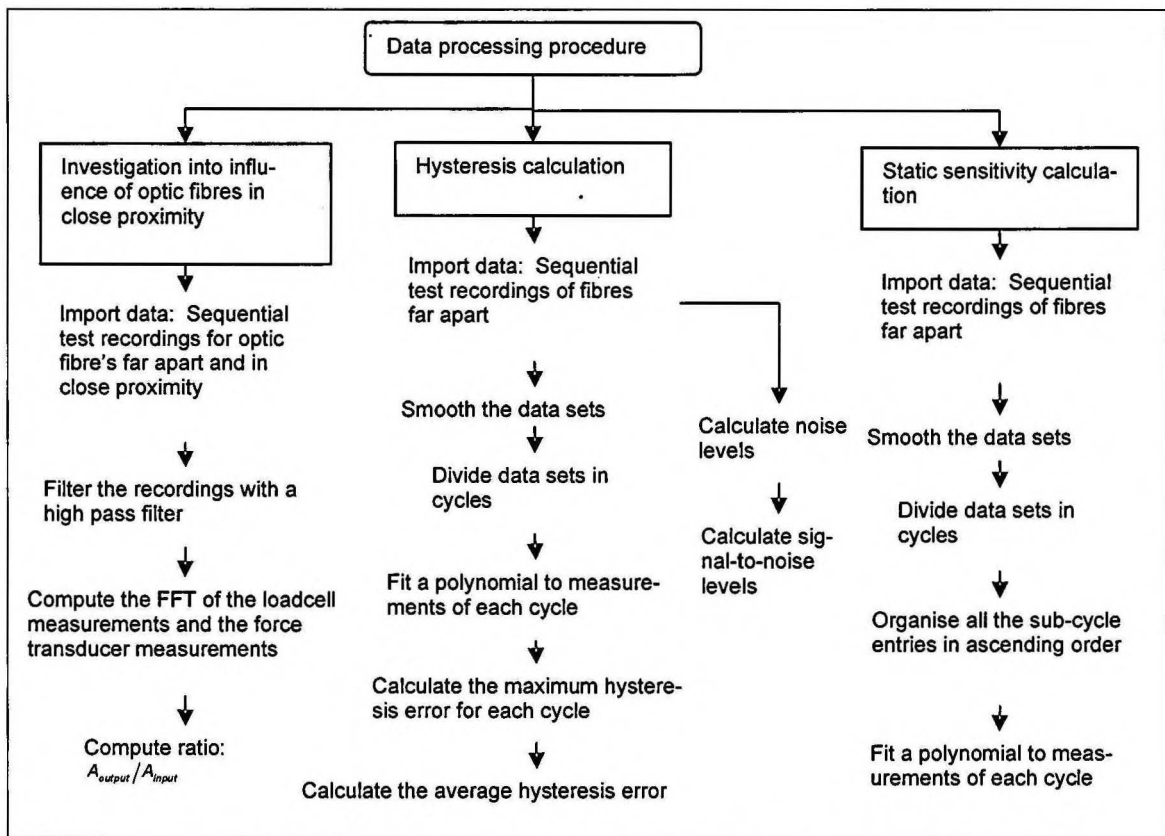


Figure 22: *In vitro* patella tendon loading test: data processing of sequential test recordings

The steps in the data processing procedure are shown in Figure 22. The influence that two optic fibres in close proximity had on the sensor output was investigated through a FFT analysis. The sensor recordings for both instances where the optic fibres were far apart and in close proximity were imported into Matlab. The hydraulic cylinder drifted while the sequential test was carried out. Unfortunately this resulted in a low frequency component (0.01 Hz) in the sensor output. The sensor output and the loadcell output were digitally filtered with a high pass filter to remove this low frequency component. The FFT was then computed for both tests using the same function that was used during the hydraulic press test. From the FFT signals the ratio of the sensor output to the loadcell output was computed.

The hysteresis in the sensor recordings, loadcell recordings and displacement sensor recordings were calculated with Equation 5 and the procedure that was used for the hydraulic press test was repeated. The hysteresis was based on the recordings when the optic fibres were far apart. Another method was implemented to test the qual-

ity of the polynomials that were fitted to the loading and unloading cycles, namely the  $\chi^2$ -test. The  $\chi^2$ -parameter was calculated as (Chernoff *et al.*, 1954)

$$\chi^2 = \sum_{i=1}^k \frac{(y_{c,i} - y_i)^2}{y_i} \quad \text{Equation 14}$$

where  $y_{c,i}$  refers to the polynomial prediction and  $y_i$  refers to the actual test recording. The polynomial that had the smallest  $\chi^2$ -error was automatically chosen. It was found that the same polynomial would be chosen when the error in force prediction as determined by the polyval-function was used. The same method as was used during the hydraulic press test was used in the calculation of the signal-to-noise ratio. The static sensitivity was determined from the derivatives of first to fifth order polynomial fits to the sequential data since a random test was not performed.

### 4.3.5 Results

In Table 6 the FFT results that were obtained for different optic fibre configurations are shown. The ratio,  $A_{output}/A_{input}$ , decreased (12.2%) while the ratio increased (1.66%) when the additional optic fibre was inserted for the anterior and posterior channel respectively. The FFT signals for the different sensors are shown in Figure 23 and Figure 24.

Table 6: FFT results on sensor output for different optic fibre configurations

Optic fibres:	Anterior		Posterior		Loadcell		Anterior	Posterior
	mV	Hz	mV	Hz	mV	Hz	$A_{output} / A_{input}$	$A_{output} / A_{input}$
far apart	6.96	0.490	10.6	0.496	24.7	0.496	0.281	0.429
close proximity	9.81	0.495	17.1	0.495	39.1	0.495	0.251	0.436

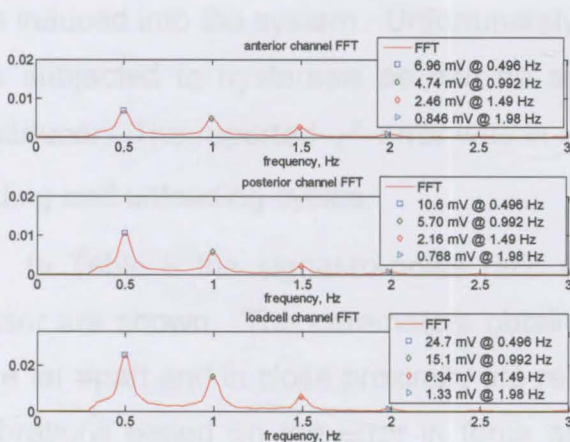


Figure 23: FFT for optic fibres far apart

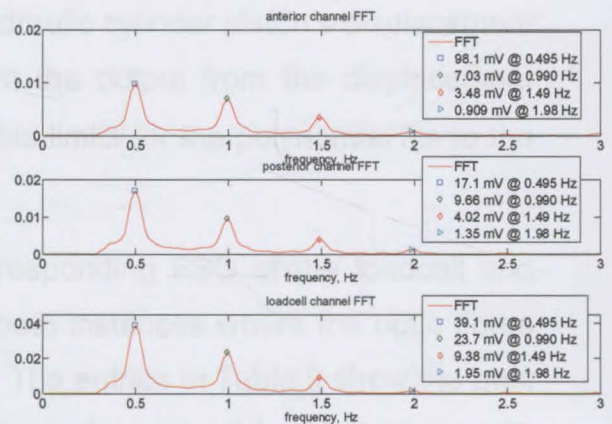


Figure 24: FFT for optic fibres in close proximity

Table 7: Hysteresis in the recordings of the sequential test

Sensor n = 10	Hysteresis %FSO [SD]	FSO V [SD]	$\chi^2_{up\ scale}$ [SD]	$\chi^2_{down\ scale}$ [SD]
Anterior channel	33.6 [8.88]	0.101 [0.00885]	9.37e-6 [2.42e-6]	8.90e-6 [1.84e-6]
Posterior channel	25.7 [7.63]	0.142 [0.0111]	5.47e-6 [1.79e-6]	4.31e-6 [1.23e-6]
Loadcell	15.2 [10.4]	0.331 [0.0152]	4.25e-4 [1.56e-4]	6.44e-4 [1.79e-4]
Displacement transducer	10.7 [7.18]	0.473 [0.0106]	1.17e-6 [1.29e-6]	4.67e-7 [4.03e-7]

Table 8: Signal to noise ratio and FSO of the loadcell and sensor

Sensor n = 10	Optic fibres far apart		Optic fibres in close proximity	
	Signal to noise, dB	FSO, N – loadcell V – sensor	Signal to noise, dB	FSO, N – loadcell V – sensor
	Loadcell	28.9	391	30.0
Anterior channel	24.4	0.183	21.6	0.129
Posterior channel	31.2	0.176	34.2	0.220

Table 9: Best calibration and average static sensitivity

Channel n = 10	Calibration	Static sensitivity N/V [SD]
Anterior	5th order	3230 [677]
Posterior	5th order	2320 [473]

In Table 7 the hysteresis that occurred in the sensor recordings, loadcell recordings and displacement recordings are reported. A greater hysteresis effect was evident in the anterior channel recordings than in the posterior channel recordings. The hysteresis in the sensor and the loadcell output can be divided into the hysteresis that is inherent to the viscoelastic nature of the patella tendon as well as the hysteresis that was induced into the system. Unfortunately the hydraulic cylinder piston's displacement was subjected to hysteresis as can be seen from the output from the displacement transducer. The reported  $\chi^2$ -error was in acceptable limits for the polynomial fits to the loading and unloading cycles.

In Table 8 the signal-to-noise ratio and corresponding FSO of the loadcell and sensor are shown. The parameters obtained for both instances where the optic fibres were far apart and in close proximity are reported. The entries in Table 9 show the best calibrations based on the error in force estimation as determined by Matlab's *polyfit*-

function. The reported static sensitivity is the average sensitivity based on a first order to fifth order polynomial fit to the sequential test recordings.

## **4.4 In vivo sensor calibration**

### **4.4.1 Introduction**

The next step in the investigation of the sensor's behaviour was to find approximate calibrations with which the *in vivo* measured patella tendon forces could be approximated. The calibrations had to be based on *in vivo* data because the same loading conditions that are experienced *in vivo* could not be replicated during the *in vitro* and the hydraulic press loading test.

A test setup was needed with which the tensile force inside the patella tendon could be measured and against which the output from the sensor could be compared. The Biodex test system (Biodex Inc.) gave the possibility of an isokinetic test that the volunteer could perform and during which the torque produced by the quadriceps muscles could be measured. Since the quadriceps muscle is connected to the patella via the quadriceps tendon which in turn is connected to the patella tendon, the torque produced by the quadriceps could be related to the patella tendon. If values for the moment arm of the patella tendon with regards to the medial/lateral axis could be obtained, approximate tensile force values for the patella tendon could be calculated.

This is a crude method of determining the tensile force inside the patella tendon since the quadriceps muscle isn't the only muscle responsible for extension. The Vastus medialis, Vastus lateralis and Vastus intermedius are also responsible for knee extension. The patella also connects to the femur through other ligaments, i.e. the patellofemoral ligament etc., which dissipates the loads that are exerted on the patella through the quadriceps tendon. The patella tendon however is distally attached to the tibial tubercle and is therefore responsible for extending the tibia relative to the femur.

Another phenomenon that must be kept in mind is the axis of rotation that shifts during knee flexion. The moment arm of the patella tendon with respect to the medial/lateral axis will therefore vary with flexion of the knee joint as is depicted by Herzog & Read (1993), Kellis & Baltzopoulos (1999) & Krevolin, Pandy & Pearce (2004). Although the procedure had its limitations, it still provided an approximate calibration that

could be used to express the *in vivo* voltage measurements of the sensor in terms of force values.

#### 4.4.2 Hardware setup

A piece of optic fibre was inserted through the volunteer's right patella tendon. It was decided to record the force values of the right leg since it was the volunteer's dominant side. The following procedure was followed when the optic fibre was inserted through the patella tendon:

The surrounding skin and flesh to the anterior proximal part of the right patella tendon was anaesthetised. After ample time was allowed for the local anaesthesia to take effect, a 22 gauge spinal needle was inserted under sonar guidance deep posterior to the patella tendon where more anaesthesia was injected into the fat pad. This procedure ensured that the nerve supply to the patella tendon was completely anaesthetised which led to the experience being less traumatic and the recovery time as short as possible after the test ended.

With the patella tendon anaesthetised, a 19 gauge needle was inserted under sonar guidance through the midsection of the proximal patella tendon in a medial/lateral direction. A piece of sterilised optic fibre was drawn through the needle and the needle was removed. The piece of optic fibre was left suspended inside the patella tendon as is shown in Figure 25. Dressing was applied to the insertion sites to avoid any contact with the outside environment.

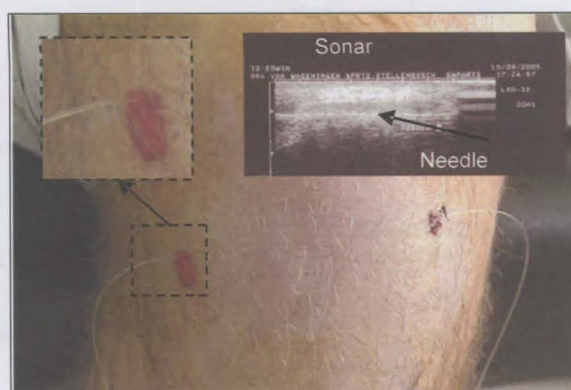


Figure 25: Insertion of optic fibre into the patella tendon

After the optic fibre was inserted through the patella tendon, the volunteer was strapped into the Biodex test system. To familiarise the volunteer to the test procedure, the system was setup for his left leg and he performed the whole set of exercises. After the familiarisation procedure, the system was setup for the volunteer's right leg and the



sensor was connected to the optic fibre. The same data acquisition system that was described in Chapter 3 was used to record the sensor output at a sampling frequency of 100 Hz. The torque measurements were captured by the Biodex control system and a computer printout was supplied after each test which reported on the test results.

#### 4.4.3 Test procedure

The volunteer completed three isokinetic tests that consisted of fifteen knee flexions in succession at maximum muscle output. The difference between the three tests was the rate at which each test was performed. The Biodex control program regulated the maximum rotational speed of the knee flexion and extension movement, which were 60 °/s flexion, 180 °/s flexion and 300 °/s flexion. The control system of the Biodex system regulated the flexion speed by adjusting the resistance of the arm. The three tests were performed in succession with a rest period of 30 s between each test.

#### 4.4.4 Data processing

The data processing procedure is illustrated in Figure 26. The sensor output recorded for the three tests were imported into Matlab and smoothed using the procedure described previously. Since the three datasets consisted of extension/flexion cycles, the cycles were subdivided into loading phases and unloading phases. The maximum and minimum voltage output for each sub-cycle. The average and standard deviation of the maximum and minimum voltage outputs and FSOs for each test were calculated.

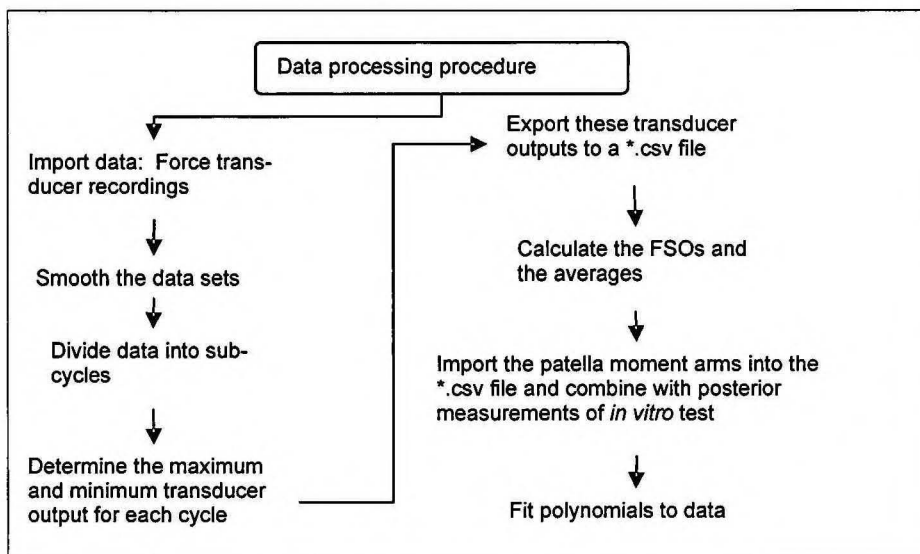


Figure 26: *In vivo* patella tendon loading test: data processing of cyclic recordings

The Biodex test system only gave a paper copy of the test results and the data could not be electronically extracted. It was therefore not possible to relate the entire sensor output to the measured torque produced by the quadriceps muscles. The report from the Biodex system only stated the maximum and average maximum torque and flexion angle at which the maximum torque occurred. The literature (Herzog *et al.*, 1993; Kellis *et al.*, 1999 & Krevolin *et al.*, 2004) was consulted to determine applicable moment arms of the patella tendon to the axis of rotation and its variation with flexion.

These moment arms were used in the calculation of the patella tendon tensile load. The values from the *in vivo* test were combined with the sensor recordings from the *in vitro* patella tendon test. Using the *polyfit*-function of Matlab, first to fifth order polynomials were fitted to the data. The one with the best predictive nature according to Matlab's *polyval*-function were chosen. From these calibrations, the average static sensitivity over the FSO experienced during the *in vivo* test was calculated.

#### 4.4.4 Results

The average maximum output, minimum output and FSO of the sensor for the three tests are shown in Table 10. The average maximum torque with its corresponding flexion angle for each test is reported in Table 11. Included in Table 11 are approximate values of the patella tendon moment arm in terms of Tibiofemoral contact point (Kellis *et al.*, 1999). The approximate maximum tensile load as derived from the torque measurements and moment arms is given in Table 11.

Table 10: Average sensor recordings for the three isokinetic tests

Test °/s	Maximum output V [SD]	Minimum output V [SD]	FSO V [SD]
60	2.85 [0.136]	1.43 [0.0780]	1.42 [0.077]
180	2.77 [0.0620]	1.84 [0.161]	0.931 [0.193]
300	2.87 [0.0440]	2.16 [0.117]	0.708 [0.127]

Table 11: Maximum exerted torque as reported by the Biodex test system

Test °/s	Torque N.m. [SD]	Flexion angle °	Moment arm mm [SD]	Tensile load N
60	237 [10.2]	66	41.7 [2.80]	5670
180	171 [6.56]	52	42.6 [4.50]	4110
300	114 [5.12]	68	41.7 [2.80]	2730

Table 12: Sensor calibration results of *in vitro* and *in vivo* patella tendon loading test

Calibration	Calibration constants						SD
	1	2	3	4	5	6	N
1st order	2.72e03	-58.7					61.3
2nd order	1.86e03	1.84e03	-34.1				49.4
3rd order	-4.54e03	8.54e03	951	-18.3			44.1
4th order	1.44e04	-3.72e04	2.73e04	-852	8.41		37.5
5th order	-3.42e04	1.03e05	-1.03e05	4.07e04	-1.66e03	17.5	45.0

Table 13: Static sensitivity of posterior channel

Calibration	Static sensitivity	
	N/V	[SD]
1st order	2722	
2nd order	4476	1526
3rd order	3870	2284
4th order	4018	3527
5th order	3972	6611
Average	3812	3487

The *in vivo* data was used together with the posterior channel data from the *in vitro* patella tendon test to derive calibrations. The results are shown in Table 12 where the calibration constants and error in force prediction are reported. It was found that a fourth order polynomial fitted the data best in terms of the error in force prediction. The average static sensitivity of the posterior channel is shown in Table 13.

## 4.5 Conclusion

The hysteresis effect in the sensor recordings was quantified through the application of a sequential test during the hydraulic press test and the *in vitro* patella tendon test. During the two tests it was found that the material properties of the optic fibre as well as the dynamics of the test medium caused a hysteresis error in the sensor recordings.

The findings from the hydraulic press test gave an indication of the hysteresis effect that the material properties of the optic fibre induced in the force measurements. The optic fibre is manufactured from polymethyl methacrylate, which is a viscoelastic material (Callister, 2000). When the optic fibre is loaded, the rate of deformation will differ from the rate of recovery, due to its viscoelastic behaviour. If the applied load is further increased, the optic fibre deforms more, and the hysteresis effect becomes more

prominent due to the difference in the deformation rate and recovery rate of the optic fibre.

There was significant variation in the hysteresis values of the hydraulic press test. The hysteresis in the loadcell output, as shown in Table 2, followed a diminishing trend as the applied loads on the optic fibre increased. The loadcell output was directly proportional to the displacement of the hydraulic cylinder's piston and the hysteresis in the loadcell recordings can therefore be related to the hysteresis induced into the system by the hydraulic cylinder. The displacement of the hydraulic cylinder during the application of the 250 N load was small and the servo valve that was used did not have a fast enough response and sensitivity. Load control at small loads was therefore difficult. Better load control was achieved for larger loads, i.e. 500 N, since these required larger displacements.

The displacement control of the MTS control unit induced hysteresis in the measurements as seen in the displacement transducer recordings, loadcell recordings and sensor recordings. The patella tendon complex in the *in vitro* patella tendon loading test also caused hysteresis, due to its viscoelastic nature. This can be seen in the larger hysteresis effect in the loadcell recordings than the displacement transducer recordings. The hysteresis effect in the sensor recordings was greater than the hysteresis effect in the loadcell recordings, and this can be attributed to the material properties of the optic fibre.

Table 14: Overall hysteresis contribution from the sensor

Test	Anterior channel % Hysteresis, $value = \left(1 - \frac{Trans}{System}\right) * 100\%$	Posterior channel % Hysteresis, $value = \left(1 - \frac{Trans}{System}\right) * 100\%$
Hydraulic press test	70.2	13.8
<i>In vitro</i> patella tendon test	120	67.9

If the hysteresis in the sensor recordings for the different tests is expressed in terms of percentages of the hysteresis induced into the overall system, the results are as shown in Table 14. Sequential tests with the sensor should therefore be avoided, since hysteresis will play a dominant role in the sensor output. By subtracting the hysteresis error from that of the test equipment used, a maximum hysteresis error of 20% FSO [SD = 8.88] is obtained. This value corresponds well to the reported value of 17% FSO by Erdemir *et al.* (2002).

The test results from the hydraulic cylinder press test showed that the signal-to-noise ratio was well in excess of 20 dB with the minimum 41.2 dB. Although the FSO of the sensor was greater during the *in vitro* patella tendon loading test than it was during the hydraulic press test, the signal-to-noise ratio was lower, indicating more noise for the *in vitro* patella tendon loading test. The signal-to-noise ratios for the other two transducers, i.e. loadcell and displacement transducer, that were used during the *in vitro* patella tendon loading test shows that there was a significant source of noise.

The USB based I/O module that was used to convert the analogue signals of the sensors into digital signals was placed beside the MTS control unit. Inside the control unit casing was a large electric cooling fan which was a source of electrical noise in the measured signals. Unfortunately the module could not be isolated from the fan motor. The noise in the reference values were therefore not measured by the sensors, but were induced into the system by means of the I/O module that lay beside the electric fan.

The frequency response of the sensor was investigated through the sequential test performed during the hydraulic press test. The FFT of the 0.1 Hz test and 1 Hz tests were compared to the force values predicted with the static calibrations. The results suggested that the sensor's sensitivity diminished as the loading frequency increased. However, the following should be kept in mind.

The optic fibre was loaded inside the hydraulic press by means of the hydraulic cylinder's piston that compressed the optic fibre between the two polished plates. The top plate lay on top of the optic fibre and it was therefore not parallel to the bottom plate due to the optic fibre's geometry when the load was applied. Part of the top plate therefore pressed onto the bottom plate, leading to a fraction of the load not being applied on the optic fibre. This effect is clear when the results in Table 4 are considered.

There is a significant difference in the prediction of the static calibration and the measured value of the 0.1 Hz test and the 1 Hz test of the anterior 250 N (20 mm plate) trial whereas better results were obtained for the posterior 250 N (20 mm plate) trial. From these results it is thus not possible to give a statistical significant judgement on the sensor's frequency response. The results from Erdemir *et al.* (2003, 2002) showed that errors resulted for differences in loading rate between the calibration and test trial runs. The errors were larger when calibrations at lower loading rates were used to predict loads from tests having higher loading rates. The calibrations of the sensor are

therefore rate dependent. This can be attributed to the viscoelastic nature of the optic fibre since its behaviour will be dependent on the applied stress and time.

The repeatability of force measurements for different optic fibres was investigated during the random test of the hydraulic press test. The repeatability was based on the FSO of the sensor. In other words, the investigation was done to see whether the same FSO would be measured for different optic fibres when the same load was applied. The results in Table 5 suggest that the FSO between different optic fibres will differ considerably for repeating loads, yielding a low repeatability. Erdemir *et al.* (2003, 2002) found that the calibrations are not only rate dependent, but also subject dependent. The results from this study and the study conducted by Erdemir *et al.* (2003, 2002) therefore suggest that a general calibration will have much variability, and that better results will be achieved if calibrations are derived for each optic fibre.

If the calibrations are based on the raw sensor output, more variability will be induced into the system due to the effect of the termination technique of the optic fibre at the ST-connector ends. It was clear during the hydraulic test that the termination procedure influenced the magnitude of the zero-sensor output.

Both the hydraulic press test and the *in vitro* patella tendon test indicated that the anterior channel is more sensitive than the posterior channel. The sensitivity of both channels of the sensor also increased with the FSO. This can also be attributed to the viscoelastic nature of the optic fibre. It was found during the hydraulic press test that a second order polynomial curve best fitted the majority of the data for both channels. For the *in vitro* patella tendon test, a fifth order polynomial fitted the data best and the final calibration derived from both the *in vitro* and *in vivo* results for the posterior channel, showed that a fourth order polynomial fitted the data best. The quality of the fits was based on the predictive ability of the calibrations as calculated with Matlab's *polyfit*-function. Erdemir *et al.* (2002, 2003) came to conclusion from their test results that a third order polynomial fitted the data best and that the curve fit didn't improve for further orders. The FSO's differed between the abovementioned tests, and an applicable calibration will therefore depend on the FSO of the tests to be conducted.

Finally the influence of optic fibres in close proximity to one another on the sensor output was considered. The influence was measured in terms of the ratio calculated from the FFT values. The results suggest that the effect is negligible since the ratio increased for the posterior channel and decreased for the anterior channel when the optic

fibre was inserted in close proximity. Since the calibrations are subject dependent, the influence that optic fibres in close proximity will have on the sensor output will not be a problem. This is because the effect will be accommodated in the calibration.

Fibre optic technology provides an attractive methodology for the measurement of *in situ* loads. This is because the sensor's disturbance in the connective tissue is negligible, it is minimally invasive, easy to implement and inexpensive (Finni *et al.*, 2000, 1998; Erdemir *et al.*, 2003, 2002; Komi *et al.*, 1996) with regards to other sensors that have previously been employed, i.e. buckle transducers, liquid metal strain gauges, implantable force transducers and pressure transducers (Ravary *et al.*, 2004). The results obtained through the study of Erdemir *et al.* (2003, 2002) and this study show that the sensor is subject to significant measurement errors if the technique is not applied carefully. Care must therefore be given when making use of a sensor.

## Chapter 5: Stress relaxation measured by a loadcell and the sensor

### 5.1 Introduction

In Chapter 2 connective tissue was classified as a viscoelastic material. Its behaviour will therefore be dependent on stress relaxation, creep and hysteresis. The behaviour of viscoelastic materials has been described by means of mathematical models of mechanical analogues. Two popular mechanical models are shown in Figure 27 and Figure 28. These are Maxwell's model (Coleman & Li, 1994; Liu & Subhash, 2006; Wu *et al.*, 2006) and the Kelvin/Voight model (Toms *et al.*, 2002; Vriend & Kren, 2004; Wills, Picton & Davies, 1972). The mathematics of these models relates the stress and strain in the framework of linear viscoelastic theory. The elastic component is simulated by a mechanical spring and a dashpot approximates the viscous component.

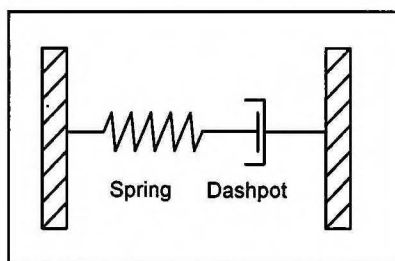


Figure 27: Maxwell model (Fung, 1965)

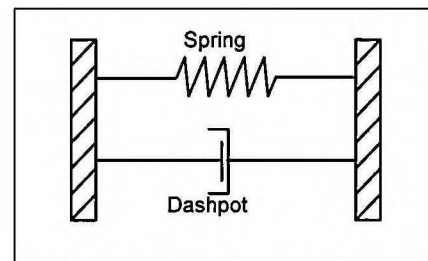


Figure 28: Kelvin/Voight model (Fung, 1965)

Maxwell's model and the Kelvin/Voight model are the simplest mechanical analogues that can be used to describe the behaviour of a viscoelastic material (Wills *et al.*, 1972). It is reasonable to expect that for small oscillations of small amplitude about an equilibrium state that the theory of linear viscoelasticity will be sufficient, but when the viscoelastic tissue experiences significant deformations, the non-linear stress and strain characteristic of the material must be accounted for. Oza, Vanderby & Lakes (2006) reports on mathematical models that are based on non-linear viscoelastic theory in a study where an interrelationship of creep and stress relaxation were investigated. One of the models is Quasi-linear Viscoelastic theory (QLV theory), a theory that have been applied extensively in the investigation of stress relaxation of connective tissue (Abramowitch *et al.*, 2004; Hashemi *et al.*, 2005; Johnson *et al.*, 1994; Moon *et al.*, 2006; Nigul *et al.*, 1987; Toms *et al.*, 2002; Wu *et al.*, 2006).



QLV theory, derived and developed by Fung (1972, 1965), approximates the viscoelastic nature of a material with five (Abramowitch *et al.*, 2004; Hashemi *et al.*, 2005; Johnson *et al.*, 1994; Moon *et al.*, 2006; Nigul *et al.*, 1987) or eight constants (Toms *et al.*, 2002; Wu *et al.*, 2006) in a mathematical expression known as the QLV-function. The constants' values are derived by fitting the QLV-function to the stress measurements recorded during a stress relaxation test. During a stress relaxation test, the test sample is strained at a constant rate until a predefined strain level is reached. That strain level is then maintained for a period of time, while the load in the test sample is recorded. After the QLV-constants' values have been derived, their predictive ability is examined by comparing the prediction from the QLV-function to the results of an additional stress vs. strain test.

QLV theory has been applied in this study to provide a measure for comparison of the overall stress relaxation measured by a loadcell and the local stress relaxation measured by the sensor in a patella tendon. Since the test sample was old (Female patella tendon,  $\pm 80$  years), the derived QLV-constants could not be used to shed more light on the biomechanical properties of the patella tendon. An in-depth analysis on the viscoelastic properties of the patella tendon has been done as depicted in Johnson *et al.* (1994). Patella tendons are used as graft materials for ACL reconstruction (Cooper, Deng, Burstein & Warren, 1993; Komistek, Dennis & Mahfouz, 2003), and samples between the ages of 17 and 55 years are normally used. Since the test sample fell outside this age range, the results of this *in vitro* investigation must only be considered for the purposes of comparing the performance of the sensor to that of the loadcell.

## 5.2 QLV theory

The principles of QLV theory can be described through the consideration of a cylindrical material that is longitudinally loaded (Fung, 1972, 1965). If the specimen is stretched from its reference length,  $\ell_0$ , to a new length,  $\ell$ , the resulting strain,  $\varepsilon$ , is defined as

$$\varepsilon = \frac{\ell - \ell_0}{\ell_0} \quad \text{Equation 15}$$

The strain will induce a tensile stress,  $\sigma$ , as is described by

$$\sigma = f(\varepsilon) \quad \text{Equation 16}$$

From viscoelastic theory it is clear that the stress,  $\sigma$ , will also be a function of time, and therefore Equation 16 becomes

$$\sigma = f(\varepsilon, t) \quad \text{Equation 17}$$

Fung (1972, 1965) proposed an expression that included two parameters with which the history of the stress in the loaded specimen could be described. The QLV-function originated and can be written as

$$\sigma(\varepsilon, t) = G(t) \times \sigma^{(e)}(\varepsilon(t)) \quad \text{Equation 18}$$

The QLV-function,  $\sigma = f(\varepsilon, t)$ , consists of the reduced relaxation function,  $G(t)$ , which is a normalised stress function of time, whereas the elastic response,  $\sigma^{(e)}(\varepsilon(t))$ , is a function of strain,  $\varepsilon(t)$ .

When an infinitesimal change in strain,  $\delta\varepsilon$ , is superposed on the specimen having a strain,  $\varepsilon(t)$ , at a time,  $\tau$ , the stress response,  $K(\varepsilon, t)$ , for  $t > \tau$ , can be calculated with

$$K(\varepsilon, t) = G(t - \tau) \frac{\partial \sigma^{(e)}(\varepsilon(t))}{\partial \varepsilon} \delta\varepsilon(\tau) \quad \text{Equation 19}$$

By applying the superposition principle, the tensile stress,  $\sigma(\varepsilon, t)$ , at any time,  $t$ , is the sum of the contributions of the past changes in strain,  $\delta\varepsilon$ , which are governed by the same reduced relaxation function,  $G(t)$ , as

$$\sigma(\varepsilon, t) = \int_{-\infty}^t \left( G(t - \tau) \frac{\partial \sigma^{(e)}(\varepsilon(t))}{\partial \varepsilon} \frac{\delta\varepsilon(\tau)}{\partial \tau} \right) d\tau \quad \text{Equation 20}$$

The lower integration limit in Equation 20 designates that the entire stress history,  $K(\varepsilon, t)$ , of the specimen should be included. In a test setup, the tensile test starts at  $t=0$ , and the stress,  $\sigma(\varepsilon, t)$ , and strain,  $\varepsilon(t)$ , at  $t < 0$ , are assumed to be constant. Equation 20 then becomes

$$\sigma(\varepsilon, t) = \sigma^{(e)}(0+)G(t) + \int_0^t \left( G(t - \tau) \frac{\partial \sigma^{(e)}(\varepsilon(t))}{\partial \varepsilon} \frac{\delta\varepsilon(\tau)}{\partial \tau} \right) d\tau \quad \text{Equation 21}$$

Fung (1972, 1965) also derived an expression with which the creep can be described when a constant stress is induced on the specimen. Since creep was not considered, the reader is referred to the literature [Dortmans, van de Ven & Sauren, 1994; Fung, 1972, 1965] if more information on the reduced creep function,  $J(t)$ , is needed.

### 5.3 Elastic response

The elastic response,  $\sigma^{(e)}(\varepsilon(t))$ , is defined as the tensile stress that is instantaneously generated inside a specimen when a step function of strain,  $1(t)$ , is imposed on the specimen (Fung, 1972, 1965). Abramowitch *et al.* (2004), Hashemi *et al.* (2005), Johnson *et al.* (1994), Moon *et al.* (2006) & Nigul *et al.*, (1987) who employed QLV theory used an exponential expression with two constants,  $A$  and  $B$ , to describe the instantaneous elastic response as

$$\sigma^{(e)}(\varepsilon(t)) = A(e^{B\varepsilon(t)} - 1) \quad \text{Equation 22}$$

The product of the two constants,  $AB$ , describes the initial slope of the stress vs. time curve. Constant  $B$  influences the non-linearity of the elastic response which is proportional to the magnitude of constant  $B$  (Johnson *et al.*, 1994).

### 5.4 Reduced relaxation function

When the trend of a stress vs. time curve from a stress relaxation test is considered, the first tendency is to analyse the stress relaxation function,  $G(t)$ , into a sum of exponential functions of a Kelvin/Voight or Maxwell function (Fung, 1972, Hashemi *et al.*, 2005). Each exponential constant is then identified with a relaxation mechanism. However, when this approach is followed, the exponential constants derived from the experimental data might lead to faulty predictions of the behaviour of relaxation outside the tested time range or a measured characteristic time of a relaxation test might be the length of the experiment (Fung, 1972).

The mechanical properties of the patella tendon are insensitive to a wide range of strain rate (Abramowitch *et al.*, 1994). Blevins, Hecker, Bigler, Boland & Hayes (1994) showed that the values for biomechanical properties of the patella tendon will stay constant for loading rates that range between 10 %/s to 100 %/s. The behaviour of a mechanical model that consists of a finite number of springs and dashpots is dependent on the strain rate though (Fung, 1972) and a discrete model will therefore correspond to a discrete spectrum of the behaviour of the connective tissue. Because of this principle the application of a continuous distribution of the exponents has to be considered (Fung, 1972).

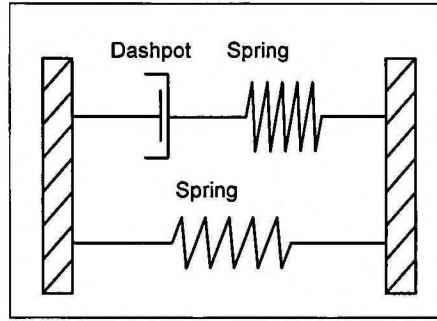


Figure 29: Linear solid model (Fung, 1965)

Fung (1972, 1965) based the QLV model on the standard linear solid model, which is a combination of the Kelvin/Voight and Maxwell model as is illustrated in Figure 29. The linear solid model's constitutive differential equation has been derived in Appendix C-1 and has been found to be

$$\tau_\epsilon \dot{\sigma} + \sigma = E_R (\tau_\sigma \dot{\sigma}^{(e)} + \sigma^{(e)}) \text{ with } \tau_\epsilon \sigma(0) = E_R \tau_\sigma \sigma^{(e)}(0) \quad \text{Equation 23}$$

The definition of the reduced relaxation function requires that

$$\sigma^{(e)}(0) = \sigma(0), \quad G(0) = 1 \quad \text{Equation 24}$$

and hence

$$E_R = \frac{\tau_\epsilon}{\tau_\sigma} \quad \text{Equation 25}$$

In order to find an expression for the reduced stress relaxation parameter,  $G(t)$ , of the linear solid model, Equation 23 is integrated for the stress,  $\sigma(\epsilon, t)$ , when there is a step increase in the elastic response

$$\sigma^{(e)}(\epsilon, t) = 1(t) \quad \text{Equation 26}$$

The result is

$$G(t) = E_R \left( 1 + \left( \frac{\tau_\sigma}{\tau_\epsilon} - 1 \right) e^{-\frac{t}{\tau_\epsilon}} \right) 1(t) \quad \text{Equation 27}$$

Equation 27 shows that the time constant,  $\tau_\epsilon$ , relates to stress relaxation at constant strain. The time constant,  $\tau_\sigma$ , relates to creep at constant stress. The constant  $E_R$  can be described as the fraction of the elastic response that is left in the specimen after a period of long relaxation (Fung, 1965).

Now that expressions for the reduced relaxation function are identified, the continuous distribution of the exponential constants can be considered in more detail. The argument begins with the substitution of

$$\sigma(t) = \sigma_0 e^{i\omega t} \text{ and } \sigma^{(e)}(t) = \sigma_0^{(e)} e^{i\omega t} \quad \text{Equation 28}$$

into Equation 23. The result is

$$\begin{aligned}\sigma_0 e^{i\omega t} + i\omega\tau_\varepsilon\sigma_0 e^{i\omega t} &= E_R \left[ \sigma_0^{(e)} e^{i\omega t} + i\omega\tau_\sigma\sigma_0^{(e)} e^{i\omega t} \right] \\ \Rightarrow \sigma_0 \left[ e^{i\omega t} (1+i\omega\tau_\varepsilon) \right] &= E_R \left\{ \sigma_0^{(e)} \left[ e^{i\omega t} (1+i\omega\tau_\sigma) \right] \right\} \\ \Rightarrow \frac{\sigma_0}{\sigma_0^{(e)}} &= \frac{e^{i\omega t} (1+i\omega\tau_\sigma)}{e^{i\omega t} (1+i\omega\tau_\varepsilon)} E_R = M(\omega)\end{aligned}\tag{Equation 29}$$

$M(\omega)$ , is defined as the complex modulus of the linear solid model and is a function of the angular frequency,  $\omega$ , and thus the strain rate,  $\frac{d\varepsilon}{dt}$ . Its practical use is giving an expression with which the ratio of the stress,  $\sigma(t)$ , and the elastic response,  $\sigma^{(e)}(\varepsilon(t))$ , can be calculated, similar to the elastic modulus in traditional structural mechanics.

Recall that the QLV-function, Equation 20, relates the stress,  $\sigma(t)$ , to the elastic response,  $\sigma^{(e)}(\varepsilon(t))$ , through the reduced relaxation parameter,  $G(t)$ . Fung (1965) substituted the time difference  $(t-\tau)$  with the parameter  $\xi$  for convenience during the derivation procedure. Equation 20 then becomes

$$\sigma(t) = \int_{-\infty}^t \left( G(\xi) \frac{\partial \sigma^{(e)}(\varepsilon(t-\xi))}{\partial t} \right) d\xi\tag{Equation 30}$$

When Equation 30 is evaluated for the elastic response input of Equation 28, the result is

$$\begin{aligned}\sigma(t) &= \int_0^{\infty} \left( G(\xi) i\omega\sigma_0^{(e)} e^{i\omega(t-\xi)} \right) d\xi \\ \Rightarrow \sigma(t) &= i\omega\sigma_0^{(e)} \int_0^{\infty} \left( G(\xi) e^{i\omega(t-\xi)} \right) d\xi \\ \Rightarrow \frac{\sigma(t)}{\sigma_0^{(e)}} &= i\omega \int_0^{\infty} \left( G(\xi) e^{i\omega(t-\xi)} \right) d\xi = M(\omega) = |M(\omega)| e^{i\delta}\end{aligned}\tag{Equation 31}$$

The angle,  $\delta$ , represents the phase shift between the strain,  $\varepsilon(t)$ , and the stress,  $\sigma(t)$ , and the tangent of the angle,  $\delta$ , represents the internal damping of the viscoelastic material (Fung, 1972, 1965). If the modulus,  $|M(\omega)|$ , and internal damping,  $\tan \delta$ , is plotted against the logarithm of  $\omega\sqrt{\tau_\sigma\tau_\varepsilon}$ , as shown in Figure 30 it is clear from the graph that the internal damping reaches a peak at  $\frac{1}{\sqrt{\tau_\sigma\tau_\varepsilon}}$ . Since the connective tissue's internal damping, and therefore the hysteresis, is insensitive to the loading rate (Blevins *et al.*

1994 & Woo *et al.*, 1999) the peak in Figure 30 needs to be spread out. This can be achieved by superposing a larger number of Kelvin models into the model and it leads to the introduction of a continuous spectrum of relaxation.

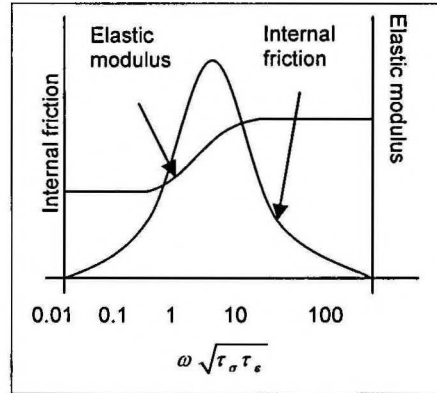


Figure 30: Modulus and internal damping plotted against frequency  $\omega$

The idea of a continuous spectrum of relaxation is implemented by defining a parameter  $S$  as (Fung, 1972, 1965)

$$S = \frac{\tau_\sigma}{\tau_\epsilon} - 1 \text{ and } E_R \text{ then becomes } E_R = \frac{1}{1+S} \quad \text{Equation 32}$$

Rewriting Equation 27 and Equation 29 in terms of  $S$ , the following is obtained

$$G(t) = \frac{1}{1+S} \left( 1 + S e^{-\frac{t}{\tau_\epsilon}} \right)$$

$$M(\omega) = \frac{1}{1+S} \left[ 1 + S \frac{\omega \tau_\epsilon}{\omega \tau_\epsilon + \frac{1}{\omega \tau_\epsilon}} + iS \frac{1}{\omega \tau_\epsilon + \frac{1}{\omega \tau_\epsilon}} \right] \quad \text{Equation 33}$$

The time constant,  $\tau_\epsilon$ , is replaced by a continuous time constant,  $\tau$ , and the parameter,  $S(\tau)$ , becomes a function of the continuous time constant,  $\tau$ . The proposed function  $S(\tau)$  is (Fung, 1972, 1965)

$$S(\tau) = \begin{cases} \frac{C}{\tau} & \text{for } \tau_1 \leq \tau \leq \tau_2 \\ 0 & \text{for } \tau < \tau_1, \tau > \tau_2 \end{cases} \quad \text{Equation 34}$$

This choice for  $S(\tau)$  leads to the modulus,  $M(\omega)$ , staying nearly constant over a wide range of frequency,  $\omega$ . The corresponding reduced relaxation function can then be evaluated in terms of the exponential integral function (Fung, 1972, 1965). Three constants  $C$ ,  $\tau_1$  and  $\tau_2$  are left that needs to be adjusted so it can be fitted to the experimental data. The final proposed reduced relaxation function is

$$G(t-\tau) = \frac{1+C \left( E_1 \left[ \frac{t-\tau}{\tau_2} \right] - E_1 \left[ \frac{t-\tau}{\tau_1} \right] \right)}{1+C \ln \left( \frac{\tau_2}{\tau_1} \right)}$$
Equation 35

where  $E_1 \left[ \frac{t-\tau}{\tau_{\#}} \right]$  is defined as the exponential integral,  $E_1[y] = \int_y^{\infty} \frac{e^{-z}}{z} dz$

Constant  $C$  relates to the elasticity of the material since the material is more elastic for decreasing values of  $C$ . The time constants  $\tau_1$  and  $\tau_2$  govern the fast and slow viscous phenomena of the material respectively (Johnson *et al.*, 1994).

## 5.5 Test setup

The same test setup that was used during the *in vitro* patella tendon loading test was utilised. A schematic of the test setup is shown in Chapter 4, Figure 19. Two sensors were used during the stress relaxation test to measure the load inside the test sample: The loadcell and the sensor. A displacement sensor that recorded the hydraulic cylinder's displacement was also used to quantify the elongation of the test sample. It was preferable to use a sensor that measured the local elongation of the test sample, since it would provide more accurate approximations of the strain. The laboratory unfortunately did not have the necessary equipment with which this could be achieved. The data acquisition system described in Chapter 3 was used.



Figure 31: Harvesting of patella tendon complex

The test sample consisted of a human patella-patella tendon-tibial tubercle complex that was cleared by the Anatomy Council. The patella tendon complex was harvested from a donor's amputated leg (Female,  $\pm 80$  years old) as is shown in Figure 31.

The patella tendon complex was wrapped in 0.9% saline soaked gauze and cling wrap to be stored at  $-20^{\circ}\text{C}$  after it was harvested. The same procedure was followed by Cooper *et al.*, (1993) and Johnson *et al.*, (1994). The patella tendon was removed from the freezer and allowed to thaw at room temperature the day before testing. Afterwards the complex was wrapped in fresh 0.9% saline soaked gauze and the connective tissue was covered in cling wrap.

The patella tendon complex was potted into steel cylinders with an epoxy (Epi-dermix 372, ABE Construction Chemicals (Pty)Ltd.), as is shown in Figure 32, and the potted complex was left to cure over night at room temperature. Before commencement of the test, the potted complex was submerged into a 0.9% saline bath for at least fifteen minutes (Johnson *et al.*, 1994). During the experiment, the connective tissue was constantly hydrated with 0.9% saline to prevent it from drying out.

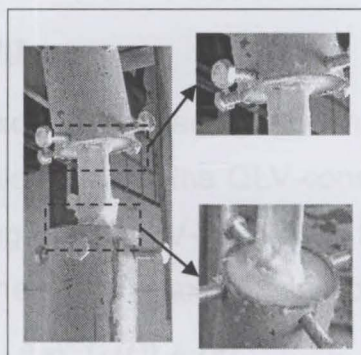


Figure 32: Patella tendon complex potted into steel cylinders

## 5.6 Test procedure

After temperature equilibration in the saline bath, the patella tendon complex was inserted into the MTS hydraulic press. The same preconditioning procedure and reference measurement procedure as described in Chapter 4 (reference length, reference width and reference depth) was used. After the preconditioning cycle, the patella tendon was held for 15 minutes at the reference state.

A stress relaxation test and a cyclic loading test were performed next. During the stress relaxation test, a ramp increase in strain was exerted on the patella tendon at a loading rate of 10 mm/min until the patella tendon reached a 5% strain level. Thereafter the patella tendon was kept at the 5% strain level for 5 minutes. A period of rest followed where the patella tendon was held at its reference state for 15 minutes. The patella tendon was then cyclically loaded at 0.5 Hz between 0% strain and 5% strain.



The elastic response expression of the QLV-function requires the tests sample to undergo a step increase in strain. In practice, it is however impossible to apply a step increase in strain. It has been shown that the connective tissue is insensitive to strain rate over a wide range however. This result suggests that tests employing high extension rates will therefore be sufficient, but this approach brings some difficulties of its own (Abramowitch *et al.*, 2004).

It is difficult to measure strain accurately, and if high extension rates are employed, it might lead to poor approximations of the strain history. Further complications are strain overshoot and vibration problems. Abramowitch *et al.* (2004) investigated what influence longer ramp times had on the analytical method that was used to obtain the QLV-constants and developed a procedure that accommodated slower loading rates.

## 5.7 Matlab programming

The “strain history approach” described by Abramowitch *et al.* (2004) was implemented in this study for the calculation of the QLV-constants. This approach is based on the simultaneous curve fitting of the QLV-function to the stress response of the ramp increase in strain section and the stress relaxation section. Recalling Equation 21,

$$\sigma(\varepsilon, t) = \sigma^{(e)}(0+)G(t) + \int_0^t \left( G(t-\tau) \frac{\partial \sigma^{(e)}(\varepsilon(t))}{\partial \varepsilon} \frac{\delta \varepsilon(\tau)}{\partial \tau} \right) d\tau \quad \text{Equation 36}$$

it can be rewritten for the ramp increase in strain section as

$$\sigma(t : 0 < t < t_0, \theta) = \frac{AB\gamma}{1 + C \ln \left[ \frac{\tau_2}{\tau_1} \right]} \int_0^t \left\{ 1 + C \left( E_1 \left[ \frac{t-\tau}{\tau_2} \right] - E_1 \left[ \frac{t-\tau}{\tau_1} \right] \right) \right\} e^{B\gamma\tau} \partial\tau \quad \text{where } \gamma = \frac{\partial \varepsilon}{\partial t} \quad \text{Equation 37}$$

and for the stress relaxation section as

$$\sigma(t : t > t_0, \theta) = \frac{AB\gamma}{1 + C \ln \left[ \frac{\tau_2}{\tau_1} \right]} \int_0^{t_0} \left\{ 1 + C \left( E_1 \left[ \frac{t-\tau}{\tau_2} \right] - E_1 \left[ \frac{t-\tau}{\tau_1} \right] \right) \right\} e^{B\gamma\tau} \partial\tau \quad \text{where } \gamma = \frac{\partial \varepsilon}{\partial t} \quad \text{Equation 38}$$

with  $\theta = f(A, B, C, \tau_1, \tau_2)$  (Abramowitch *et al.*, 2004). The steps followed in the derivation of Equation 37 and Equation 38 is shown in Appendix C-2.

Simpson’s rule, was used to solve the integrals in Equation 37 and Equation 38 and is defined as, (Stewart, 1999)

$$\int_a^b f(x)dx \approx S_n = \frac{\Delta X}{3} [f(x_0) + 4f(x_1) + 2f(x_2) + 4f(x_3) + \dots + 2f(x_{n-2}) + 4f(x_{n-1}) + f(x_n)] \quad \text{Equation 39}$$

where  $n$  is even and  $\Delta X = (b - a) / n$

The exponential integrals,  $E_1[\tau]$ , were solved with Matlab's *expint*-function.

Since only two equations, i.e. Equation 37 and Equation 38, are available and the system needs to be solved for the values of five constants, it is indeterminate. In Chapter 2 two tools, namely optimisation techniques and reduction methods, have been described with which indeterminate systems can be solved. Abramowitch *et al.* (2004) made use of the former technique and combined Equation 37 and Equation 38 into an objective function. This objective function was based on the sum of the squared error of the stress recordings and the predictions of the QLV-function. The stress recordings taken during the ramp phase was grouped in a vector,  $\mathbf{r}$ , while the stress recordings taken during the stress relaxation phase were grouped in a vector,  $\mathbf{s}$ . This resulted in the objective function,  $OBJ_1$ , as

$$OBJ_1 = f(\theta) + g(\theta) \\ = \sum_i [r_i - \sigma_i(t : 0 < t_i < t_0, \theta)]^2 + \sum_i [s_i - \sigma_i(t : t_0 < t_i < t, \theta)]^2 \quad \text{Equation 40}$$

In this study, Equation 40 as well as another function was used. The second objective function,  $OBJ_2$ , was based on a the  $\chi^2$ -error and was derived as

$$OBJ_2 = \sum_i \frac{[r_i - \sigma_i(t : 0 < t_i < t_0, \theta)]^2}{r_i} + \sum_i \frac{[s_i - \sigma_i(t : t_0 < t_i < t, \theta)]^2}{s_i} \quad \text{Equation 41}$$

The aim therefore was to find the combination of the QLV-constants for which the objective functions, i.e. Equation 40 and Equation 41, would be equal to zero. The results from the two objective functions would also serve as a confirmation of the global minimum.

Abramowitch *et al.* (2004) found that the fitted curves to the experimental data were non-Gaussian and that the QLV-constants  $A$  and  $\tau_1$  became closely correlated as the ramp times increased. If the fits were found to be Gaussian, the QLV-constants that were obtained with the "strain history approach" would be the same as for the case where a step input would have been used given that the global minimum was obtained. Since constant  $A$  did not describe the relaxation of the connective tissue during the relaxation test and since the stress vs. time graph was insensitive to a wide range of

strain rate, it could be determined separately from the other QLV-constants. Constant  $A$  was obtained by fitting Equation 22 to the ramp part of the stress vs. time graph of the relaxation test (Abramowitch *et al.*, 2004). Its value was kept constant for the remainder of the analysis.

In this study, the same approach was followed. The difference was that the optimisation process was started with the value of  $A$  being kept constant. When the objective function converged for the first time, the optimisation process was started again using the final values for constants  $B$ ,  $C$ ,  $\tau_1$  and  $\tau_2$  from the first trial as initial values for the second trial run. The value of constant  $A$  was also allowed to be varied by the optimisation algorithm during the second trial run.

Abramowitch *et al.* (2004) utilised the Levenberg-Marquardt-algorithm (Levenberg, 1944). Since the objective functions are highly non-linear, it was decided to make use of an optimisation algorithm that does not depend on the derivatives, i.e. Hessian matrix of the second partial derivatives of the objective function with respect to the design variables,  $\theta$ , of the objective function. It was found during the analysis that the objective function underwent small changes in its value, for large changes in the values of the design variables. This indicates that the first derivatives are small, and an optimisation algorithm using the first derivatives, will therefore not perform optimally.

The *patternsearch* toolbox of Matlab provided a tool with which Equation 40 and Equation 41 could be optimised, and this optimisation tool did not require information regarding the derivatives of Equation 40 and Equation 41. The principles of the *patternsearch*-algorithm are described in Appendix C-3. It should be noted that Matlab also have a build-in function with which non-linear curve fitting problems can be solved namely the *lsqcurvefit*-tool. The *lsqcurvefit*-tool is based on the interior-reflective Newton method Coleman *et al.* (1996, 1994) and was utilised to confirm the solution from the *patternsearch*-algorithm.

## 5.8 Data processing procedure

The schematic in Figure 33 illustrates the optimisation procedure that was followed. The stress relaxation data was loaded into the Matlab workspace and stored under global variable names. In the previous section it was shown that the objective functions consisted of two parts, namely the ramp increase in strain section and the

stress relaxation section. The stress relaxation data therefore needed to be separated into these parts.

During the stress relaxation test, the MTS hydraulic press cylinder drifted and therefore experienced small perturbations while the ramp strain was applied and when it was held at constant displacement. Since the QLV-theory does not account for these small fluctuations, the test data needed to be smoothed to remove these fluctuations. A moving average could not be employed since the amount of points that needed to be averaged was too large and the stress relaxation trend was modified too much when applying it. Instead, Matlab's *polyfit*-function was used to fit a polynomial to the two sections respectively.

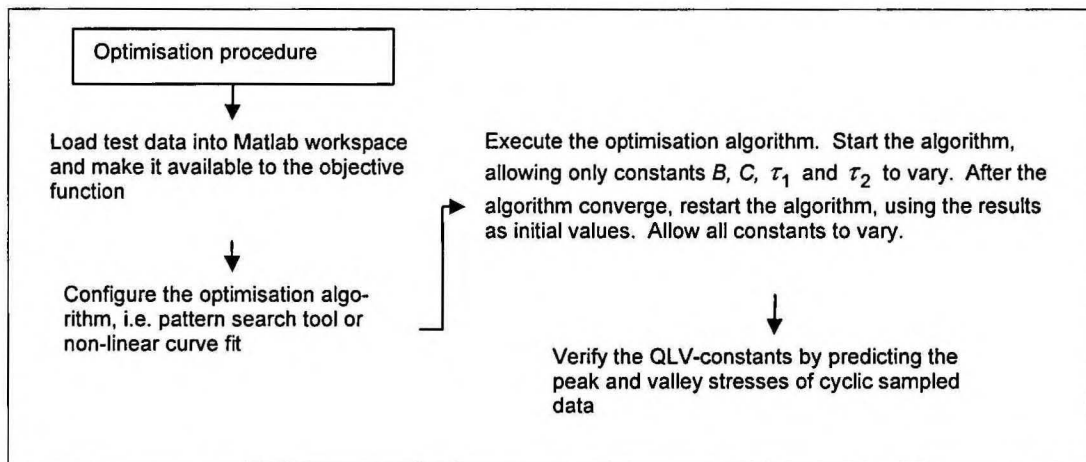


Figure 33: Optimisation strategy

After the recorded stress relaxation data was loaded into the work space, the optimisation procedure could be started. Initial values for the QLV-constants were gathered from the study conducted by Johnson *et al.* (1994) on human patella tendons. The initial values were loaded into the optimisation algorithm and the options were configured. The optimisation algorithm was first executed with only constants  $B$ ,  $C$ ,  $\tau_1$  and  $\tau_2$  allowed to vary. After the algorithm converged, the QLV-constant values were used as initial values for the next trial run and all the QLV-constants were allowed to vary.

When the objective function converged on the new solution it was verified through the results of separate cyclic tests. The test sample was subjected to a cyclic elongation between the strain limits used during stress relaxation tests, i.e. 0% and 5%. The same cyclic strain input that was applied onto the connective tissue was fed into Equation 21 and the maximum loads measured during the experiment were compared to the maximum theoretical loads predicted by the QLV-function.

## 5.9 Results

The perturbations that occurred in the movement of the MTS hydraulic press cylinder are depicted in Figure 34. This resulted in perturbations in the loadcell and sensor output which are not accommodated in QLV-theory. The perturbations in the strain and stress data, was removed by fitting polynomials to the stress response as are shown in Figure 35 and Figure 36 for the loadcell and sensor output respectively. The polynomials were visually inspected to see which order maintained the trend of the relaxation test best. A straight line was fitted to the ramp increase in strain/stress response and third order polynomials were found to maintain the stress relaxation trend best.

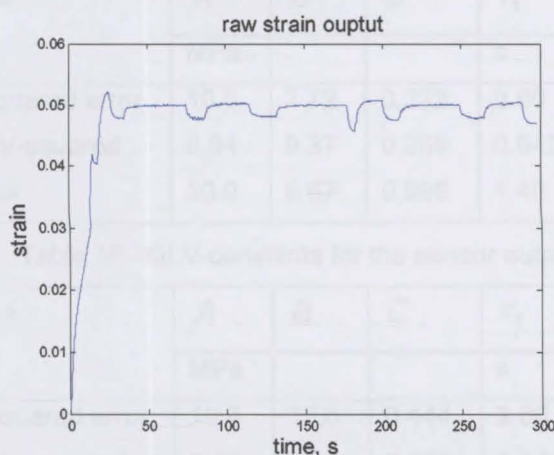


Figure 34: Raw strain measured by displacement sensor

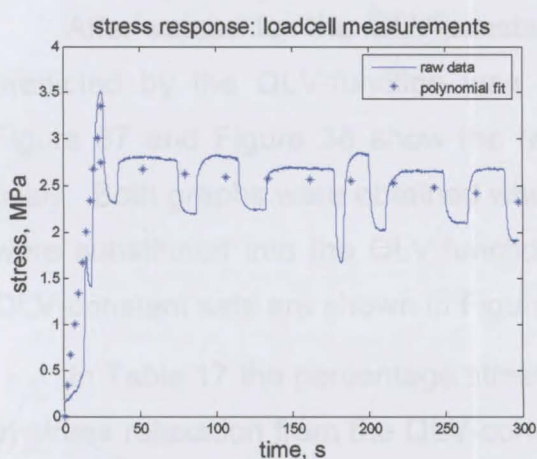


Figure 35: 3<sup>rd</sup> order polynomial fit to loadcell measurements

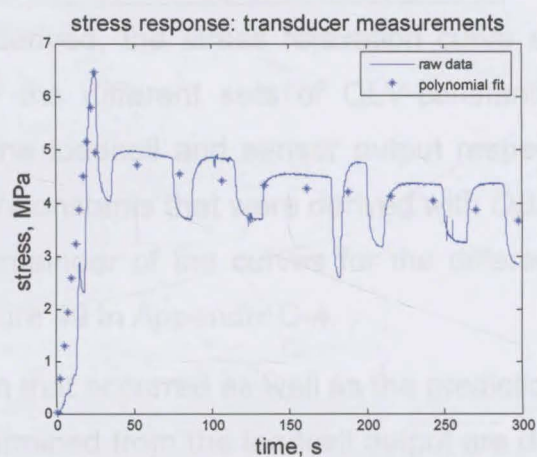


Figure 36: 3<sup>rd</sup> order polynomial fit to sensor measurements

After the polynomials were fitted, discrete points (11 for the ramp increase in strain/stress response, and 11 for the stress relaxation phase) were entered into the optimisation algorithms. The QLV-constants,  $\theta$ , as determined from the loadcell and sen-

sensor output are shown in Table 15 and Table 16 respectively. Included in the tables are the objective function values for the different objective functions and the two optimisation algorithms. The average values for constants  $A$ ,  $C$ , and  $\tau_1$  as derived from the loadcell and sensor output is in the same order of magnitude. There is an order of magnitude difference in the values for constant  $B$  between the loadcell and sensor output with the constants derived from the sensor output being greater. There was considerable variability for the time constant  $\tau_2$  values within the different optimisation algorithms and the objective functions, i.e.  $SD_{loadcell} = 3.37e05$  and  $SD_{sensor} = 6.03e06$ .

Table 15: QLV-constants for the loadcell output

Optimisation technique	$A$	$B$	$C$	$\tau_1$	$\tau_2$	$OBJ$
	MPa			s	s	
<i>patternsearch</i> -tool: squared error	10.0	7.72	0.322	2.00	36.3	0.172
<i>patternsearch</i> -tool: chi-squared	6.94	9.37	0.259	0.942	2.21E+04	0.763
Non-linear curve fit-tool	10.0	6.67	0.998	1.46	5.94E+05	0.295

Table 16: QLV-constants for the sensor output

Optimisation technique	$A$	$B$	$C$	$\tau_1$	$\tau_2$	$OBJ$
	MPa			s	s	
<i>Patternsearch</i> -tool: squared error	10.0	13.6	0.444	2.00	51.3	0.735
<i>Patternsearch</i> -tool: chi-squared	2.52	24.0	0.468	1.11	1.04E+07	0.359
Non-linear curve fit-tool	10.0	11.7	0.841	2.000	1.47E+04	1.03

After values for the QLV-constants were derived, the stress relaxation curve as predicted by the QLV-function was plotted for the different sets of QLV-constants. Figure 37 and Figure 38 show the results for the loadcell and sensor output respectively. Both graphs were obtained when the QLV-constants that were derived with  $OBJ_1$  were substituted into the QLV-function. The remainder of the curves for the different QLV-constant sets are shown in Figure 46 to Figure 49 in Appendix C-4.

In Table 17 the percentage stress relaxation that occurred as well as the prediction in stress relaxation from the QLV-constants determined from the loadcell output are depicted. The percentage stress relaxation was calculated as the percentage of stress left in the sample at the end of the relaxation period,  $\sigma_f$ , to the stress in the sample at the end of the ramp phase,  $\sigma_0$ , as

$$\% \sigma_{relax} = \frac{\sigma_f}{\sigma_0} \times 100$$

Equation 42

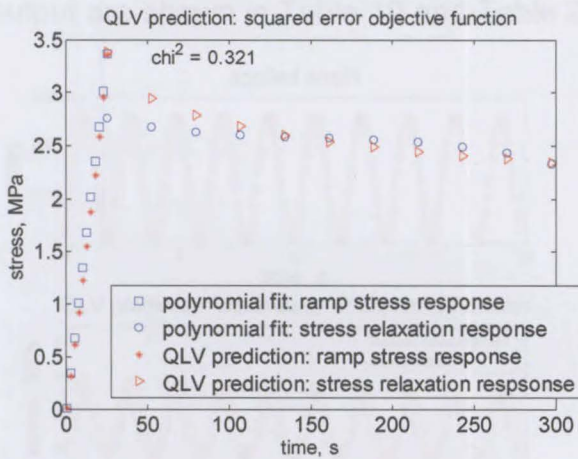


Figure 37: Loadcell stress relaxation prediction: squared error objective function

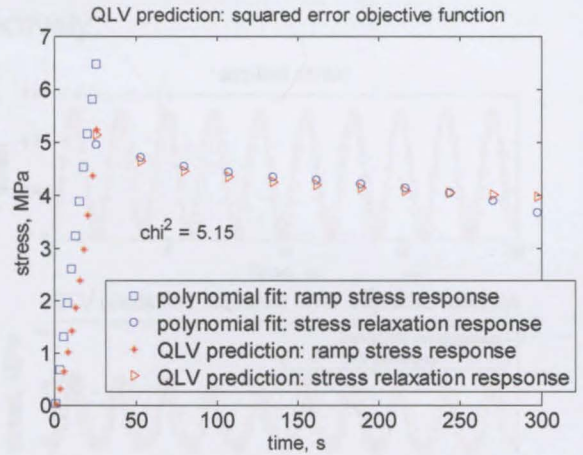


Figure 38: Sensor stress relaxation prediction: squared error objective function

Table 17: Stress relaxation measured by loadcell for relaxation test

Optimisation technique	Maximum stress, $\sigma_f$	Minimum stress, $\sigma_0$	Stress relaxation, $\% \sigma_{relax}$
	MPa	MPa	%
Raw measurements	3.36	2.34	30.5
<i>patternsearch</i> -tool: squared error	3.33	2.51	24.6
<i>patternsearch</i> -tool: chi-squared	3.36	2.34	30.2
Non-linear curve fit-tool	3.30	2.36	28.4

Table 18: Stress relaxation measured by sensor for relaxation test

Optimisation technique	Maximum stress, $\sigma_f$	Minimum stress, $\sigma_0$	Stress relaxation, $\% \sigma_{relax}$
	MPa	MPa	%
Raw measurements	6.47	3.68	43.1
<i>patternsearch</i> -tool: squared error	5.23	3.97	23.9
<i>patternsearch</i> -tool: chi-squared	6.61	4.09	38.1
Non-linear curve fit-tool	6.43	3.71	42.4

The predictive ability of the QLV-function was tested by comparing the predicted stress relaxation that would result from a cyclic strain input to the actual measurements of a cyclic test. Figure 39 and Figure 40 show the results for the loadcell and sensor output respectively. Both graphs were obtained from the QLV function when the QLV-constants that were derived from  $OBJ_1$  were substituted into the function. The curves for the other objective functions are shown in Figure 50 to Figure 53 in Appendix C-5. The values of the actual maximum stress level and predicted maximum stress level for each cycle of the cyclic tests are shown in Table 35 and Table 36 in Appendix C-5 for the loadcell and sensor output respectively. As a summary for Table 35 and Table 36,

the actual stress relaxation and predicted stress relaxation for the loadcell and sensor output are shown in Table 19 and Table 20 respectively.

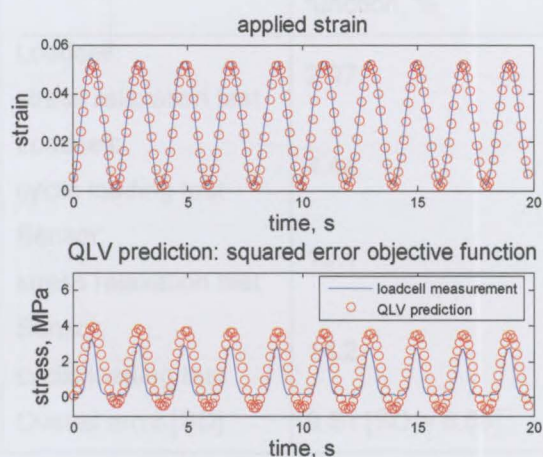


Figure 39: Loadcell output: squared error objective function

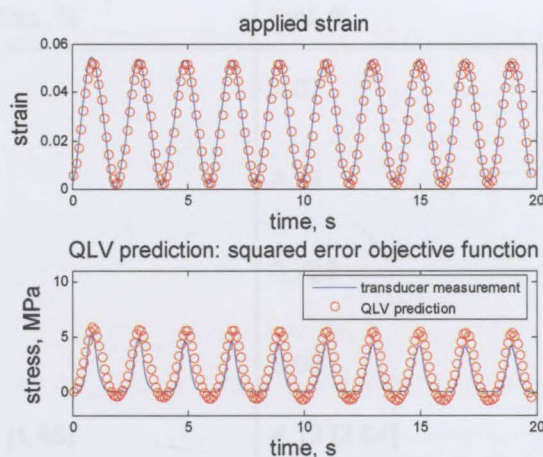


Figure 40: Sensor output: squared error objective function

Table 19: Stress relaxation measured by loadcell for cyclic loading

Optimisation technique	Maximum stress, $\sigma_f$	Minimum stress, $\sigma_0$	Stress relaxation, $\% \sigma_{relax}$
	MPa	MPa	%
Raw measurements	3.27	2.76	15.7
<i>patternsearch</i> -tool: squared error	3.95	3.51	11.2
<i>patternsearch</i> -tool: chi-squared	4.46	3.72	17.1
Non-linear curve fit-tool	3.78	3.37	10.9

Table 20: Stress relaxation measured by sensor for cyclic loading

Optimisation technique	Maximum stress, $\sigma_f$	Minimum stress, $\sigma_0$	Stress relaxation, $\% \sigma_{relax}$
	MPa	MPa	%
Raw measurements	5.44	4.27	21.5
<i>patternsearch</i> -tool: squared error	5.86	5.42	7.4
<i>patternsearch</i> -tool: chi-squared	9.31	7.59	18.5
Non-linear curve fit-tool	7.693	6.725	12.58

From the results in Table 17 to Table 20 it is apparent that the QLV-function overestimates the stress relaxation, except for the cyclic loading results for the sensor output where the QLV-constants were obtained from  $OBJ_1$ . The QLV-constants derived with  $OBJ_1$  resulted in an overestimation of 9.51% [SD = 8.66].  $OBJ_2$  and the least-squares-curve fit tool resulted in an overestimation of 3.84% [SD = 8.66] and 4.13% [SD = 3.64] respectively. The overestimation in stress relaxation for the loadcell and sensor output are shown in Table 21.



Table 21: Estimation error for the QLV-constants

Measurements	Squared error objective function, %	Chi squared objective function, %	Least squares curve fit-tool, %
Loadcell: stress relaxation test	2.97	5.87	2.07
Loadcell: cyclic loading test	4.44	1.45	4.74
Sensor: stress relaxation test	19.1	4.99	0.728
Sensor: cyclic loading test	14.2	3.05	8.98
Overall error [SD]	9.51 [SD = 8.66]	3.84 [1.98]	4.13 [3.64]

## 5.10 Conclusion

Figure 34 shows that there occurred overshoot in the ramp increase in strain. It was stated earlier in the chapter that fast loading rates will result in overshoot, but the loading rate for this study was 10 mm/min, which is slow. The displacement control of the hydraulic cylinder was therefore not tuned to perfection, which resulted in the overshoot as well as the perturbations in the hydraulic cylinder displacement. The motion of the cylinder was however more stable during the cyclic tests.

The system that was used dates from the 1970's, and it is therefore old and not in perfect condition anymore. It was attempted to improve the control over the hydraulic cylinder displacement but it could unfortunately not be improved. Although the test conditions were not perfect, they were sufficient for this study, since the aim was not the determination of representative QLV-constant values for the patella tendon, as was done by Johnson *et al.* (1994).

The polynomials that were fitted to the stress data, i.e. stress response to ramp increase in strain and stress relaxation response, induced errors into the analysis, but it was attempted to minimise its effect. The straight lines fitted to the ramp increase in strain stress response are crude approximations of the actual non-linear stress response that would occur. The induced error stays constant however and it doesn't influence the analysis since the loadcell and sensor output was processed similarly.

The difference in the magnitudes of the different loads as measured with the loadcell and the sensor, can be ascribed to the alignment of the tendon in the test setup, as well as the difference in length of the tendon fibres (Basso *et al.*, 2002). The alignment

of the patella tendon in the test setup might induce greater loads within regions of the patella tendon. This was unlikely in this study since it was ensured that the patella tendon was correctly aligned with regards to its loading axis when it was potted into the steel cylinders.

The loadcell measures an average value of the tendon load whereas the sensor measures local loads. The optic fibre was inserted through the patella tendon in a proximal posterior location. Basso *et al.* (2002) has shown that the posterior fibres are shorter than the anterior fibres, and it has been shown in Chapter 5 that the posterior patella tendon fibres endure greater loads. The loads measured by the sensor will therefore be different to the average load measured by the loadcell. The calibration that was used for the sensor was derived during the *in vitro* tests of Chapter 4. A first order calibration has been used, and the standard error that resulted from this has been shown to be in the region of 12.8 N or 0.105 MPa, which is negligible in terms of the FSO for these tests. Erdemir *et al.* (2002) have shown though that the sensor output must be calibrated with a third order polynomial. Some error will therefore be induced into the analysis with the use of the first order calibration.

The values of constants  $A$  and  $B$  correspond to the ramp increase in strain stress response, and their magnitudes are therefore influenced by the approximation of the straight line. Constant  $C$  corresponds to the elasticity of the patella tendon. The values obtained in this study relates to the value obtained by Johnson *et al.* (1994) which was 0.68. The elasticity of the tendon tested, therefore was in the same range as the tendons tested in the study of Johnson *et al.* (1994). The value of the constant  $\tau_1$  is however an order of magnitude greater than the value obtained in the study of Johnson *et al.* (1994).

This time constant relates to the lower boundary value of the continuous spectrum of relaxation. It is associated with the fast viscous phenomena of the patella tendon. The sample tested was old and it was stored in a frozen environment for at least six months. The moisture content in the tendon would therefore differ from the moisture content of a fresh sample as is depicted by Moon *et al.* (2006), and this would influence its viscous behaviour. The same goes for time constant  $\tau_2$ .

Constant  $\tau_2$  relates to the slow viscous phenomenon of the patella tendon. There is not only variability between the values derived from this study and the literature

(Johnson *et al.*, 1994), but also between the loadcell and sensor output and within the different derivations from the optimisation procedures. The allowed relaxation times for the tests were short, i.e. 5 minutes. Other studies employed relaxation times of 15 minutes (Johnson *et al.*, 1994) and one hour (Abramowitch *et al.*, 2004). The expected value for  $\tau_2$ , i.e.  $5.03e+06$  as derived in the literature (Johnson *et al.*, 1994), falls outside the tested time frame of this study. It is hypothesised that there will be less variability in the derived values if longer relaxation times were allowed.

The test results indicate that the values of constants  $A$ ,  $C$ ,  $\tau_1$  and  $\tau_2$  are not that sensitive to whether the loadcell or sensor output is used in their derivation. The values of constants  $B$  seem to be dependent on whether the loadcell or sensor output is used. The value of constant  $B$  corresponds to the non-linearity of the initial slope of the stress vs. strain curve. If the initial slope of the loadcell output is compared to that of the sensor's, it is clear that the local loads as measured with the sensor were greater than the overall loads measured with the loadcell.

This occurrence of the difference in the measured load with the loadcell and sensor will therefore influence the value of constant  $B$  and can be considered the reason for the difference in the value of constant  $B$ . Overall, there seems to be a difference between the values derived from the loadcell and the sensor output. More tests need to be done in order to see whether the differences are statistically significant.

It was shown that the QLV-function overestimates the stress relaxation except for the case where the QLV-constants are derived from the loadcell output and  $OBJ_1$ . Overall  $OBJ_1$  performed worse whereas  $OBJ_2$  seemed to be more stable in delivering good estimates of the QLV-constants. If  $OBJ_2$  is considered more closely, it is apparent that the error between the QLV-function prediction and the actual measurement, is divided through the value of the actual measurement and the errors are therefore normalised. This enables the optimisation algorithm to perform better.

From the study, the following conclusions can be made: the sensor enables the measurement of local loads within the patella tendon. It is thus possible to investigate the stress relaxation of certain areas within the tendon, something that is not possible with the loadcell. This can help researchers to investigate the biomechanics of the patella tendon and other connective tissues in order to explain certain phenomena and occurrences. The use of  $OBJ_2$  yielded better results than the other applied optimisation

procedures. This can be ascribed to the normalisation of the error, something that was lacking in  $OBJ_1$ . The non-linear curve fit-tool also applied a normalisation procedure, but was dependent on the derivatives of the objective function. Since the objective function is non-linear and the change in function value is small for a large change in the variable values, it did not perform as well as  $OBJ_2$  and the *patternsearch*-tool.

## Chapter 6: *In vivo* investigation into the loading patterns of the patella tendon

### 6.1 Introduction

There is uncertainty on which part of the patella tendon – anterior or posterior – is more highly loaded. Two *in vitro* studies have been conducted with conflicting results (Basso, Amis, Race & Johnson, 2002; Almekinders *et al.*, 2002). The two *in vitro* studies were performed on cadavers and it was not possible to exert the patella tendon to everyday loading conditions. The fibre optic force sensor provides a minimal invasive technique, and the simultaneous instrumentation of the anterior and posterior patella tendon fibres of a volunteer is possible. This will enable the *in vivo* measurement of the differential forces within the patella tendon of a volunteer that performs everyday exercises.

The results of this study will not only give an indication of what part is more highly loaded, but will also lay the way for *in vivo* investigations into the aetiology<sup>vi</sup> and pathogenesis<sup>vii</sup> of pathologies that are known to affect the patella tendon. One of these is Patellar Tendinopathy (PT) that exists within the posterior fibres of the proximal patella tendon. It affects athletes that take part in sports that require jumping, running, cycling or kicking (Martens, Wouters, Burssens & Muller, 1982). This condition is associated with focal tenderness, pain and swelling in the central part of the proximal patella tendon and its characteristic features are disrupted collagen chains, increased ground substance<sup>viii</sup>, more prominent and rounded tenocytes<sup>ix</sup>, neovascularisation<sup>x</sup> and calcifying tendinopathy. Figure 41 shows the common location of PT lesions in the proximal posterior region of the patella tendon on a MRI photograph.

---

<sup>vi</sup> Aetiology: Science that deals with the causes or origin of disease. As described by <http://www.medterms.com/script/main/art.asp?articlekey=2166>, (11/07/2006)

<sup>vii</sup> Pathogenesis: The mechanism by which a certain aetiological factor causes disease. As described by <http://en.wikipedia.org/wiki/Pathogenesis>, (11/07/2006)

<sup>viii</sup> Ground substance: The amorphous extra-cellular material, in which the cells and fibers of connective tissue are embedded, also referred to as the extracellular matrix. As described by <http://en.wikipedia.org/wiki/Groundsubstance>, (02/11/2006)

<sup>ix</sup> Tenocyte: The cell of a tendon, as defined by <http://www.neurolaw.com/Index.cfm?file=t.htm>, (02/11/2006)

<sup>x</sup> Neovascularization: The formation of functional micro-vascular networks with red blood cell perfusion. Perfusion is the process of nutritive delivery of arterial blood to a capillary bed in the biological tissue. As described by <http://en.wikipedia.org/wiki/Groundsubstance>, (02/11/2006)

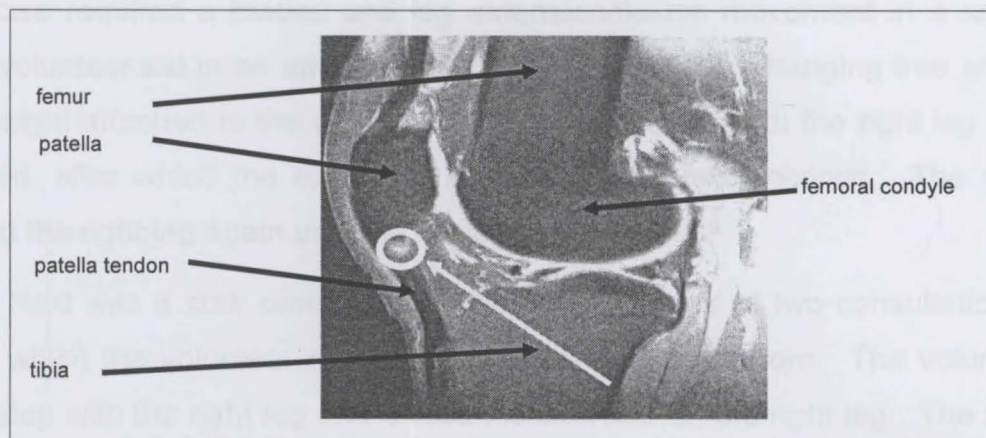


Figure 41: Indication of Patellar Tendinopathy on a MRI photograph

The results of this study will be useful to the treatment and rehabilitative measures for patients suffering from PT and other pathologies. Although the aetiology and pathogenesis of PT is still unknown, it has been hypothesised that the condition might be the result of chronic stress overload (Warden & Brukner, 2003). The flexion angles at which loads inside the patella tendon is a maximum will be identified for the different exercises. Patients suffering from PT should avoid these exercises at these flexion angles since it might cause more damage.

## 6.2 Hardware setup and test procedure

The same anaesthesia procedure that was described in Chapter 4 during the section on the *in vivo* patella tendon test was followed. After the anaesthetic took effect, a 19 gauge needle was inserted under ultrasound guidance through the anterior third and then through the posterior third of the proximal patella tendon in a medial/lateral direction. A piece of sterilised optic fibre was drawn through the needle, leaving the pieces of optic fibre suspended inside the patella tendon after the needle was pulled out.

The two pieces of optic fibre were connected to the sensor which was fixed on a knee brace containing a goniometer. Care was taken during the attachment of the knee brace onto the volunteer's leg to ensure alignment of the brace's hinge joint and the rotation axes of the knee joint. The test procedure involved four exercises that each consisted of at least three trials with a maximum of five trials.

The first exercise was a one leg squat. The volunteer had to rise and sit back down from a chair unassisted. The exercise started with the knee at a flexion angle of  $110^\circ$  and ended in the same position. During the exercise the volunteer was asked to keep a controlled contraction in order to load the patella tendon maximally. The second

exercise required a loaded one leg extension/flexion movement in a seated position. The volunteer sat in an upright position with the right leg hanging free at 90° with a 10 kg weight attached to the ankle. The exercise started with the right leg being fully extended, after which the extension was held for a few seconds. The volunteer then flexed the right leg again until the flexion angle was 90°.

Next was a stair climbing exercise that consisted of two consultation room steps, onto which the volunteer needed to walk up and down from. The volunteer gave the first step with the right leg and ended the exercise on the right leg. The fourth and last exercise entailed a jump from a 34 cm high elevation where the volunteer needed to land only on the right leg. A comfortable landing was ensured by allowing the volunteer to flex the right leg as much as was needed on impact. After completion of the four exercises and removal of the two pieces of optic fibre under sterile conditions, new dressing was applied onto the insertion sites and they were covered. Each volunteer received pain killers and were instructed by the orthopaedic surgeon to contact him if they experienced any discomfort.

The test population consisted of ten volunteers (nine males {ages 20 to 32} and one female {age 20}) from the engineering faculty and the health sciences faculty of the University of Stellenbosch. Each volunteer was informed of the test procedure and the risks involved before commencement of a test and were free to abandon the test at any time. The study was approved by the Committee for Human Research of the University of Stellenbosch, project number N05/02/023.

### **6.3 Data processing procedure**

The data processing procedure is illustrated in Figure 42. The data was imported and smoothed as described in Chapter 4. The anterior and posterior loads were then compared to one another on the basis of the FSO. Analysis of the raw sensor recordings showed that the anterior channel had a positive offset from the posterior channel, i.e. the maximum sensor output from the anterior channel were greater than that from the posterior channel. The mean offset between the anterior channel and the posterior channel was 0.471 V [SD = 0.158V]. The test results in Chapter 4 indicated an inherent offset between the two channels averaging at 0.0367 V [SD = 0.00121V] when the optic fibre was unloaded, and this offset therefore represented 8% of the offset that occurred during the *in vivo* study.

When the forces were recorded during a test, it was unlikely that the patella tendon was unloaded at any time during the test. The maximum raw voltage output from any two of the sensor's channels would therefore not correspond to a zero load condition, but rather to a minimum load condition<sup>xi</sup>. When the FSO of the anterior channel was calculated, the anterior signal was scanned for the maximum voltage output and the remaining voltage outputs were subtracted from this value. Since the patella tendon was loaded, it meant that the proposed difference in load between the anterior tendon fibres and posterior tendon fibres would be measured by the sensor. This principle serves as a plausible explanation for the additional recorded offset in the anterior and posterior output.

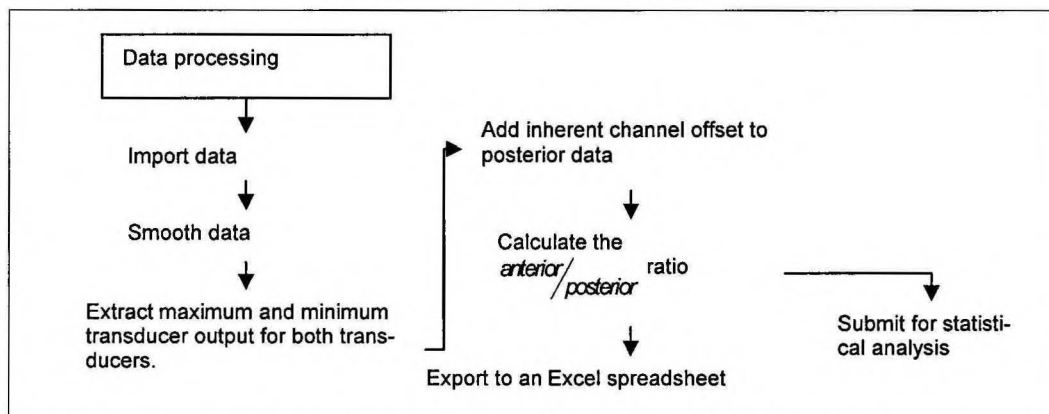


Figure 42: Steps followed during processing of the *in vivo* data

When the FSO of the posterior channel was calculated, the voltage values were also subtracted from the reference value determined for the anterior signal. In following this approach, it was ensured that the proposed difference in the anterior tendon fibres and posterior fibres for the maximum sensor output was maintained. The inherent offset between the anterior channel and the posterior channel was then subtracted from the posterior FSO to remove the bias in the output signals.

After the FSO was computed the ratio of the anterior and posterior values were computed. A ratio greater than one indicated that the load in the anterior tendon fibres was greater than the load in the posterior tendon fibres and vice versa for a ratio less than one.

The static sensitivity determined during the *in vivo* calibration procedure in Chapter 4 was used to give a ballpark indication of the force values for the recordings by the

<sup>xi</sup> Recall that the force transducer output diminishes as the load increases inside the patella tendon



posterior channel. This static sensitivity was also used for the anterior channel, but since it became clear that the anterior channel is more sensitive, the static sensitivity needed to be adapted for the anterior channel. This was achieved by multiplying the static sensitivity for the posterior channel by the ratio of the posterior sensitivity and anterior sensitivity determined during the *in vitro* patella tendon test. The results were also submitted for statistical analysis by a statistician.

## 6.4 Results

Tables with the results for the different tests are shown in Appendix B. A summary of the test results is shown in Table 22. It is clear that the posterior loads were all greater than the associated anterior loads when the ratios in Table 22 are considered. The FSO values for the anterior channel and the posterior channel were submitted for statistical analysis. A repeated measures analysis was done to see whether the posterior loads were greater than the anterior loads.

Table 22: *In vivo* test results for the different exercises

Exercise	<i>anterior</i> / <i>posterior</i>	Anterior load, N [SD]	Posterior load, N [SD]
Squat: concentric contraction, n=8	0.556 [0.399]	1380 [878]	3870 [1810]
Squat: eccentric contraction, n=8	0.540 [0.410]	1280 [790]	3880 [2040]
Leg extension, n=8	0.331 [0.168]	693 [336]	3280 [1557]
Step up, n=7	0.278 [0.0939]	629 [349]	3090 [1440]
Step down, n=7	0.294 [0.0662]	696 [309]	3280 [1520]
Jump, n=7	0.338 [0.145]	1150 [482]	6420 [3240]

From the repeated measures analysis for the different tests the probabilities of the posterior loads being greater than the anterior loads could be derived. The following probabilities were derived for a confidence interval of 95% as given in Table 23. A probability value of  $p < 0.025$  indicated a statistical significant condition for the confidence interval of 95%.

Samples of the sensor output for the anterior channel and posterior channel as well as box plots for the different tests are shown in Appendix B. The results of Table 22 suggest that the posterior loads in the proximal patella tendon were greater than the anterior loads for all the exercises. Table 23 shows that the results for the leg extension exercise, step exercise and jump exercise were statistically significant with  $p < 0.025$  for a confidence interval of 95%. The results for the squat exercise were not statistically

significant, but the trend of the posterior loads being greater than the anterior loads still applied. The assumption can thus be made that, had there been more volunteers, a statistical significant condition would exist for the squat exercise.

Table 23: Probabilities as determined by the repeated measures analysis for the condition that the anterior loads are smaller than the posterior loads for the different exercises

Exercise	Probability, $p$
Squat: concentric contraction	0.132
Squat: eccentric contraction	0.115
Leg extension: concentric contraction	0.0213
Leg extension: eccentric contraction	0.0211
Step up	0.0194
Step down	0.0188
Jump	0.00193

## 6.5 Conclusion

The results for this *in vivo* study support the hypothesis that there exist differential forces inside the patella tendon and that the posterior loads are significantly greater than the anterior loads for the exercises that were performed. The results of this study can provide some guidance in the rehabilitation and treatment of patients who suffer from pathologies such as PT.

Table 22 and the graphs in Appendix B show that the loads in the posterior fibres were greatest when the volunteers took part in exercises where there were shock impacts on the knee joints, i.e. step and jump exercises. These exercises should therefore be avoided, since the elevated loads might cause more damage to the already damaged posterior tendon fibres. Non-impact exercises are proposed, but with the following advice. During the squat exercise, the maximum load occurred at maximum flexion. It is suggested that patients should not perform squat exercises where the flexion angle exceeds 80°. The same principle applies for the leg extension exercise. In order to avoid stress overload, the patient should not fully extend the injured leg while doing leg extensions, but rather stop at 10° flexion.

It has been shown that the posterior loads occurring in patella tendon when volunteers jumped from an elevation are five times greater than the anterior loads. Since PT is most common in patients who take part in exercises that require jumping, and since the lesion occurs in the posterior fibres, the chronic stress overload theory might be

true. More tests need to be done in order to prove the hypothesis beyond doubt. These tests' populations should include patients who suffer from PT.

During the study the following limitations were experienced. When the first volunteer was tested, the posterior optic fibre snapped when the subject performed his second jump. The reason for this was because the brace to which the sensor was attached shifted when the subject landed and this caused the fibre to tighten and snap. This was corrected by tightening the brace more during the jumps and also inserting longer pieces of fibre to allow relative movement. Tests confirmed that the allowed relative movement didn't influence the force measurements.

During the test on the second volunteer, the batteries driving the optic fibre force transducer's circuit ran low and although it was still possible to distinguish between the anterior and posterior optic fibre outputs, the FSO for both channels were too low and the measurements were discarded. For the third volunteer and the step and jump exercises of the ninth volunteer, the anterior channel receiver circuit experienced technical difficulties which could not be rectified during the test. These recordings were also discarded.

## Chapter 7: Conclusions

Three types of transducers were considered for this study. The first type's working principle was based on the variation of magnetic fields, the second type on the variation of electrical resistance, and the third type was based on light intensity modulation. It was decided to make use of a sensor that is based on light intensity modulation through the mechanical deformation of the optic fibre geometry. This sensor is minimally invasive, which leads to fast instrumentation of volunteers and shorter recovery periods after testing. The optic fibre is inserted through the cross-section of the ligament or tendon and its presence has a negligible effect on the normal orientation of the connective tissue's fibres due to its small diameter. The sensor consisted of two transmitter units, two receiver units, two pieces of optic fibre and the transducer driving circuit.

Three tests were conducted which aided in the characterisation of the sensor's capabilities and performance - a loading test in a hydraulic press and an *in vitro* loading test in a patella tendon. The aim was to characterise:

- the hysteresis in the force recordings;
- the sensor's frequency response;
- the signal-to-noise ratio for the different tests;
- the sensitivity of the two channels of the sensor;
- the measurement repeatability of the sensor; and
- the influence of two optic fibres in close proximity on force measurements.

The sensor displays significant hysteresis in its force measurements, i.e. 20%FSO [SD = 8.88], which is in the same order of magnitude compared to the results of Erdemir *et al.* (2002) who tested a similar sensor. The frequency response of the sensor was found to be sufficient for the purposes of this study, although biomechanical experiments will require better frequency response in other applications. Due to the termination technique of the optic fibre ends when it is connected to the ST-connectors, the force measurement repeatability of the sensor is poor, i.e. 102%FSO [SD = 53.2] and 83.1%FSO [SD = 7.50] for the anterior and posterior channels respectively.

General calibrations for the sensor will lead to inaccurate force approximations of the actual occurring loads and subject specific calibrations should therefore be used in-

stead of general calibrations, as was found in this study and by Erdemir *et al.* (2002). The influence of optic fibres in close proximity on sensor force recordings appears to be negligible if subject-specific calibrations are used.

The use of the sensor for the derivation of the QLV-constants resulted in slightly different values from the QLV-constants derived from the loadcell during the *in vitro* loading test of the patella tendon. Since the sensor measures local loads, the derived QLV-constants will correspond to the local area where the measurements were taken. If the patella tendon had a uniform load distribution, the QLV-constants' values derived from the loadcell and the sensor would be similar.

It was found that the  $\chi^2$ -error objective function gave the best results and that its use with the *patternsearch*-tool resulted in the best predictions of the QLV-constants. Although test conditions were not ideal during the *in vitro* test, it was sufficient for the purpose of this study. It is however advised that similar experiments in future studies be conducted on more accurate and reliable test equipment, in order to deliver publishable results.

During the *in vivo* study posterior fibre loads were found to be greater than anterior fibre loads in the proximal patella tendon for the set of exercises that were performed. The results were statistically significant ( $P = 95\%$ ,  $p < 0.025$ ) for the leg extension, step and jump exercises. The results of the squat exercises support the tendency that the posterior loads are greater, but the results were not statistically significant. This is the first *in vivo* study that investigates the differential loads to the author's knowledge.

The results have a positive contribution on rehabilitative and treatment measures for PT patients. It was possible to determine flexion ranges in which the loads were a maximum. If patients suffering from PT perform these exercises, they run the risk of damaging the patella tendon further due to the greater loads that occur in the affected areas. The following exercises should be avoided:

- Squat exercise: avoid flexion beyond 90°
- Knee extension exercise: avoid extension beyond 10°
- Jump exercise: avoid exercises that involve jumping altogether

## Chapter 8: Recommendations

During the property characterisation of the sensor, it was apparent that the performance of the patella tendon is highly influenced by the material properties of the optic fibres as well as by the termination of the optic fibre ends at the ST-connectors. No published studies could be found that characterises the influence of the optic fibre properties on the sensor output. There might be commercially available optic fibres that will be better suited for use with the sensor. The problem with commercial fibres is that they are designed to minimise transmission losses whereas the working principle of the sensor is based on transmission losses.

The termination techniques of the optic fibre ends induce variability and have a negative impact on force measurement repeatability. Other connectors are available and might decrease the force measurement errors that result from the use of the ST-connectors. A study that investigates the sensor performance for different types of optic fibres and connectors will definitely make a contribution to the biomechanical field, since sensors have a huge advantage over other sensors because of its ease of use and minimal invasive character.

The *in vitro* study into the stress relaxation behaviour of the patella tendon with the sensor opened new possibilities since a more detailed analysis of the stress relaxation for different regions within the patella tendon can be done. This will yield more detailed empirical mathematical models. Due to the minimal invasive character of the patella tendon, its use in *in vivo* investigations into the viscoelastic properties of the patella tendon can result in significant contributions to research, due to the novelty of such studies.

## References

- Abramowitch SD & Woo SL-Y. 2004. An improved method to analyze the stress relaxation of ligaments following finite ramp time based on the quasi-linear viscoelastic theory. *Journal of Biomechanics* 126: 92-97.
- Almekinders LC, Vellema JH & Weinhold PS. 2002. Strain patterns in the patellar tendons and the implication for patellar tendinopathy. *Knee Surgery, Sports Traumatol, Arthroscopy* 10: 2-5.
- Anderson FC & Pandy MG. 2001. Dynamic optimisation of human walking. *Journal of Biomechanical Engineering* 123: 381-390.
- Arndt AN, Komi PV, Brüggemann G-P & Lukkariniemi J. 1998. Individual muscle contributions to the in vivo Achilles' tendon force. *Clinical Biomechanics* 13: 532-541.
- Bailey D. 2003. *Practical fiberoptics*. Elsevier, First edition: 42-82.
- Basso O, Amis AA, Race A, Johnson DP. 2002. Patella tendon fibre strains: Their differential responses to quadriceps tension. *Clinical Orthopaedics Related Research* 400: 246-253.
- Blevins FT, Hecker AT, Bigler GT, Boland AL & Hayes WC. 1994. The effects of donor age and strain rate in the biomechanical properties of bone-patella tendon – bone allografts. *The American Journal of Sports Medicine* 22: 328-333.
- Callister, W.D. Jr 2000. *Material science and engineering, an introduction*. 5th edition. John Wiley & Sons, Inc. 487-91.
- Chernoff H. 1954. The use of maximum likelihood estimates in chi square tests for goodness of fit. *The Annals of Mathematic Statistics* 25: 579-586.
- Coleman TF, Li Y. 1996. An interior trust region approach for non-linear minimisation subject to bounds. *SIOPT* 6: 418-445.
- Coleman TF, Li Y. 1994. On the convergence of reflective Newton methods for large-scale nonlinear minimisation subject to bounds. *Mathematical programming* 67: 189-224.
- Cooper DE, Deng XH, Burstein AL & Warren RF. 1993. The strength of the central third patellar tendon graft. *American Journal of Sports Medicine* 23: 818-824.
- Crowinshield RD. 1978. Use of optimisation techniques to predict muscle forces. *Journal of Biomechanics* 100: 88-92.
- Dortmans LJMG, van de Ven AAF & Sauren AAHJ. 1994. A note on the reduced creep function corresponding to the quasi-linear viscoelastic model proposed by Fung. *Journal of Biomechanical Engineering* 116: 373-375.
- Erdemir A, Hamel AJ, Piazza SJ & Sharkey NA. 2003. Fiberoptic measurement of tendon forces is influenced by skin movement artifact. *Journal of Biomechanics* 36: 449-455.

- Erdemir A, Piazza SJ & Sharkey NA. 2002. Influence of loading rate and cable migration on fiberoptic measurement of tendon force. *Journal of Biomechanics* 35: 857-862.
- Figliola RS & Beasley DE. 2006. Basic concepts of measurement methods. In: *Theory and design for mechanical measurements, Fourth edition*. Wiley & Sons Inc.: 1-29.
- Figliola RS & Beasley DE. 2006. Probability and statistics. In: *Theory and design for mechanical measurements, Fourth edition*. Wiley & Sons Inc.: 109-141.
- Finni T, Komi PV & Lepola V. 2000. In vivo human triceps surae and quadriceps femoris muscle function in a squat jump and counter movement jump. *European Journal of Applied Physiology* 83: 416-426.
- Finni T, Komi PV & Lukkariniemi J. 1998. Achilles tendon loading during walking, application of a novel optic fiber technique. *European Journal of Applied Physiology* 77: 289-291.
- Fung YC. 1993. *Biomechanics: Mechanical properties of living tissue*. Springer, New York, second edition.
- Fung YC. 1972. Biomechanics, its foundations and objectives, in *Stress-strain-history relations of soft tissues in simple elongations*. Prentice-Hall, Inc. 181-208.
- Fung YC. 1965. Prototypes of theory of elasticity and viscoelasticity. In: *Foundations of solid mechanics*. Prentice Hall Inc. 1-30.
- Hamilton B & Purdam C. 1973. Patellar tendinosis as an adaptive process: a new hypothesis. *British Journal of Sports Medicine* 38: 758-761.
- Hansen P, Bojsen-Moller J, Aagaard P, Kjaer M & Magnusson SP. 2006. Mechanical properties of the human patellar tendon, in vivo. *Clinical Biomechanics* 21: 54-58.
- Hashemi J, Chandrashekar N & Slaughterbeck J. 2005. The mechanical properties of the human patellar tendon are correlated to its mass density and are independent of sex. *Clinical Biomechanics* 20: 645-652.
- Haut RC & Powlison AC. 1990. The effects of test environment and cyclic stretching on the failure properties of the human patellar tendon. *Journal of Orthopaedic Research* 8: 532-540.
- Herzog, W. & Read, L.J. 1993. Lines of action and moment arms of the major force-carrying structures crossing the human knee. *Journal of Anatomy*, 182: 213-230.
- Hewitt J, Guilak F, Glisson R & Vail TP. 2001. Regional material properties of the human hip joint capsule ligaments. *Journal of Orthopaedic Research* 19: 359-364.
- Johnson GA, Tramaglino DM, Levine RE, Ohno K, Choi N-Y & Woo SL-Y. 1994. Tensile and viscoelastic properties of human patellar tendon. *Journal of Orthopaedic Research* 12: 796-803.
- Kellis, E. & Baltzopoulos, V. 1999. In vivo determination of the patella tendon and hamstring moment arms in adult males using videofluoroscopy during submaximal knee extension and flexion. *Clinical Biomechanics*, 14:118-124.



- Komi PV, Belli A, Huttunen V, Bonnefoy R, Geysantt A & Lacour JR. 1996. Optic fibre as a transducer of tendomuscular forces. *European Journal of Applied Physiology* 72: 278-280.
- Komistek RD, Kane TR, Mahfouz M, Ochoa JA & Dennis DA. 2005. Knee mechanics: A review of past and present techniques to determine in vivo loads. *Journal of Biomechanics* 38: 215-228.
- Komistek RD, Dennis DA & Mahfouz M. 2003. In Vivo fluoroscopic analysis of the normal human knee. Symposium: Knee Kinematics and Total Knee Replacement Design. Lippincott Williams & Wilkins, Inc. 410: 69-81.
- Komistek RD, Sthiel JB & Dennis DA. 1998. Mathematical model of the lower extremity joint reaction forces using Kane's method of dynamics. *Journal of Biomechanics* 31: 185-189.
- Krevolin, J.L., Pandy, M.G. & Pearce, J.C. 2004. Moment arm of the patella tendon in the human knee. *Journal of Biomechanics* 37: 785-788.
- Levenberg K. 1944. A method for the solution of certain problems in least squares. *Quarterly Applied Mathematics* 2:164-168.
- Liu Q & Subhash G. 2006. Characterisation of viscoelastic properties of polymer bar using iterative deconvolution in the time domain. *Mechanics of Materials* 38: 1105-1117.
- Lu TW, O'Connor JJ, Taylor SJG & Walker PS. 1998. Validation of a lower limb model with in vivo femoral forces telemetered from two subjects. *Journal of Biomechanics* 31: 63-69.
- Lu TW, Taylor SJG, O'Connor JJ & Walker PS. 1997. Influence of muscle activity on the forces in the femur: an in vivo study. *Journal of Biomechanics* 30: 1101-1106.
- Martens M, Wouters A, Bursens A & Muller JC. 1982. Patellar tendonitis: pathology and results of treatment. *Acta Orthopaedic Scand* 53: 445-450.
- Meyer K. 2003. Standard handbook of biomedical engineering and design. New York: McGraw Hill. 5.1-5.26.
- Mikosz RP, Andriacchi TP & Anderson GB. 1988. Model analysis of factors influencing the prediction of muscle forces at the knee. *Journal of Orthopaedic Research* 6: 205-214.
- Moon DK, Woo SL-Y, Takakura Y, Gabriel MT & Abramowitch SD. 2006. The effects of refreezing on the viscoelastic and tensile properties of ligaments. *Journal of Biomechanics* 39: 1153-1157.
- Nigul I & Nigul U. 1987. On algorithms of evaluation of Fung's relaxation function parameters. *Journal of Biomechanics* 4: 343-352.
- Oza A, Vanderby R & Lakes RS. 2006. Generalised solution for predicting relaxation from creep in soft tissue: Application to ligament. *International Journal of Mechanical Sciences* 48: 662-673.
- Piazza SJ & Delp SL. 2001. Three dimensional dynamic simulation of total knee replacement motion during a step-up task. *Journal of Biomechanical Engineering* 123: 559-606.

- Ravary B, Pourcelot P, Bortolussi C, Konieczka S & Crevier-Denoix N. 2004. Strain and force transducers used in human and veterinary tendon and ligament biomechanical studies. *Clinical Biomechanics* 19: 433-447.
- Schipplein OD & Andriacchi TP. 1991. Interaction between active and passive knee stabilisers during level walking. *Journal of Orthopaedic Research* 9: 113-119.
- Seireg A & Arvikar RJ. 1973a. The prediction of muscular load sharing and joint forces in the lower extremities during walking. *Journal of Biomechanics* 8: 89-102.
- Seireg A & Arvikar RJ. 1973b. A mathematical model for evaluation of forces in lower extremities of the musculo-skeletal system. *Journal of Biomechanics* 6: 313-326.
- Shigley JE & Mischke CR. 2001. Stress. In: *Mechanical Engineering and Design, 6<sup>th</sup> edition*. McGraw Hill. 103-104.
- Stewart J. 1999. Techniques of integration. In: *Calculus: 4<sup>th</sup> edition*. GWO: 550-554
- Thomopoulos S, Williams GR, Gimbel JA, Favata M & Soslowky LJ. 2003. Variation of biomechanical, structural and compositional properties along the tendon to bone insertion site. *Journal of Orthopaedic Research* 21: 413-419.
- Toms SR, Dakin GJ, Lemons JE & Eberhardt AW. 2002. Quasi-linear viscoelastic behaviour of the human periodontal ligament. *Journal of Biomechanics* 35: 1411-1415.
- Vriend NM & Kren AP. 2004. Determination of the viscoelastic properties of elastomeric materials by the dynamic indentation method. *Polymer Testing* 23: 369-375.
- Warden SJ & Brukner P. 2003. Patellar tendinopathy. *Clinical Sports Medicine* 22: 743-759.
- Wills DJ, Picton DCA & Davies WIR. 1972. An investigation of the viscoelastic properties of the periodontum in monkeys. *Journal of Periodontal Research* 7: 42-51.
- Woo SL-Y, Debski RE, Withrow JD & Jansushek MA. 1999. Biomechanics of knee ligaments. *The American Journal of Sports Medicine* 27: 533-543.
- Wu X, Levenston ME & Chaikof EL. 2006. A constitutive model for protein-based materials. *Biomaterials* 27: 5315-5325.
- Yamamoto K, Hirokawa S & Kawada T. 1998. Strain distribution in the ligament using photoelasticity. A direct application to the human ACL. *Medical Engineering & Physics* 20: 161-168.

## Appendix A: Results from the sensor output tests

### A-1 Hydraulic press loading test

The calibration constants and standard deviation as calculated for the anterior and posterior channel of the sensor are shown in Table 24 to Table 28.

Table 24: Anterior channel calibration: 250 N, 20 mm plate

Calibration	Calibration constants						SD
	1	2	3	4	5	6	N
1st order	2390	-21.7					19.4
2nd order	1.19e04	112	-0.124				16.1
3rd order	1.03e05	-3.61e03	1.70e03	-3.33			17.5
4th order	6.80e06	-1.31e06	8.90e04	-182	-0.642		18.5
5th order	-1.19e08	3.75e07	-4.09e06	1.92e05	-1.50e03	-0.179	20.6

Table 25: Anterior channel calibration: 500 N, 20 mm plate

Calibration	Calibration constants						SD
	1	2	3	4	5	6	N
1st order	3.60e3	5.44					13.2
2nd order	-4.79e03	4.26e03	-8.39				10.3
3rd order	-2.35e04	-20.5	4.01e03	-6.15			11.2
4th order	1.71e06	-4.92e05	3.99e04	2.93e03	-1.96		10.9
5th order	-5.17e07	1.94e07	-2.61e06	1.43e05	1.20e03	0.790	10.6

Table 26: Anterior channel calibration: 500 N, 15 mm plate

Calibration	Calibration constants						SD
	1	2	3	4	5	6	N
1st order	2.54e03	4.79					32.9
2nd order	1.21e03	2.31e04	11.1				35.9
3rd order	2.51e04	-5.84e04	2.82e03	4.25			39.2
4th order	-1.96e05	9.55e04	-1.36e04	3.09e03	2.96		43.7
5th order	9.10e06	-4.49e06	8.04e05	-6.06e04	4.10e03	2.00	49.1

Table 27: Posterior channel calibration: 250 N, 20 mm plate

Calibration	Calibration constants						SD
	1	2	3	4	5	6	N
1st order	2.81e03	-4.27					9.41
2nd order	5.87e03	2.31e03	2.00				8.93
3rd order	-9.38e04	1.81e04	1.90e03	3.93			9.67
4th order	-6.11e06	9.65e05	-3.95e04	2.91e03	1.61		10.3
5th order	3.68e08	-8.52e07	6.92e06	-2.23e05	4.86e03	-0.734	10.7

Table 28: Posterior channel calibration: 500 N, 20 mm plate

Calibration	Calibration constants						SD
	1	2	3	4	5	6	N
1st order	2.63e03	5.77					16.1
2nd order	-2.51e03	3.10e03	-7.64				14.5
3rd order	-1.18e04	805	2.87e03	-4.64			15.8
4th order	1.89e05	-8.25e04	9.03e03	2.56e03	-2.92		17.4
5th order	-5.80e06	2.92e06	-5.30e05	3.86e04	1.90e03	-1.66	19.4

In Table 29 and Table 30 the parameters, i.e. linearity error, static sensitivity error, zero error, repeatability and sensor FSO, are reported which was based on the sensor calibrations. Table 31 and Table 32 contain the static sensitivity of the sensor's channels.

N (Plate)	Calibration	Linearity error, % FSO	Static sensitivity error, mV	Zero error, mV	Repeatability, FSO	Sensor FSO, V
250 (20 mm)	1st order	5.48	102	6.33		
	2nd order	5.87	14.1	4.31		
	3rd order	5.20	10.5	5.39	0.27	0.0050
	4th order	4.53	104	5.44		
	5th order	4.82	107	5.80		
500 (20 mm)	1st order	3.81	31.7	8.71		
	2nd order	3.76	71.7	7.05		
	3rd order	4.21	18.3	6.78	0.0768	0.160
	4th order	3.81	33.8	8.83		
	5th order	3.93	31.8	8.74		

Table 29: Results from the calibrations for anterior channel

Load, N (Plate)	Calibration	Linearity error, % FSO	Static sensitivity error, N/V	Zero error, N	Repeatability, FSO	Sensor FSO, V
250 (20 mm)	1st order	9.31	182	12.6	0.15423	0.101
	2nd order	9.06	147	9.93		
	3rd order	8.63	156	10.5		
	4th order	7.11	162	10.9		
	5th order	7.26	179	12.0		
500 (20 mm)	1st order	3.90	91.9	7.18	0.0807	0.137
	2nd order	3.16	69.7	5.44		
	3rd order	2.85	73.9	5.77		
	4th order	2.58	70.8	5.53		
	5th order	1.95	67.8	5.30		
500 (15 mm)	1st order	13.0	163	18.0	0.125	0.185
	2nd order	12.9	173	19.1		
	3rd order	12.3	185	20.5		
	4th order	12.0	202	22.4		
	5th order	11.4	225	24.9		

Table 30: Results from the calibrations for posterior channel

Load, N (Plate)	Calibration	Linearity error, % FSO	Static sensitivity error, N/V	Zero error, N	Repeatability, FSO	Sensor FSO, V
250 (20 mm)	1st order	5.38	102	5.32	0.207	0.0859
	2nd order	5.87	94.1	4.91		
	3rd order	5.20	99.5	5.19		
	4th order	4.53	104	5.44		
	5th order	4.62	107	5.60		
500 (20 mm)	1st order	3.81	81.7	8.71	0.0758	0.188
	2nd order	3.79	71.7	7.65		
	3rd order	4.21	76.3	8.14		
	4th order	3.81	82.8	8.82		
	5th order	3.93	91.3	9.74		

## Appendix A: Results from the sensor output tests

Table 31: Static sensitivity for each test – anterior channel.

Sensor	Load, N (plate, mm)	Calibration	Mean, N/V	SD
Anterior	250 (20) FSO = 0.101	1st	2.39e03	
		2nd	1.83e03	390
		3rd	1.9e03	261
		4th	1.72e03	713
		5th	1.58e03	1.08e03
Average			1.89 e03	612
	500 (20) FSO = 0.137	1st	3.60e03	
		2nd	3.94e03	213
		3rd	3.86e03	149
		4th	3.65e03	287
		5th	3.41e03	793
Average			3.69e03	361
	500 (15) FSO = 0.185	1st	2.54e03	
		2nd	2.42e03	75.1
		3rd	2.58e03	104
		4th	2.63e03	178
		5th	2.74e03	467
Average			2.58e03	206

Table 32: Static sensitivity for each test – posterior channel.

Sensor	Load, N (plate, mm)	Calibration	Mean, N/V	SD
Posterior	250 (20) FSO = 0.0859	1st	2.81e03	
		2nd	2.57e03	167
		3rd	2.45e03	295
		4th	2.65e03	156
		5th	2.95e03	705
Average			2.69e03	331
	500 (20) FSO = 0.188	1st	2.63e03	
		2nd	2.88e03	152
		3rd	2.80e03	93.1
		4th	2.74e03	100
		5th	2.65e03	272
Average			2.74e03	154

## A-2 In vitro patella tendon loading test

The calibration constants and each calibration's estimated error in force prediction are shown for the anterior channel and posterior channel in Table 33 and Table 34 respectively.

Table 33: Calibration constants for anterior channel

Calibration	Calibration constants						SD
	1	2	3	4	5	6	N
1st order	3.22e03	11.5					19.5
2nd order	-1.07e04	4.35e03	2.19				17.1
3rd order	-1.23e04	-8.40e03	4.24e03	2.83			17.4
4th order	1.26e05	-5.02e04	-4.93e03	4.14e03	3.31		17.5
5th order	-5.37e07	2.11e07	-2.81e06	1.39e05	1.63e03	12.7	16.8

Table 34: Calibration constants for posterior channel

Calibration	Calibration constants						SD
	1	2	3	4	5	6	N
1st order	2.36e03	0.932					12.8
2nd order	1.38e04	2.17e03	3.41				12.6
3rd order	-102385	2.50e04	831	13.8			9.55
4th order	1.09e06	-4.62e05	6.21e04	-397	21.0		8.67
5th order	-6.02e06	3.65e06	-8.42e04	8.53e04	-908	23.5	8.62



Figure 44: Dashpot and elastic spring in series free body diagram.

First consider the dashpot and elastic spring in series. The free body diagram shown in Figure 44, illustrates that the force will stay constant through the dashpot and the elastic spring.

$$F = F_s = F_d = F_c = \mu \dot{x} = kx \quad \text{Equation 45}$$

Equation 45

The total displacement for the dashpot and elastic spring will be

$$x = x_s + x_d = \frac{F}{k} + \frac{F}{c} \quad \text{Equation 46}$$

Equation 46

After manipulation of Equation 45 and Equation 46, the following can be derived.

## Appendix B: QLV model of patella tendon stress relaxation

### B-1 Linear solid model

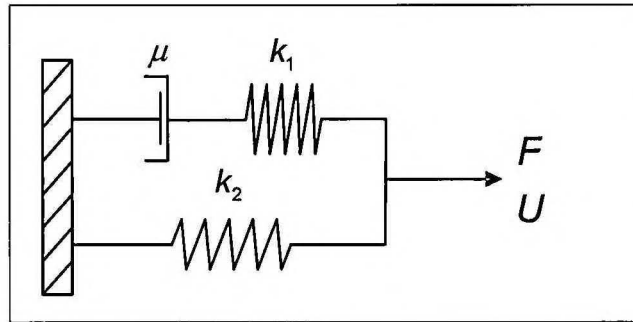


Figure 43: Linear solid model

Consider the linear solid model having a dashpot and elastic spring in parallel with another elastic spring, Figure 43. The dashpot has a viscosity constant,  $\mu$ , the elastic spring in series with the dashpot has a spring constant,  $k_1$ , and the spring in parallel has a spring constant,  $k_2$ . If a constant force,  $F$ , is exerted on the model as is shown in Figure 43, the kinematical behaviour of the linear elastic model can be described by

$$U(t)_{total} = U(t)_{c+k_1} = U(t)_{k_2}, \tag{Equation 43}$$

whereas the dynamic behaviour can be described by

$$F(t)_{total} = F(t) = F(t)_{\mu+k_1} + F(t)_{k_2} = \alpha F(t)_1 = (1-\alpha)F(t)_2 \text{ with } \alpha \text{ a constant} \tag{Equation 44}$$

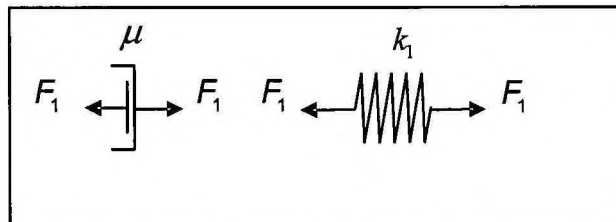


Figure 44: Dashpot and elastic spring in series free body diagram

First consider the dashpot and elastic spring in series. The free body diagram shown in Figure 44, illustrates that the force will stay constant through the dashpot and the elastic spring

$$F_1 = F_\mu = F_{k_1} \Rightarrow F_1 = \mu \dot{u}(t) = k u(t) \tag{Equation 45}$$

The total displacement for the dashpot and elastic spring will be

$$u_{total} = u_\mu + u_{k_1} \Rightarrow \dot{u}_{total} = \dot{u}_\mu + \dot{u}_{k_1} \tag{Equation 46}$$

After manipulation of Equation 45 and Equation 46, the following can be derived



$$\dot{u} = \frac{F_1}{\mu} + \frac{\dot{F}_1}{k_1} \Rightarrow F_1 = \mu \left( \dot{u} - \frac{1}{k_1} \dot{F}_1 \right)$$

since

$$F_1 = \alpha F \Rightarrow \dot{F}_1 = \alpha \dot{F}$$

Equation 47

therefore

$$F_1 = \mu \left( \dot{u} - \frac{1}{\alpha k_1} \dot{F} \right)$$

If the other spring is considered, the force,  $F_2$ , can be defined by means of Hooke's law as

$$F_2 = k_2 u$$

Equation 48

Substituting Equation 47 and Equation 48 into Equation 44, the result is

$$F = \mu \left( \dot{u} - \frac{1}{\alpha k_1} \dot{F} \right) + k_2 u \Rightarrow \frac{\mu}{\alpha k_1} \dot{F} + F = \mu \dot{u} + k_2 u$$

Equation 49

If the reference area,  $A_0$ , and a reference length,  $\ell_0$ , is incorporated into Equation 49, it can be written in terms of the stress,  $\sigma$ , and the strain,  $\varepsilon$ , that the material that are simulated through the model experience

$$\frac{\mu}{\alpha k_1} \frac{\dot{F}}{A_0} + \frac{F}{A_0} = \mu \frac{\dot{u}}{\ell_0} + k_2 \frac{u}{\ell_0} \Rightarrow \frac{\mu}{\alpha k_1} \dot{\sigma} + \sigma = \mu \dot{\varepsilon} + k_2 \varepsilon$$

Equation 50

Equation 50 can further be simplified if the following constants are defined

$$\tau_\varepsilon = \frac{\mu}{\alpha k_1}, \tau_\sigma = \frac{\mu}{k_2}, E_R = k_2$$

Equation 51

and substituted into Equation 50. The result is

$$\tau_\varepsilon \dot{\sigma} + \sigma = E_R (\tau_\sigma \dot{\varepsilon} + \varepsilon)$$

Equation 52

Introducing the elastic response as is defined by Fung (1972), Equation 52 becomes

$$\tau_\varepsilon \dot{\sigma} + \sigma = E_R (\tau_\sigma \dot{\sigma}^{(e)} + \sigma^{(e)}) \text{ with } \tau_\varepsilon \sigma(0) = E_R \tau_\sigma \sigma^{(e)}(0)$$

Equation 53

## B-2 Reformulation of QLV theory for programming

The tensile stress inside a specimen that undergoes stress relaxation can be computed via this expression derived by Fung *et al.* (1972)

$$\sigma(\varepsilon, t) = \sigma^{(e)}(0+)G(t) + \int_0^t \left( G(t-\tau) \frac{\partial \sigma^{(e)}(\varepsilon(\tau))}{\partial \varepsilon} \frac{\delta \varepsilon(\tau)}{\partial \tau} \right) d\tau$$

Equation 54

The reduced relaxation function,  $G(t-\tau)$ , and the elastic response,  $\sigma^{(e)}(\varepsilon(t))$ , have been defined as

$$G(t-\tau) = \frac{1 + C \left( E_1 \left[ \frac{t-\tau}{\tau_2} \right] - E_1 \left[ \frac{t-\tau}{\tau_1} \right] \right)}{1 + C \ln \left( \frac{\tau_2}{\tau_1} \right)}$$

Equation 55

where  $E_1 \left[ \frac{t-\tau}{\tau_1} \right]$  is defined as the exponential integral or  $E_1 [y] = \int_y^\infty \frac{e^{-z}}{z} dz$

and

$$\sigma^{(e)}(\varepsilon(t)) = A(e^{B\varepsilon(t)} - 1)$$

Equation 56

During a relaxation test, the specimen is strained at a constant strain rate,  $\gamma$ , until a predetermined strain level is reached. The specimen is then held at the resulting strain level for a set period of time. The strain history for the stress relaxation test is therefore

$$\varepsilon(t) = \begin{cases} \gamma t & \text{for } 0 \leq t \leq t_0 \\ \gamma t_0 & \text{for } t > t_0 \end{cases}$$

Equation 57

and the first derivative is

$$\frac{d\varepsilon(t)}{dt} = \begin{cases} \gamma & \text{for } 0 \leq t \leq t_0 \\ 0 & \text{for } t > t_0 \end{cases}$$

Equation 58

By substituting Equation 57 into Equation 56, Equation 56 becomes

$$\sigma^{(e)}(\varepsilon(t)) = \begin{cases} A(e^{B\gamma t} - 1) & \text{for } 0 \leq t \leq t_0 \\ A(e^{B\gamma t_0} - 1) & \text{for } t > t_0 \end{cases}$$

Equation 59

$$\frac{\partial \sigma^{(e)}(\varepsilon(t))}{\partial \varepsilon} = \begin{cases} AB e^{B\gamma t} & \text{for } 0 \leq t \leq t_0 \\ 0 & \text{for } t > t_0 \end{cases}$$

If the specimen was unloaded before commencement of the stress relaxation test, and if the superposition principle is applied, Equation 54 becomes

$$\sigma(\varepsilon, t) = \begin{cases} \int_0^t \left( G(t-\tau) \frac{\partial \sigma^{(e)}(\varepsilon(\tau))}{\partial \varepsilon} \frac{\delta \varepsilon(\tau)}{\partial \tau} \right) d\tau & \text{for } 0 \leq t \leq t_0 \\ \int_0^{t_0} \left( G(t-\tau) \frac{\partial \sigma^{(e)}(\varepsilon(\tau))}{\partial \varepsilon} \frac{\delta \varepsilon(\tau)}{\partial \tau} \right) d\tau + \int_{t_0}^t \left( G(t-\tau) \frac{\partial \sigma^{(e)}(\varepsilon(\tau))}{\partial \varepsilon} \frac{\delta \varepsilon(\tau)}{\partial \tau} \right) d\tau & \text{for } t > t_0 \end{cases}$$

Equation 60

Substituting Equation 55, Equation 58 and Equation 59 into Equation 60, the result is

$$\sigma(\varepsilon, t) = \begin{cases} \int_0^t \left( \frac{1+C \left( E_1 \left[ \frac{t-\tau}{\tau_2} \right] - E_1 \left[ \frac{t-\tau}{\tau_1} \right] \right)}{1+C \ln \left( \frac{\tau_2}{\tau_1} \right)} \times A B e^{B\gamma\tau} \times \gamma \right) d\tau & \text{for } 0 \leq t \leq t_0 \\ \int_0^{t_0} \left( \frac{1+C \left( E_1 \left[ \frac{t-\tau}{\tau_2} \right] - E_1 \left[ \frac{t-\tau}{\tau_1} \right] \right)}{1+C \ln \left( \frac{\tau_2}{\tau_1} \right)} \times A B e^{B\gamma\tau} \times \gamma \right) d\tau \\ + \int_{t_0}^t \left( \frac{1+C \left( E_1 \left[ \frac{t-\tau}{\tau_2} \right] - E_1 \left[ \frac{t-\tau}{\tau_1} \right] \right)}{1+C \ln \left( \frac{\tau_2}{\tau_1} \right)} \times 0 \times \gamma \right) d\tau & \text{for } t > t_0 \end{cases} \quad \text{Equation 61}$$

After some simplification, Equation 61 becomes

$$\sigma(\theta, t) = \begin{cases} \frac{A B \gamma}{1+C \ln \left( \frac{\tau_2}{\tau_1} \right)} \int_0^t \left( \left( 1+C \left( E_1 \left[ \frac{t-\tau}{\tau_2} \right] - E_1 \left[ \frac{t-\tau}{\tau_1} \right] \right) \right) e^{B\gamma\tau} \right) d\tau & \text{for } 0 \leq t \leq t_0 \\ \frac{A B \gamma}{1+C \ln \left( \frac{\tau_2}{\tau_1} \right)} \int_0^{t_0} \left( \left( 1+C \left( E_1 \left[ \frac{t-\tau}{\tau_2} \right] - E_1 \left[ \frac{t-\tau}{\tau_1} \right] \right) \right) e^{B\gamma\tau} \right) d\tau & \text{for } t > t_0 \end{cases} \quad \text{Equation 62}$$

with  $\theta = f(A, B, C, \tau_1, \tau_2)$ .

### B-3 Patternsearch-algorithm

The *patternsearch*-algorithm does not utilise the derivatives of the objective function, which makes it ideal for the optimisation of non-linear discontinuous functions like the QLV-function. An initial start point is specified from which the algorithm starts to search for the optimum. The following steps are performed for each iteration step:

A mesh grid is generated around the current point, i.e. the initial point if it is the first iteration step or the current point that delivers the best function value. The size of the mesh grid depends on the user specified size if it is the first generation, or on the results of the previous iteration step.

The algorithm then polls the mesh grid points that surround the current point by computing the value of the objective function at each grid points.

If a point is found that improves the value of the objective function that point becomes the new reference point. The mesh grid size is then increased and the algorithm moves onto the new iteration step.

If an improvement is not found, the mesh grid size is decreased and the polling of the new mesh grid points follows.

This will continue until one of the stopping criteria is met, i.e. minimum mesh grid size, maximum number of iterations performed, maximum number of function evaluations computed or if the function tolerance or variable tolerance is reached.

It is also possible to perform a specific search method at each iteration step before polling of the mesh grid points. If an improvement is found, the algorithm moves onto the next iteration step without polling of the mesh grid points. If an improvement is not found, the algorithm continues with the polling process. The user can also specify whether all the grid points need to be polled, or whether the next iteration can be begin as soon as an improvement is found.

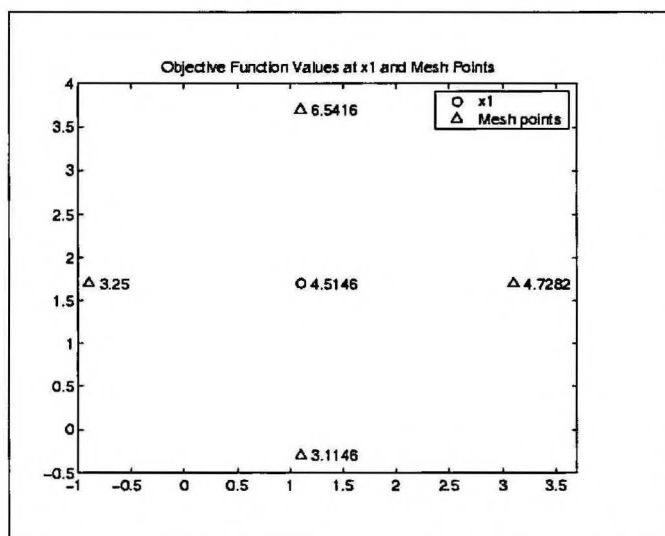


Figure 45: Poll method

The search and polling method that was used in this project was the so-called positive basis 2N method. The method is described in Figure 45. The mesh points are displayed as blue triangles whereas the current point is displayed as a red circle. The values beside the points in Figure 45 represent the objective function value. The positive basis 2N method implies that the mesh points are obtained through

$$\begin{aligned}
 2 * [ 1 \quad 0 ] + x_1 &= \text{mesh point 1} \\
 2 * [ 0 \quad 1 ] + x_1 &= \text{mesh point 2} \\
 2 * [-1 \quad 0 ] + x_1 &= \text{mesh point 3} \\
 2 * [ 0 \quad -1 ] + x_1 &= \text{mesh point 4}
 \end{aligned}$$

Equation 63

for an objective function that are dependent on two variables. More information with regards to the *patternsearch*-algorithm can be found in the release notes of Matlab.

### B-4 Stress relaxation graphs

The stress relaxation curves as predicted by the QLV-function are shown in Figure 46 to Figure 49 for the different sets of QLV-constants.

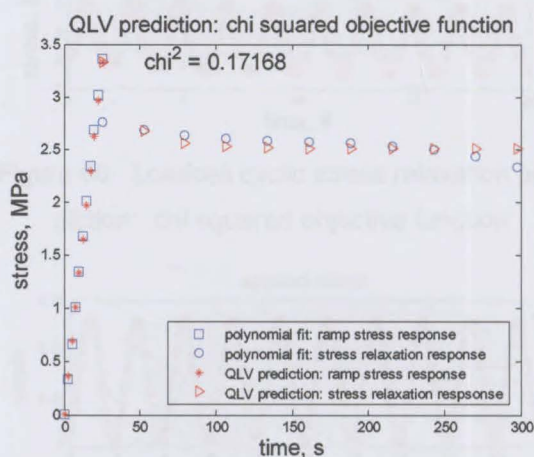


Figure 46: Loadcell stress relaxation prediction: chi squared objective function

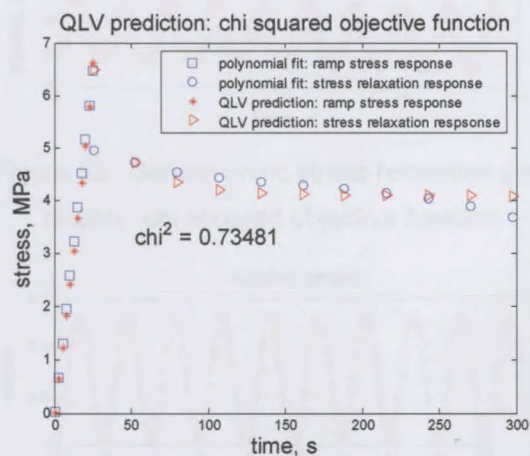


Figure 48: Sensor stress relaxation prediction: chi squared objective function

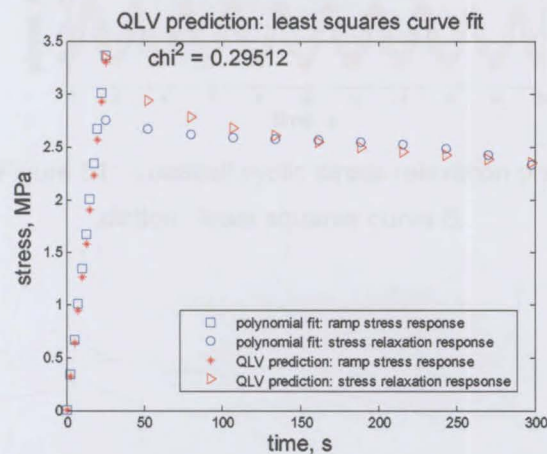


Figure 47: Loadcell stress relaxation prediction: least squares curve fit

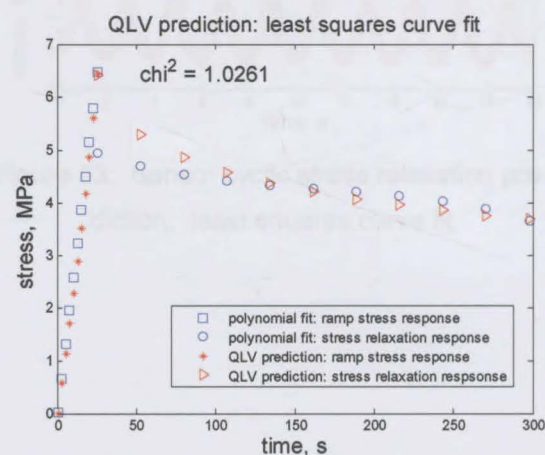


Figure 49: Sensor stress relaxation prediction: least squares curve fit

### B-5 Cyclic loading graphs

The cyclic loading curves as predicted by the QLV-function are shown in Figure 46 to Figure 49 for the different sets of QLV-constants.

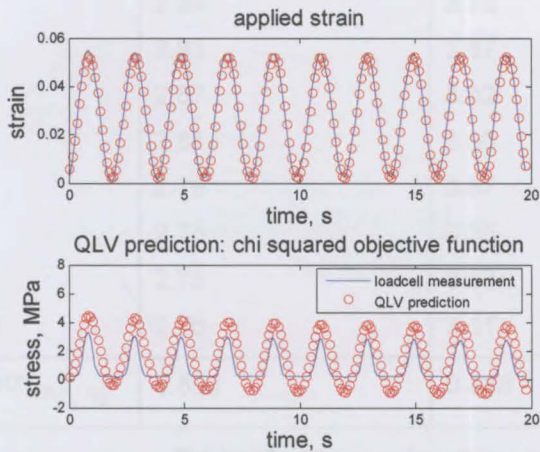


Figure 50: Loadcell cyclic stress relaxation prediction: chi squared objective function

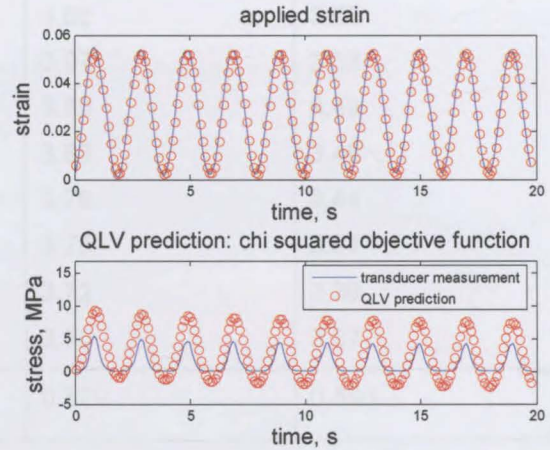


Figure 52: Sensor cyclic stress relaxation prediction: chi squared objective function

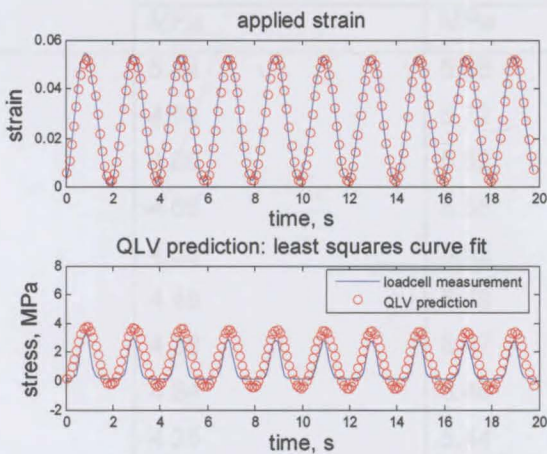


Figure 51: Loadcell cyclic stress relaxation prediction: least squares curve fit

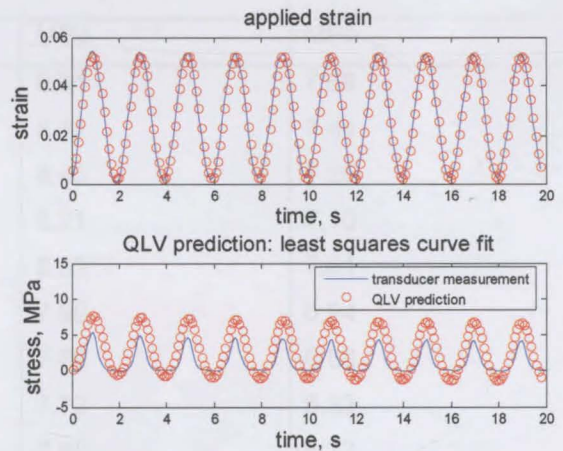


Figure 53: Sensor cyclic stress relaxation prediction: least squares curve fit

## Appendix B: QLV model of patella tendon stress relaxation

Table 35: Stress relaxation prediction for cyclic loading: loadcell predictions

Cycle	Raw measurements,	<i>patternsearch</i> -tool: squared error	<i>patternsearch</i> -tool: chi-squared	Non-linear curve fit-tool
#	MPa	MPa	MPa	MPa
1	3.27	3.95	4.46	3.78
2	3.03	3.82	4.24	3.67
3	2.94	3.73	4.08	3.59
4	2.93	3.67	3.97	3.53
5	2.87	3.62	3.89	3.49
6	2.81	3.60	3.83	3.46
7	2.79	3.57	3.79	3.44
8	2.78	3.55	3.75	3.41
9	2.75	3.53	3.72	3.39
10	2.76	3.51	3.70	3.37
$\% \sigma_{relax}, \%$	0.843	0.888	0.829	0.890

Table 36: Stress relaxation prediction for cyclic loading: sensor predictions

Cycle	Raw measurements,	<i>patternsearch</i> -tool: squared error	<i>patternsearch</i> -tool: chi-squared	Non-linear curve fit-tool
#	MPa	MPa	MPa	MPa
1	5.44	5.86	9.31	7.69
2	4.94	5.72	8.81	7.44
3	4.69	5.62	8.46	7.25
4	4.65	5.55	8.21	7.10
5	4.53	5.52	8.02	7.01
6	4.45	5.49	7.90	6.94
7	4.38	5.47	7.80	6.88
8	4.34	5.46	7.72	6.82
9	4.25	5.44	7.65	6.77
10	4.27	5.42	7.59	6.73
$\% \sigma_{relax}, \%$	0.784	0.926	0.815	0.874

## Appendix C: *In vivo* investigation into the loading patterns of the patella tendon

### C-1 Results

The results for the squat exercise are shown in Table 37 and Table 38. Results for the leg extension exercise and the step exercises are shown in Table 39 to Table 41. Finally Table 42 contains the results for the jump exercise.

Table 37: Squat: Concentric contraction

Volunteer	FSO,V [SD]		Load, N [SD]		<i>anterior</i> / <i>posterior</i>
	Anterior	Posterior	Anterior	Posterior	
1	0.359 [0.0457]	0.898 [0.0704]	981 [125]	3420 [268]	0.403 [0.0769]
2	-	-	-	-	-
3	-	-	-	-	-
4	0.199 [0.0138]	0.601 [0.0113]	544 [37.7]	2290 [43.1]	0.331 [0.0204]
5	0.399 [0.0734]	1.76 [0.0104]	1090 [201]	6690 [39.8]	0.227 [0.0411]
6	0.477 [0.0149]	1.72 [0.0488]	1300 [40.7]	6540 [186]	0.278 [0.00608]
7	0.987 [0.0489]	1.42 [0.0428]	2700 [134]	5400 [163]	0.697 [0.0213]
8	0.266 [0.0193]	0.774 [0.0221]	729 [52.8]	2950 [84.3]	0.344 [0.0173]
9	0.827 [0.0113]	0.562 [0.0497]	2260 [30.8]	2140 [189]	1.48 [0.113]
10	0.233 [0.0437]	0.411 [0.0428]	637 [120]	1570 [163]	0.563 [0.0603]



Appendix C: *In vivo* investigation into the loading patterns of the patella tendon

Table 38: Squat: Eccentric contraction

Volunteer	FSO, V [SD]		Load, N [SD]		<i>anterior/posterior</i>
	Anterior	Posterior	Anterior	Posterior	
1	0.342 [0.0693]	0.943 [0.163]	936 [190]	3590 [622]	0.362 [0.0105]
2	-	-	-	-	-
3	-	-	-	-	-
4	0.231 [0.0188]	0.639 [0.0167]	632 [51.5]	2440 [63.6]	0.362 [0.0235]
5	0.388 [0.0560]	1.74 [0.0359]	1060 [153]	6620 [137]	0.223 [0.0310]
6	0.502 [0.0300]	1.53 [0.0378]	1370 [82.0]	5840 [144]	0.327 [0.0136]
7	0.996 [0.0745]	1.38 [0.0764]	2720 [204]	5280 [291]	0.720 [0.0383]
8	0.271 [0.0273]	0.757 [0.0186]	742 [74.7]	2880 [70.7]	0.358 [0.0289]
9	1.01 [0.0255]	0.698 [0.0241]	2770 [69.6]	2660 [91.8]	1.45 [0.0259]
10	0.278 [0.0547]	0.430 [0.0230]	761 [150]	1640 [87.6]	0.643 [0.0946]

Table 39: Leg extension

Volunteer	FSO, V [SD]		Load, N [SD]		<i>anterior/posterior</i>
	Anterior	Posterior	Anterior	Posterior	
1	0.255 [0.0443]	0.706 [0.0363]	697 [121]	2691 [138]	0.363 [0.0815]
2	-	-	-	-	-
3	-	-	-	-	-
4	0.139 [0.00699]	0.551 [0.00391]	381 [19.1]	2100 [14.9]	0.253 [0.0135]
5	0.235 [0.00898]	1.72 [0.0244]	644 [24.6]	6570 [92.9]	0.136 [0.00490]
6	0.236 [0.0150]	1.13 [0.175]	645 [41.2]	4290 [668]	0.213 [0.0321]
7	0.194 [0.0194]	0.746 [0.0240]	530 [53.2]	2840 [91.5]	0.260 [0.0153]
8	0.194 [0.00474]	0.746 [0.00541]	530 [13.0]	2840 [20.6]	0.260 [0.00527]
9	0.544 [0.0388]	0.875 [0.0358]	1490 [106]	3340 [137]	0.621 [0.0372]
10	0.231 [0.112]	0.407 [0.127]	631 [306]	1550 [485]	0.540 [0.123]

Appendix C: *In vivo* investigation into the loading patterns of the patella tendon

Table 40: Step up

Volunteer	FSO, V [SD]		Load, N [SD]		<i>anterior</i> / <i>posterior</i>
	Anterior	Posterior	Anterior	Posterior	
1	0.125 [-]	0.641 [-]	341 [-]	2440 [-]	0.194 [-]
2	-	-	-	-	-
3	-	-	-	-	-
4	0.125 [0.00327]	0.485 [0.0302]	342 [8.95]	1850 [115]	0.259 [0.0135]
5	0.480 [0.00906]	1.57 [0.0148]	1310 [24.8]	5970 [56.4]	0.306 [0.00333]
6	0.145 [0.0180]	0.791 [0.0415]	396 [49.3]	3010 [158]	0.183 [0.0235]
7	0.285 [0.0504]	0.975 [0.0413]	781 [138]	3720 [158]	0.294 [0.0598]
8	0.188 [0.0255]	0.758 [0.0200]	515 [69.8]	2890 [76.1]	0.248 [0.0269]
9	-	-	-	-	-
10	0.263 [0.258]	0.457 [0.288]	719 [706]	1740 [1100]	0.464 [0.223]

Table 41: Step down

Volunteer	FSO, V [SD]		Load, N [SD]		<i>anterior</i> / <i>posterior</i>
	Anterior	Posterior	Anterior	Posterior	
1	0.170 [-]	0.669 [-]	465 [-]	2552 [-]	0.254 [-]
2	-	-	-	-	-
3	-	-	-	-	-
4	0.151 [0.0153]	0.535 [0.0132]	412 [41.9]	2040 [50.4]	0.282 [0.0227]
5	0.467 [0.0177]	1.63 [0.0371]	1280 [48.4]	6200 [141]	0.287 [0.00717]
6	0.188 [0.00354]	0.786 [0.0343]	513 [9.68]	3000 [131]	0.239 [0.0104]
7	0.337 [0.0558]	1.13 [0.0317]	922 [153]	4320 [121]	0.297 [0.0436]
8	0.209 [0.0302]	0.799 [0.0246]	571 [82.7]	3050 [93.7]	0.261 [0.0304]
9	-	-	-	-	-
10	0.260 [0.259]	0.481 [0.323]	712 [708]	1830 [1230]	0.437 [0.200]

Appendix C: *In vivo* investigation into the loading patterns of the patella tendon

Table 42: Jump

Volunteer	FSO, V [SD]		Load, N [SD]		<i>anterior</i> / <i>posterior</i>
	Anterior	Posterior	Anterior	Posterior	
1	0.198 [-]	0.819 [-]	542 [-]	3120 [-]	0.242 [-]
2	-	-	-	-	-
3	-	-	-	-	-
4	0.200 [0.0192]	1.23 [1.30]	548 [52.4]	4690 [4950]	0.267 [0.133]
5	0.535 [0.0572]	3.01 [1.56]	1460 [157]	1190 [5960]	0.214 [0.0991]
6	0.188 [-]	0.831 [-]	514 [-]	3170 [-]	0.226 [-]
7	0.582 [0.0270]	2.28 [1.34]	1590 [73.9]	8680 [5090]	0.326 [0.152]
8	0.457 [0.0855]	1.31 [1.02]	1250 [234]	4990 [3880]	0.445 [0.187]
9	-	-	-	-	-
10	0.550 [0.0280]	0.870 [0.0877]	1500 [76.7]	3310 [334]	0.639 [0.0851]

In Figure 54 to Figure 59 samples of the sensor output obtained for the different exercises for volunteer #4 are shown.

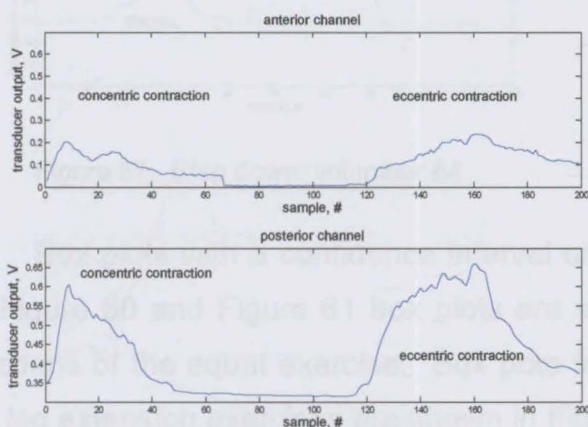


Figure 54: Squat exercise: volunteer #4

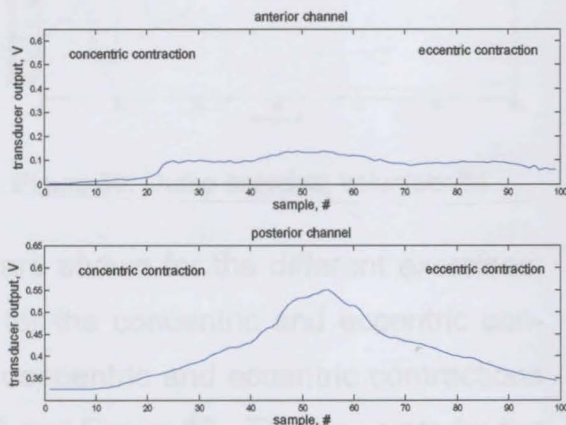


Figure 55: Leg extension: volunteer #4

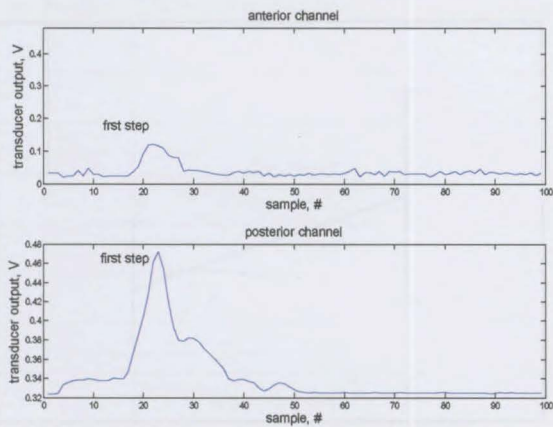
Appendix C: *In vivo* investigation into the loading patterns of the patella tendon

Figure 56: Step up: volunteer #4

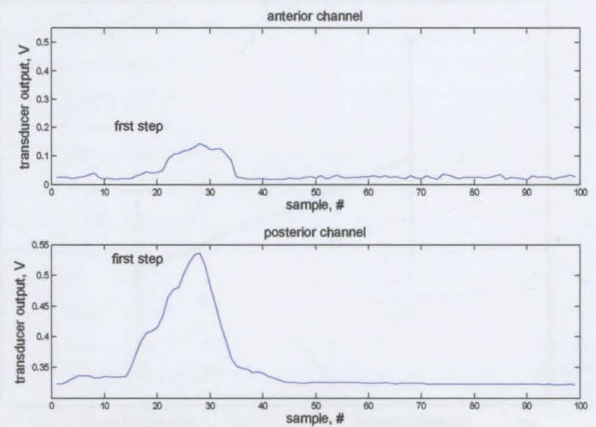


Figure 58: Step down: volunteer #4

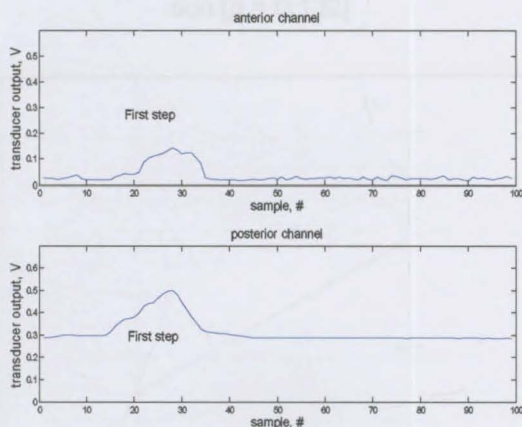


Figure 57: Step down: volunteer #4

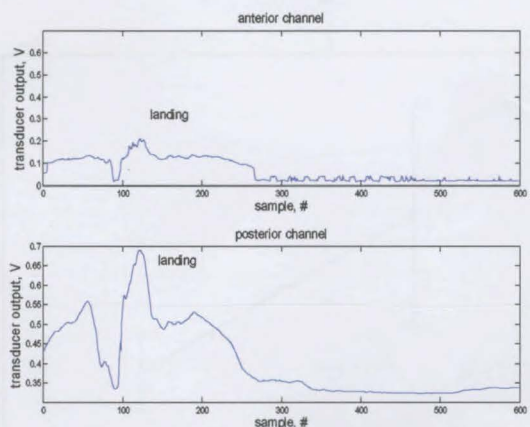


Figure 59: Jump exercise: volunteer #4

Box plots with a confidence interval of 95% are shown for the different exercises. In Figure 60 and Figure 61 box plots are shown for the concentric and eccentric contractions of the squat exercise. Box pots for the concentric and eccentric contractions for leg extension exercises are shown in Figure 62 and Figure 63. The box plots for the step exercises are shown in Figure 64 and Figure 65. Figure 64 shows the box plot when the volunteers walked up the steps and Figure 65 shows the box plot when the volunteers walked down the steps. The box plot for the jump exercise is shown in Figure 66.

Appendix C: *In vivo* investigation into the loading patterns of the patella tendon

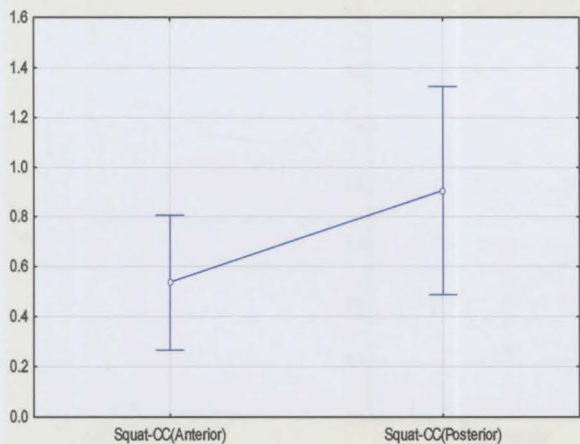


Figure 60: Squat exercise: Concentric contraction [ $p = 0.132$ ]

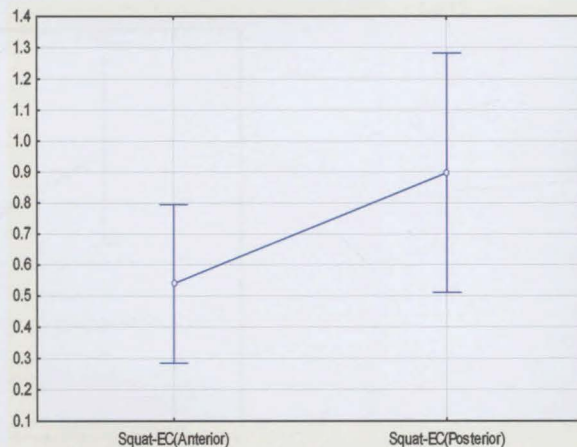


Figure 61: Squat exercise: Eccentric contraction [ $p = 0.115$ ]

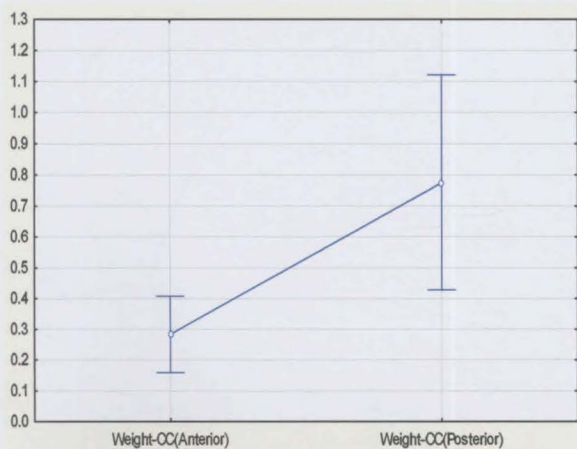


Figure 62: Leg extension exercise: Concentric contraction [ $p = 0.0213$ ]

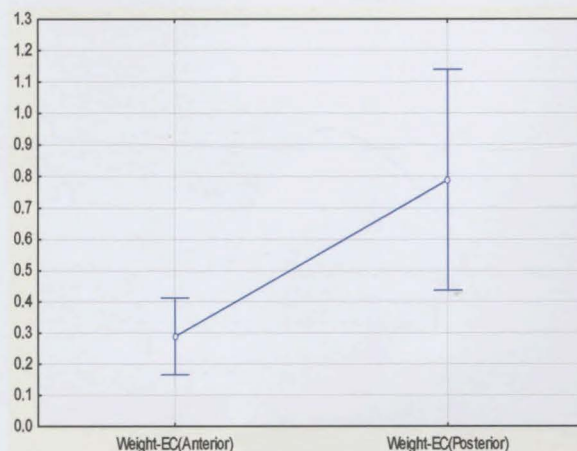


Figure 63: Leg extension exercise: Eccentric contraction [ $p = 0.0211$ ]

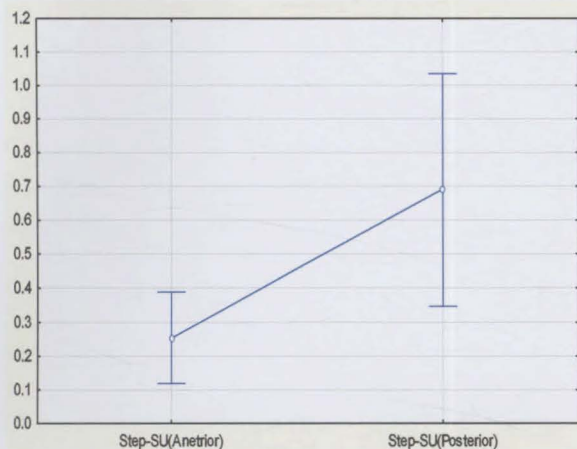


Figure 64: Step up exercise [ $p = 0.0194$ ]

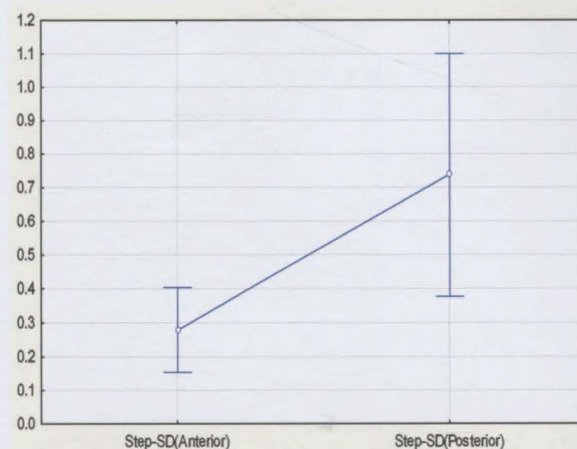


Figure 65: Step down exercise [ $p = 0.0188$ ]

Appendix C: *In vivo* investigation into the loading patterns of the patella tendon

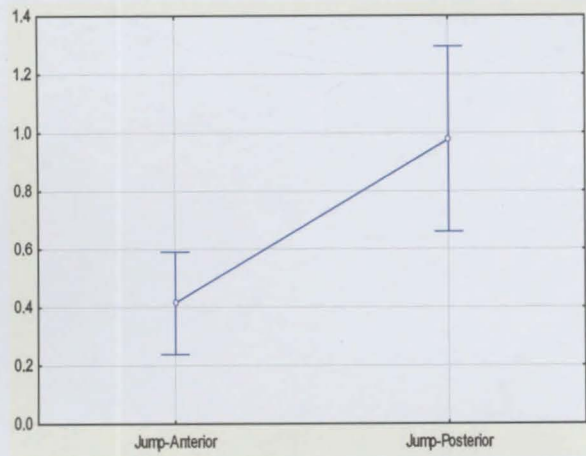


Figure 66: Jump exercise [ $p = 0.00193$ ]